THE PHYSIOLOGY OF MAMMALIAN ER QUALITY CONTROL: UNFOLDED PROTEIN RESPONSE AND ER-ASSOCIATED DEGRADATION

A Dissertation

Presented to the Faculty of the Graduate School

of Cornell University

In Partial Fulfillment of the Requirements for the Degree of

Doctor of Philosophy

by

Liu Yang

January 2014

THE PHYSIOLOGY OF MAMMALIAN ER QUALITY CONTROL: UNFOLDED PROTEIN RESPONSE AND ER-ASSOCIATED DEGRADATION

Liu Yang, Ph.D.

Cornell University 2014

Endoplasmic Reticulum (ER) is the site for secretory and transmembrane protein synthesis and maturation. Disrupted ER homeostasis activates a cascade of ER-to-nucleus signaling pathways termed the Unfolded Protein Response (UPR) to alleviate ER stress and restore ER homeostasis. Causal links between ER stress and a variety of human diseases have been suggested. However, as physiological ER stress is subtle and hard to detect relative to pharmacologically induced ER stress, the significance of ER stress and UPR activation in the pathogenesis of these disorders remains controversial.

To this end, our lab developed a Phos-tag based SDS-PAGE method to sensitively detect the phosphorylation of UPR sensors (IRE1α/PERK), a direct indicator of ER stress levels and UPR activation. This method was verified and showed to quantitatively monitor UPR activation in cells expressing misfolded proteins. More significantly, this assay revealed delicate changes in IRE1α phosphorylation in mouse tissues under basal or stimulated physiological conditions that could not be visualized with a regular SDS-PAGE gel. Using this powerful tool in a screen for anti-diabetic reagents, we showed that phenformin, an anti-diabetic drug, stimulated the IRE1α and PERK pathways in both

AMPK- and ER stress-dependent manners, revealing a novel crosstalk between UPR and metabolic pathways.

To further expand our understanding of physiological ER stress, we turned to a model of chronic ER stress and UPR activation. Specifically, we generated a mouse model deficient for SEL1L, a core factor in ER associated degradation (ERAD). Animals with SEL1L deficiency in B cells ($SEL1L^{CD19}$) exhibited severely impaired B cell development. Unexpectedly, the developmental defect in SEL1L-null B cells was independent of ER stress-mediated cell death, as UPR sensor phosphorylation and chaperone induction were not detected. Additional data supported a model that the phenotypic defect was due to a block in degradation of VpreB, a key component for a critical checkpoint during B cell developmental. In addition, our method, for the first time, showed an uncoupling between the activation status of UPR sensors and downstream targets in B cell to plasma cell differentiation.

Taken together, our Phos-tag gel has proven to be a sensitive and reliable tool for investigating physiological ER stress. We believe this method will be critical in further understanding and elucidating the physiological role of mammalian ER quality control system, and may provide insights into future diagnosis for ER-associated conformational diseases.

BIOGRAPHICAL SKETCH

Liu Yang was born in 1985 in Nanjing, China. She was fortunate to enter High School Affiliated to Nanjing Normal University in 2001, where she gradually developed interests in Biology. She majored in Biological Sciences during her four-year undergraduate study at Fudan University, China. After receiving her bachelor's degree in July 2008, she joined the program of Biochemistry, Molecular and Cell Biology in the department of Molecular Biology and Genetics at Cornell University, Ithaca, New York. In June 2009, she joined the laboratory of Dr. Ling Qi. Her research involved broad topics in the ER (endoplasmic reticulum) quality control system and its physiological significance in maintaining cellular homeostasis.

ACKNOWLEDGMENTS

I would like to thank my Ph.D. supervisor Dr. Ling Qi for taking me into his lab, for his guidance and training, and for giving me the chance of independent research.

I would like to thank my committee members, Dr. Martha Harney Stipanuk and Dr. Marcus Smolka for their great support, encouragement and advices on my projects; thank Dr. Robin Davisson and Dr. Qiaoming Long for great collaborations.

Also, I would like to thank the members of the Qi Lab for their support and help, especially the UPR subgroup members Dr. Haibo Sha, Dr. Yin He (past member), Zhen Xue, Xiaoqing Li (past member), Angela Lee (past member), and Mahindra Mohan (past member) for insightful discussion and experimental support on my UPR projects. Also thank Dr. Yewei Ji and Hana Kim for providing expertise to my ERAD project.

Many thanks to my nine-year friends Xinyin Jiang and Cheng Chen, and new friends in Ithaca Botao Liu, Xian Qu, Xuanxuan Shen, Tao Sun, Jianfeng Zhang, Shanshan Zhang and my BMCB classmates, who make the summer more fun and winter less intolerable.

Final special thanks to my husband, my parents and my parents-in-law, whose infinite love, support and encouragement always help me throughout the hard time, and are the best treasure in my life.

TABLE OF CONTENTS

BIOGRAPHICAL SKETCH ..... **III**

ACKNOWLEDGMENTS ..... **IV**

TABLE OF CONTENTS ..... **V**

LIST OF FIGURES ..... **X**

LIST OF TABLES ..... **XII**

CHAPTER 1. INTRODUCTION AND LITERATURE REVIEW **1**

1.1 ENDOPLASMIC RETICULUM 1

1.2 PROTEIN HOMEOSTASIS AND ER STRESS 3

1.3 ERAD 6

1.3.1 Substrate recognition *6*

1.3.2 Dislocation *8*

1.3.3 Core organizers of ERAD – E3 complex *10*

1.3.4 Physiological significance of ERAD *12*

1.4 UNFOLDED PROTEIN RESPONSE 14

1.4.1 IRE1 PATHWAY *17*

1.4.2 PERK PATHWAY *27*

1.4.3 ATF6 PATHWAY *29*

1.4.4 Physiological and pathological UPR *31*

1.5 RESEARCH AIMS AND DISSERTATION ORGANIZATION 42

CHAPTER 2. A PHOS-TAG-BASED APPROACH REVEALS THE EXTENT OF PHYSIOLOGICAL ENDOPLASMIC RETICULUM STRESS **48**

2.1 ABSTRACT 48

2.2 INTRODUCTION 49

2.3 MATERIALS AND METHODS 51

2.4 RESULTS 55

2.4.1 Visualization of sensor phosphorylation and quantitation of ER stress 55

2.4.2 Accumulation of misfolded proteins induces mild ER stress 59

2.4.3 Many tissues exhibit basal ER stress under feeding conditions 61

2.4.4 Refeeding induces mild ER stress in the pancreas 64

2.5 DISCUSSION 66

2.6 ACKNOWLEDGMENTS 69

CHAPTER 3. PHENFORMIN ACTIVATES UNFOLDED PROTEIN RESPONSE IN AN AMP-ACTIVATED PROTEIN KINASE (AMPK)-DEPENDENT MANNER 70

3.1 ABSTRACT 70

3.2 INTRODUCTION 71

3.3 MATERIALS AND METHODS 73

3.4 RESULTS 77

3.4.1 Phenformin induces IRE1α and PERK phosphorylation 77

3.4.2 Phenformin-mediated IRE1α and PERK activation is a general phenomenon 82

3.4.3 AMPK is required for phenformin-mediated IRE1α and PERK activation 84

3.4.4 LKB1 is dispensable for phenformin effect 86

3.4.5 AMPK activation is not sufficient to activate IRE1α and PERK 88

3.4.6 Kinase activities of both IRE1α and PERK are indispensable for their activation by phenformin 90

3.4.7 Activation of IRE1α-XBP1 pathway partially mediates the cytotoxicity of phenformin 92

3.5 DISCUSSION 94

3.6 ACKNOWLEDGEMENT 97

CHAPTER 4. SEL1L, A CORE ERAD COMPONENT MAINTAINS THE PRE-BCR CHECKPOINT AND IS INDISPENSIBLE FOR B CELL DEVELOPMENT 98

4.1 ABSTRACT 98

4.2 INTRODUCTION 99

4.3 MATERIALS AND METHODS 102

4.4 RESULTS 107

4.4.1 Sel1L BKO mice exhibit systemic B cell reduction. 107

4.4.2 B cell development is defective in BKO bone marrows 113

4.4.3 ER stress is not the cause for developmental defect in SEL1L null B cells. 116

4.4.4 Loss of SEL1L leads to dysregulated preBCR signaling pathways 122

4.5 DISCUSSION 128

4.6 ACKNOWLEDGEMENT 131

CHAPTER 5. SUMMARY AND FUTURE DIRECTIONS 132

APPENDIX A. TRANSCRIPTION UPREGULATION OF XBP1 RESETS PROTEOSTASIS BOUNDARY DURING PLASMA CELL DIFFERENTIATION WITH NO OVERT UPR ACTIVATION 137

A.1 INTRODUCTION 137

A.2 MATERIALS AND METHODS 138

A.3 RESULTS 142

A.4 DISCUSSION 149

APPENDIX B. FARP1, A NOVEL IRE1A INTERACTING PROTEIN 151

B.1 INTRODUCTION 151

B.2 MATERIALS AND METHODS 152

B.3 RESULTS 155

B.4 DISCUSSION 160

APPENDIX C. CIRCADIAN EXPRESSION OF UPR GENES IN MULTIPLE ORGANS 161

C.1 INTRODUCTION 161

C.2 MATERIALS AND METHODS 163

C.3 RESULTS 166

C.4 DISCUSSION 175

REFERENCE 176

LIST OF FIGURES

CHAPTER 1. INTRODUCTION AND LITERATURE REVIEW 1

Figure 1.1 Three major UPR pathways in mammals 15

Figure 1.2 Phos-tag molecules and phosphorylated compounds 47

CHAPTER 2. A PHOS-TAG-BASED APPROACH REVEALS THE EXTENT OF PHYSIOLOGICAL ENDOPLASMIC RETICULUM STRESS 48

Figure 2.1 Immunoblots of p-Thr980 PERK, IRE1α (left) and total PERK (right) in different MEFs treated with or without Tg 57

Figure 2.2 Visualization and quantitation of ER stress under pharmacological stress 58

Figure 2.3 Accumulation of misfolded proteins induces mild ER stress 60

Figure 2.4 Many tissues exhibit basal ER stress under feeding conditions 62

Figure 2.5 Tissue-specific UPR 63

Figure 2.6 Fasting-refeeding induces mild ER stress in pancreas 65

CHAPTER 3. PHENFORMIN ACTIVATES UNFOLDED PROTEIN RESPONSE IN AN AMP-ACTIVATED PROTEIN KINASE (AMPK)-DEPENDENT MANNER 70

Figure 3.1. Phenformin treatment activates UPR sensors IRE1α and PERK 80

Figure 3.2 Phenformin effect on UPR activation is a general phenomenon 83

Figure 3.3 AMPK is required for phenformin-mediated UPR activation 85

Figure 3.4 LKB1 is dispensable for phenformin-mediated UPR activation 87

Figure 3.5 AMPK activation is not sufficient to activate UPR 89

Figure 3.6 Kinase activities of IRE1α and PERK are required for the phenformin effect 91

Figure 3.7 Activation of the IRE1α pathway in part mediates the cytotoxicity of phenformin and the model 93

CHAPTER 4. SEL1L, A CORE ERAD COMPONENT MAINTAINS THE PRE-BCR CHECKPOINT AND IS INDISPENSIBLE FOR B CELL DEVELOPMENT 98

Figure 4.1 Mouse genotyping examples 110

Figure 4.2 Impairment of B cell development in bone marrow leading to decrease of B cellularity in peripheral tissues 111

Figure 4.3 The residual B cells in BKO spleen are normal B cells resulted from CRE leakage 115

Figure 4.4 No ER stress in BKO mice compared to WT mice 118

Figure 4.5 Bone marrow CD19+ B cell purification efficiency 120

Figure 4.6 Western blots against additional ER chaperones.....121

Figure 4.7 Loss of SEL1L leads to dysregulated preBCR signaling pathways 125

Figure 4.8 Surface expression of receptors that are critical for B cell development on early B cell progenitors 126

Figure 4.9 preBCR downstream signaling pathways are impaired in BKO 127

APPENDIX A. TRANSCRIPTION UPREGULATION OF XBP1 RESETS PROTEOSTASIS BOUNDARY DURING PLASMA CELL DIFFERENTIATION WITH NO OVERT UPR ACTIVATION.....137

Figure A1 Flow cytometric analysis of purified splenic B cells.....144

Figure A2 Increases of XBP1s and its targets during B cell to plasma cell differentiation 145

Figure A3 Expansion of ER capacity precedes immunoglobulin synthesis 146

Figure A4 No overt UPR activation during B cell to plasma cell differentiation 147

Figure A5 Dynamics of each event during plasma cell differentiation 148

APPENDIX B. FARP1, A NOVEL IRE1A INTERACTING PROTEIN 151

Figure B1. FARP1 interacts with both IRE1α and PERK independently of ER stress ...157

Figure B2 Over-expression of FARP1 doesn't promote UPR activation.....158

Figure B3 Knockdown of FARP1 doesn't impair UPR activation 159

APPENDIX C. CIRCADIAN EXPRESSION OF UPR GENES IN MULTIPLE ORGANS 161

Figure C1 Circadian rhythm of UPR genes in heart.....169

Figure C2 Activity of ER stress sensor IRE1α remains constant in heart 170

Figure C3 Circadian rhythm of UPR genes in liver 171

Figure C4 Circadian rhythm of UPR genes in white adipose tissue (WAT).....172

Figure C5 XBP1 regulates core circadian components at transcriptional level.....173

Figure C6 Knockdown of XBP1 influences multiple circadian genes 174

LIST OF TABLES

CHAPTER 2. A PHOS-TAG-BASED APPROACH REVEALS THE EXTENT OF PHYSIOLOGICAL ENDOPLASMIC RETICULUM STRESS 48

Table 2.1 Primer list.....54

CHAPTER 1. INTRODUCTION AND LITERATURE REVIEW

1.1 ENDOPLASMIC RETICULUM

Endoplasmic reticulum (ER) is a eukaryotic organelle consisted of interconnected networks of tubules, flattened cisternae and nuclear envelope, which share a common luminal space (Hu et al., 2011). The ER network dynamically interacts with other cellular organelles such as nucleus, Golgi, and mitochondria, functions as the site for protein synthesis, lipid production and calcium storage (Shibata et al., 2006).

There are two types of ER in most cell types classified by their morphology -rough ER (rER) and smooth ER (sER). Ribosomal particles attach to the outer surface of certain ER sub-compartment synthesizing nascent peptides into its lumen. These ER subdomains attached with ribosomes exhibit a rough appearance under electron microscope and thus defined as rER. Meanwhile, the ones in the absence of ribosomal particle attachment showing a smooth structure are determined as sER (Shibata et al., 2006).

In addition to their morphological differences, rER and sER perform distinct biological functions. rER is the first unit in the factory of transmembrane and secretory protein synthesis (CARO and PALADE, 1964). The translation complex of ribosome and mRNA encoding ER protein is directed to rER surface with the assistance of signal recognition

particle (SRP). SRP binding to the hydrophobic signal sequence on the terminus of nascent peptide arrests translation. Subsequently, SRP-ribosome-mRNA complex is directed to ER surface by docking to SRP receptor on the ER membrane. Release of SRP from the complex results in resumed translation, followed by insertion of growing polypeptide into ER lumen through translocons such as Sec61(Akopian et al., 2013; Nicchitta, 2002). Besides SRP dependent co-translational targeting, post-translational ER localization of newly synthesized polypeptides can also be achieved with the assistance of chaperones (Rapoport et al., 1999). Alternately, cis-ER targeting sequence on the untranslated mRNA can promote ER location of the translation complex in an SRP-independent pathway (Kraut-Cohen and Gerst, 2010). Proteins synthesized into rER lumen are then folded, modified, transported to Golgi for further modification and ultimately incorporated into plasma membrane/lysosomal vesicles or secreted into extra-cellular space.

Despite the common luminal space connected to rER, sER does not participate in protein synthesis. Rather, sER majors in phospholipids and steroid synthesis, providing material for membrane reparation and hormone production, and is highly abundant in hormone-producing cells (Black et al., 2005). In addition, sER is also the compartment for dynamic cellular calcium storage (Meldolesi and Pozzan, 1998). Particularly, a specialized sER – Sarcoplasmic reticulum found in muscle serves as the sink and source of free calcium. Voltage-dependent calcium pump releasing calcium from Sarcoplasmic reticulum couples excitation signals to the initiation of muscle contraction in stimulated muscle cells (Wray and Burdyga, 2010).

1.2 PROTEIN HOMEOSTASIS AND ER STRESS

rER network (which will be referred as ER for simplicity in the rest of the chapters) is responsible for about one-third of cellular protein synthesis, mostly secretory and integral membrane protein in all eukaryotic cells (Kaufman, 1999). Proteins destined for plasma membrane, lysosomal or extracellular space are processed in this organelle in a distinct way compared to those synthesized in the cytosol: ER proteins are synthesized at higher rates in the oxidizing environment, and bears more modification to create structural complexity (Stephens and Nicchitta, 2008). Without correct conformation, proteins are retained in ER, and cannot proceed to Golgi for further sorting and decoration.

An array of chaperones and foldases participate in the sophisticated folding cycles for correct conformation, covalent modification and multimer assembly. Many of the general folding chaperones (Hsp70 and Hsp90) and co-chaperones (Hsp110 and Hsp40) belong to the heat shock protein family. The most well-studied heat shock chaperone is Hsp70 family member BIP (also known as glucose-related protein 78, GRP78), which facilitates folding of a broad range of newly synthesized peptides by various mechanisms: BIP ensures translocation and keeps the synthesized part soluble before generation of the complete polypeptides(Nguyen et al., 1991; Vogel et al., 1990). It also holds early-produced subunit in prevention for aggregation, until displaced by the rest subunits for complex assembly (Hendershot, 1990).

Lectin chaperones such as calnexin (CXN) and calreticulin (CRT) specialize in glycoprotein folding. A large portion of ER client peptides co-transitionally obtain N-

glycosylation on asparagine (N) at the N-X-T/S (X is any amino acid) motif, which rarely occurs on cytosolic proteins. The glycan modification consists of two N-acetylglucosamine, nine mannose and three glucose, and are sequentially processed by ER glycosidase and mannosidase, to generate various barcodes representing different folding status (Ruddock and Molinari, 2006). ER exportation of folded proteins requires complete removal of glucose from the original triglucosylated oligosaccharide by glucosidases I and II. However, the trimmed glucose-free, mannose-rich glycan on non-natively folded proteins can be reglucosylated by the folding sensor UDP-glucose:glycoprotein glucosyltransferase (UGGT) (Ritter and Helenius, 2000). Lectin chaperones calnexin (CXN) and calreticulin (CRT) specifically recognize the monolglucosylated glycan tag, prolong retention of associated cargos in the ER and promote their entry/re-entry into the folding cycles (Hebert et al., 1995; Helenius and Aebi, 2004). Terminally misfolded polypeptides are removed from de- and re-glucosylation circulation. These misfolded cargos are targeted to the ER degradation system, once the N-glycan is dismantled by mannosidase (Jakob et al., 2001; 1998; Nakatsukasa et al., 2001).

Another feature of ER folding is the formation of structure-stabilizing disulfide bond, which is enabled by the reducing environment in ER. Disulfide bonds occur between two cysteine residues on the same or two individual peptides catalyzed by members of PDI (protein disulfide isomerase) family (Wilkinson and Gilbert, 2004). The example of immunoglobulin indicates that disulfides serve to stabilize subunits of multimer complexes, affecting their folding and secretion (Elkabetz et al., 2008; Vinci et al., 2004).

In addition, a PDI family member, ERp57 assists non-native disulfide bonds in the cysteine-rich unstructured regions of its substrates, allowing formation of temporary intermediates that facilitate final folding processes (Jessop et al., 2007).

Despite various folding machineries, protein folding is by nature a slow and inefficient process, with many peptides repetitively trapped into the low-energy pits on the folding-energy landscape before achieving their native conformation. Many physiological and pathological stimuli, such as sudden burst of protein synthesis and secretion, genetic mutation on critical amino acids, virus infection, depletion of chaperone co-factor calcium, interrupt with folding processes and induce large amount of misfolded protein accumulation. In fact, even under basal condition, a considerable fraction of polypeptides are terminally misfolded and never reach their native state. Misfolded proteins accumulated in the ER may cause ER stress, which is deleterious for the folding of other peptides. Alternatively, they escape the ER folding checkpoint, execute dominant negative effects, and become toxic to the tissues. To solve the problem, cells developed two major quality control pathways- the ER-associated degradation (ERAD) pathway, and the unfolded protein responses (UPR) pathway, to enhance folding capacity, ensure qualified protein functions, prevent exportation of failed products and degrade potential toxic misfolded peptides. Efficient ERAD at basal conditions, and the adaptive UPR upon stress challenges are required for maintenance of the healthy ER environment. Remarkably, these two machineries inter-regulate each other under various physiological and pharmacological conditions, synergistically alleviate ER stress and contribute to ER homeostasis (Travers et al., 2000).

1.3 ERAD

Timely removal of the failed folding products prevent unnecessary occupation of chaperones and folding space in the ER. The system eliminating terminally misfolded ER proteins is collectively termed as ER-associated degradation (ERAD) pathway. ERAD pathway has an invert pyramid structure formed by a variety of chaperones and glycan-binding adaptors, a limited number of E3 complexes, and one shared terminal proteasome degradation complex. Glycan-binding adaptors recognize misfolded proteins through yet unclear mechanisms, and deliver substrates to the ERAD central organizer- E3 complexes on the ER membrane for dislocation and ubiquitination. In both yeast and metazoans, there are different ERAD pathways defined by the E3 central organizers, responsible for distinct but overlapping ranges of substrates. Regardless of the specific E3 complex, all misfolded proteins end up being extracted by P97/cdc48p AAA ATPase and ultimately degraded by the cytosolic p26 proteasome (Smith et al., 2011).

1.3.1 Substrate recognition

The first step in ERAD is substrate recognition. Based on experiments using model ERAD substrates, several theories of recognition and delivery have been established. The most detailed mechanism is “glycan-clock” model revealed by the study of luminal glycosylated proteins. The Glc3Man9GlcNAc2 modification on glycoproteins can be trimmed by mannosidase upon prolonged retention in ER, removing the branch A terminal mannose. Exposed alpha-1,6 mannose prevents re-glucosylation which is required for re-association with calnexin/calreticulin chaperone system (Parodi, 2000). Hence, polypeptides are released from folding cycle and can be recognized as

degradation substrates by glycan-binding protein (lectin adaptors) such as Yos9p/OS-9/XTP3-B (Quan et al., 2008). Mannosidase EDEM1 (Htm1p in yeast) has been shown to act upstream of the lectins to generate such glycan marker(Quan et al., 2008) or promote disassociation of polypeptide from calnexin (Oda et al., 2003). However, this glycan signal model doesn't explain the whole story, as non-glycosylated proteins are also degraded by ERAD machinery comprised of ER lectin and EDEM1 (Shenkman et al., 2013). Thus, alternative model has been proposed in which ERAD target misfolded proteins by direct binding to structural features exposed only in misfolded conditions. This strategy has been seen in many cases of quantity regulation of ER located enzymes in response to metabolite levels. The structure of HMG-CoA, the rate-limiting enzyme in cholesterol synthesis, changes upon cholesterol binding, and is recognized as misfolded protein by E3 ligase in yeast, or by specialized adaptors Insig-1 and Insig-2 in mammalian cells (Shearer and Hampton, 2005; Song et al., 2005). Investigation of the major histocompatibility class I (MHC-I) protein reveals another model in which virus hijacked ERAD pathway. In the human cytomegalovirus-infected cells, antigen presenting molecule MHC-I is recruited to ERAD by virus transmembrane adaptors US11 and US2 for dislocation and degradation, allowing virus to escape from immune defending system (Lilley and Ploegh, 2004; Rehm et al., 2002). Despite the in vitro results, we still know little about how endogenous misfolded proteins are distinguished from folding intermediates. The underlying mechanism by which degradation is initiated remains to be a puzzling but interesting question.

In addition to ERAD specific adaptors, housekeeping chaperones may also participate in substrate recognition. Binding of BIP to the ERAD substrates increases their solubility and prevents aggregation formation (Kabani et al., 2003; Nishikawa et al., 2001). GRP94 associates with OS-9 to deliver misfolded alpha-antitrypsin to E3 complex (Christianson et al., 2008). The disulfide isomerases (PDIs) participate in retro-translocation of bacteria and virus antigens (Schelhaas et al., 2007; Tsai et al., 2001). The fact that folding and degradation machineries share common components suggests a possible role of these chaperones as gatekeepers, recruiting terminally misfolded proteins to ERAD while preventing degradation of peptides in folding process. However, this hypothesis requests further studies.

1.3.2 Dislocation

ERAD targeted misfolded proteins are spatially separated from cytosolic proteasome by ER membrane. Thus, efficient dislocation system is required to retro-transport large and sometimes covalently modified ER luminal and membrane-integral peptides without disrupting ER membrane integrity. Reducing disulfide bonds by PDIs may be needed to breakdown large multimers into individual molecules before dislocation (Tsai et al., 2001). Pores or channels consisted of transmembrane proteins warrant misfolded peptide retro-translocation. Two major candidate channel proteins are Sec61 and the Derlin family members (Bagola et al., 2011).

Sec61, the translocon for protein synthesis obtains ideal properties as a candidate ERAD channel. However, research regarding the involvement of Sec61 as dislocation channel

has reached controversial conclusions. In the human cytomegalovirus-hijacked ERAD system, co-immunoprecipitation of MHC-1 and US2 virus adaptor recovers Sec61, indicating a physical interaction between Sec61 and ERAD substrates (Wiertz et al., 1996). Mutation of Sec61p significantly delays degradation of ERAD model substrate CPY* (mutated luminal yeast carboxypeptidase ycsY) in yeast (Plemper et al., 1997). However, real-time fluorescence-based detection shows that blockage of Sec61 has no effect on in vitro reconstituted substrate retrotranslocation (Wahlman et al., 2007). Hence, more studies are needed to establish the function of Sec61 in ERAD.

Transmembrane Derlin-1/VIMP complex has been shown to associate with both misfolded polypeptides and p97 (Ye et al., 2004) and to be indispensable for retro-translocation of mutant α-1 antitrypsin (Greenblatt et al., 2011). This idea that Derlin-1 is the dislocation channel in ERAD machinery is also supported by the real-time assay detecting in vitro retrotranslocation (Wahlman et al., 2007). Deletion of Derlin-1 causes misfolded protein accumulation and thus leads to ER stress (Ye et al., 2004).

Substrate dislocation is facilitated by the AAA (ATPases Associated with diverse cellular Activities) ATPase p97, its yeast homolog cdc48, as well as their binding partners UFD1 and NPL4 in the cytosol (Braun et al., 2002). Cdc48/p97 complex binds both ubiquitinated and non-ubiquitinated substrates in an ATP dependent manner. ATP hydrolysis provides energy for the extraction of aberrant polypeptides into the cytosol (Ye et al., 2003).

1.3.3 Core organizers of ERAD – E3 complex

E3 complexes ubiquitinate misfolded substrates, and deliver them to the cytosol for degradation. They are the core organizers defining distinct ERAD pathways. Reported E3s include Hrd1p and Doa10p in yeast, and many more in metazoans, such as HRD1, GP78, TRC8, RMA1 and TEB4. Depending on the topology (luminal protein or transmembrane protein) and the location of lesion (in the luminal, transmembrane or cytosolic domains), substrates can be sorted by adaptors for particular E3 complexes. For example, secretory substrates are mainly targeted to ERAD-L pathway defined by HRD1 in both mammalian and yeast cells (Bernasconi et al., 2010; Christianson et al., 2012). However, the categorization is not always clear-cut, as GP78 is shown to degrade both luminal and transmembrane proteins at equal extents (Christianson et al., 2012).

Among the known E3 complexes, the most well characterized E3 complex is the Hrd1/SEL1L complex, which is evolutionally conserved through yeast to mammals. At the center of this complex is HRD1, the E3 ubiquitin ligase with six transmembrane segments and a cytosolic catalytic ring (Kikkert et al., 2004). Ubiquitination by HRD1 is selectively facilitated by E2 ubiquitin-conjugating enzyme, UBC6e in mammals (Mueller et al., 2008) and Ubc7p in yeast (Bazirgan et al., 2006). Mammalian UBC6e has a transmembrane region and a cytosolic catalytic domain, while in yeast, Ubc7p is a soluble protein in cytosol, and requires ubiquitin binding protein Cue1p for membrane anchoring and full-length ubiquitination (Bagola et al., 2013; Metzger et al., 2013).

The central adaptor in HRD1 E3 complex is SEL1L and its yeast counterpart Hrd3p (Mueller et al., 2006), which nucleate, stabilize and bring ERAD target proteins to the complex. Both SEL1L and Hrd3p are type I ER transmembrane proteins with a large luminal domain and a small proline-rich tail in the cytosol (Biunno et al., 2006). The luminal domain contains multiple tetratricopeptide repeats, a feature commonly found on interaction hubs for assembly of macromolecular complexes (Mittl and Schneider-Brachert, 2007). SEL1L nucleates the whole complex by interacting with multiple ERAD components including HRD1, Derlin1/2, p97, OS-9, XTP3-B, ancient ubiquitous protein 1 (AUP1), UBXD8 and several housekeeping chaperones (Christianson et al., 2012; Mueller et al., 2006; 2008). Dramatic decrease of Hrd1p protein is resulted from Hrd3p deletion in yeast (Gardner et al., 2000) while mammalian HRD1 in SEL1Li (RNAi) cells skews to smaller fractions in sucrose gradient assay (Iida et al., 2011). Vice versa, silencing HRD1 rapidly reduces mammalian SEL1L (Iida et al., 2011). These findings together point out the fact that SEL1L and HRD1 critically optimize the stability of the ERAD complex. As the substrate loading dock for HRD1 ubiquitination, SEL1L/Hrd3p recruits misfolded proteins by binding to lectins such as mammalian OS-9 and XTP3-B (Christianson et al., 2008) and yeast Yos9p (Gauss et al., 2006a). Direct binding of ERAD targets by SEL1L/Hrd3p is also possible. For instance, N-terminal fraction of Hrd3p interacts with CPY* connecting it to membrane-associated Cdc48p (Gauss et al., 2006b). Interestingly, SEL1L is heavily glycosylated on its luminal domain. This modification may be necessary for its binding to lectin adaptors OS-9, XTP3-B as well as mannosidase EDEM1 (Cormier et al., 2009).

1.3.4 Physiological significance of ERAD

ERAD eliminates the misfolded proteins preventing them from forming potentially toxic aggregation. Various knockout mouse models have demonstrated the physiological importance of ERAD as housekeeping machinery. Deletion of HRD1, SEL1L or VCP/p97 causes embryonic lethality (Francisco et al., 2010; Müller et al., 2007; Yagishita et al., 2005). Remarkably, only SEL1L but not HRD1 null embryos showed retarded growth, suggesting HRD1-independent roles of SEL1L in development (Francisco et al., 2010; Yagishita et al., 2005). On the other hand, knockout of different Derlin family members results in various outcomes: Derlin-1 deficiency is embryonic lethal, Derlin-2 deficiency impairs protein dislocation in chondrocytes, while Derlin-3 deficient mice appear normal (Dougan et al., 2011; Eura et al., 2012).

Animals with conditional knockout or genetic mutations were generated and examined to understand tissue-specific ERAD functions related to human diseases. The importance of SEL1L in pancreas is not only demonstrated by the developmental blockage of embryonic pancreatic epithelial cells in SEL1L-/- mice, but also proved by the observation that haploid insufficiency of SEL1L predisposes mice to β-cell degeneration and insulin deficiency upon high-fat diet (Francisco et al., 2011; Li et al., 2010b). R155H or A232E mutations on VCP/p97 cause pathology in muscle, brain and bones in mice, fully resembling syndromes of human IBMPFD (inclusion body myopathy associated with Paget's disease of bone and frontotemporal dementia) (Custer et al., 2010). In nature, progressive loss of ERAD occurs with aging, contributing to pathogenic protein accumulation and organ dysfunction. In the nerve system, E3 enzyme HRD1 degrades

amyloid precursor protein to prevent APP aggresome formation-mediated neuron apoptosis. Significant decrease of HRD1 is detected in patients' brain neurons, which likely initiates pathogenesis of Alzheimer's disease (AD) (Kaneko et al., 2010). The animal and human studies establish the biological significance of ERAD pathway in physiological and pathological context, particularly in the tissues with high protein synthesis rates, or cells expressing error-prone polypeptides. Hence, it is not surprising that high levels of ERAD components such as SEL1L are detected in secretory organs such as salivary tissues, colon, stomach and pancreas (Biunno et al., 2006).

Despite the protective effect on normal cells, ERAD may also be involved in carcinogenesis. In vitro experiments reveal two novel SEL1L variants, p28 and p38, secreted by human breast cancer cells in response to ER stress. The functional relevance of the new variants remains unclear (Cattaneo et al., 2011). Analysis of human pancreatic adenocarcinoma and breast cancer suggests a negative correlation between SEL1L levels and tumor outcomes (Cattaneo et al., 2003; Orlandi et al., 2002). Overexpression of SEL1L dramatically reduces proliferation and anchorage-independent colony formation of breast cancer cells, implicating that SEL1L may inhibit tumor transition (Orlandi et al., 2002). On the contrary, proteasome inhibitors blocking the downstream of ERAD trigger myeloma cell apoptosis, and thus have been proposed as potential anti-cancer drugs. More loss-of- and gain-of-function studies are needed for the comprehensive understanding of individual ERAD players in tumorgenesis and treatment before they can be aimed as therapeutic targets and/or diagnostic markers.

1.4 UNFOLDED PROTEIN RESPONSE

The Unfolded Protein Response (UPR) is the collection of signaling cascades that communicate ER with other cellular organelles when accumulated misfolded protein causes ER stress. Thus it is also termed as ER stress response (Fig. 1.1). Mammalian UPR is mainly initiated by three ER stress sensors, IRE1α (Inositol-requiring enzyme 1 α), PERK (PKR-like endoplasmic reticulum kinase) and ATF6 (Activating transcription factor 6). The sensors initiate downstream transcriptional, translational and post-translational events to reduce nascent peptide loading, increase folding machinery and degrade misfolded proteins. IRE1α and PERK are type I transmembrane proteins with kinase activities for both autophosphorylation and phosphorylation of downstream targets. In addition, IRE1α has an RNase domain adjacent to its kinase domain to promote synthesis of a key transcription factor XBP1s, which exhibits mainly pro-survival functions by transcriptionally increasing the UPR genes. The third member ATF6 is a type II transmembrane-anchored transcription factor, upregulating the UPR genes synergistically with XBP1s (Walter and Ron, 2011). Short-term activation of these pathways has been implicated as an adaptive response, which protects cells against acute or mild stress. However, prolonged UPR activation induces apoptosis under severe stress conditions (Tabas and Ron, 2011). Mechanistic and physiological details of each pathway will be discussed below.

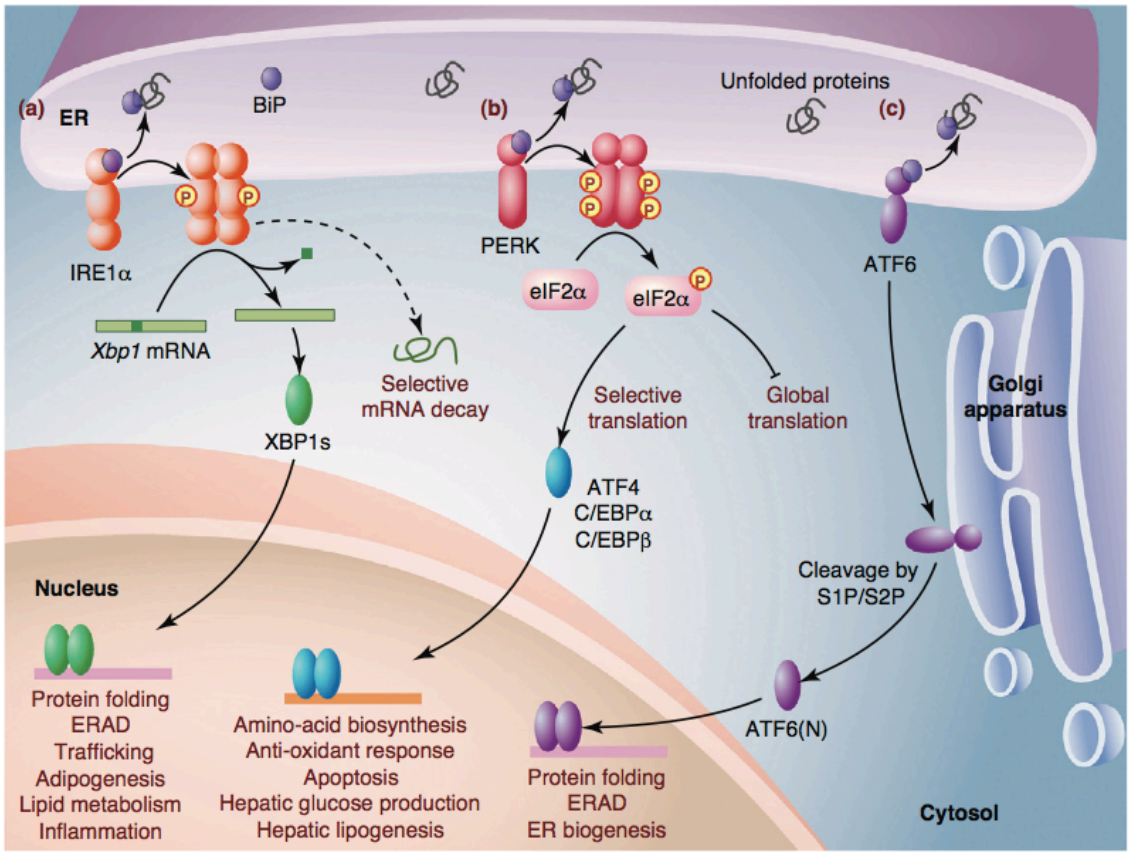

Figure 1.1 Three major UPR pathways in mammals are shown. Homeostatic alterations in the ER result in the accumulation of unfolded or misfolded proteins, and these induce dissociation of BiP and subsequently permit activation of three ER membrane sensors: IRE1a, PERK and ATF6. (a) IRE1a undergoes dimerization or oligomerization, and trans-autophosphorylation, activating its cytosolic endoRNase activity. IRE1a then removes a 26-base intron from Xbp1 mRNA to generate a potent transcription factor XBP1s (XBP1 spliced) that translocates into the nucleus and regulates a diverse array of genes. In addition, activated IRE1a could selectively degrade particular mRNAs. (b) Activated PERK phosphorylates Ser51 on the translation initiation factor eIF2a to attenuate global translation, but also preferentially upregulates the translation of selected mRNAs including ATF4, C/EBPa, and C/EBPb. ATF4 activates the expression of the

UPR target genes involved in amino acid biosynthesis, the anti-oxidant response, and apoptosis, whereas C/EBPa and C/EBPb activate genes regulating glucose production and lipogenesis in the liver. (c) Activated ATF6 translocates to the Golgi, where it is cleaved by the proteases S1P/S2P, yielding the mature transcription factor ATF6(N), which then activates the transcription of the UPR target genes. (Adopted from Sha, H., He, Y., **Yang, L.** and Qi, L. (2011) Stressed out about obesity: IRE1α-XBP1 in metabolic disorders. Trends Endocrinol Metab *22*, 374–381)

1.4.1 IRE1 PATHWAY

Overview of IRE1

Inositol-requiring enzyme 1 (IRE1) initiates the most evolutionally conserved branch out of the three UPR pathways. Ire1p was first identified as an indispensable gene for yeast growth on inositol-deficient medium (Nikawa and Yamashita, 1992). It is a transmembrane kinase critical for transcriptional induction of ER-resident protein genes, such as *KAR2* and *PDI1* (Cox et al., 1993; Mori et al., 1993). Later, the Walter group discovered that Ire1p also contained site-specific endonuclease activity to splice *HAC1* mRNA in collaboration with tRNA ligase. The spliced *HAC1* mRNA encodes a basic-leucine zipper (bZIP) transcription factor, Hac1p which is the master regulator of Ire1p-induced ER-resident chaperones under ER stress (Cox and Walter, 1996; Sidrauski and Walter, 1997; Sidrauski et al., 1996).

In mammalian cells, researchers have identified two isoforms of IRE1- IRE1α and IRE1β, both of which display kinase and RNase domains highly conserved to yeast Ire1p. The splicing target for mammalian IRE1 is *Xbp1*, the ortholog of yeast *HAC1* gene. Interestingly, IRE1α also splices yeast *HAC1* mRNA in vitro, demonstrating the structural and functional conservativeness of this protein(Tirasophon et al., 2000; 1998). IRE1α is universally found in almost all mammalian tissues while IRE1β is uniquely expressed in gut epithelial cells (Bertolotti et al., 2001). Meanwhile, mammalian counterpart of the tRNA ligase has not been found yet. However, in vitro exon-exon ligation of mammalian *XBP1* mRNA can be achieved by adding yeast and amphioxus

tRNA ligases, suggesting similar ligation mechanism may be applied in mammals (Iwawaki and Tokuda, 2011).

Current work regarding to IRE1 pathway mainly focuses on IRE1α. IRE1α is a type I transmembrane protein consisted of a luminal fraction, a 20 amino acid transmembrane segment and a cytosolic domain with non-conventional RNase activity and kinase activity. It is the most well characterized UPR sensor. Currently major theories on IRE1α activation include binding of misfolded proteins to the grooves formed by dimer luminal domains, disassociation of inhibitory chaperone BIP, and composition changes of ER membrane lipid content. Upon activation, the IRE1α RNase domain cleaves its cytosolic mRNA targets for either targeted upregulation of the transcription factor XBP1s or downregulation of nascent peptide loading into the ER. In specialized conditions, the kinase domain may phosphorylate associating adaptors and kinases, branching out to modulate various stress response pathways.

Mechanisms of IRE1 activation

In the past decade, researchers have been interested in mapping out the detailed mechanisms by which Ire1/IRE1α is activated by ER stress and/or other physiological and pathological stimuli. In vitro studies and crystal structure analyses have greatly advanced our understanding of how different domains of IRE1α sense the surrounding misfolded proteins, and/or contribute to its activation.

It is natural to believe that the Ire1p/IRE1α luminal domain exposed directly to the misfolded/unfolded peptides plays a key role in initiating the kinase and RNase activities on the cytosolic side. Crystal structure of yeast Ire1 core luminal domains shows that Ire1 luminal domains form dimers, together to create a central groove reminiscent of the peptide binding groove on the major histocompatibility complex (MHC) (Credle et al., 2005). In vitro experiments demonstrate that an endogenous misfolded ER protein CYP* as well as synthesized basic and hydrophobic peptides directly bind into the Ire1p core luminal domains and activate the UPR signaling, which provide direct evidence for the peptide-binding model (Gardner and Walter, 2011). However, crystal structure of human IRE1α raises questions against the application of direct binding model in mammalian cells, as the diameter of luminal groove formed by human IRE1α is too narrow to accommodate amino acid chains (Zhou et al., 2006).

BIP-binding model was brought up by the analysis of the IRE1α linker region, which reveals dynamic BIP binding to an IRE1α luminal site next to the dimerization domain (Bertolotti et al., 2000). In this model, BIP associates with IRE1α under basal conditions to inhibit its activation. Under ER stress condition, misfolded proteins compete with IRE1α for BIP association. The resulting depletion of BIP from IRE1α allows IRE1α luminal domain dimerization and/or oligomerization as well as its subsequent activation (Bertolotti et al., 2000). However, a mutant Ire1p, Ire1^{bipless} lacking the BIP binding segment, can still form oligomers and splice *HAC1* mRNA, suggesting that BIP binding is not required for the responsiveness of yeast Ire1p to ER stress. Instead, elevated basal foci formation and delayed deactivation of Ire1^{bipless} after drug washout are observed,

comparing to wild type Ire1. Hence, it is more likely that the association of BIP raises the threshold of IRE1α activation by sequestering inactive Ire1 molecules and preventing oligomerization, rather than directly modulating its activity (Pincus et al., 2010).

Regardless, following the direct or indirect initiation by misfolded proteins are IRE1 trans-autophosphorylation and dimerization/oligomerization. The occurring orders for the two events are not full appreciated yet. Transient dimer/oligomers may be stabilized by misfolded protein bindings, allowing subsequential trans-autophosphorylation on the adjacent IRE1α activation loops (Ali et al., 2011). Phosphorylation on the activation loop in turn leads to conformational changes of IRE1α cytosolic domains, further boosting oligomer formation and splicing. The IRE1 oligomerization in both yeast and mammals has been demonstrated by various methodologies including crystal structure analysis (Korennykh et al., 2009), sucrose gradient centrifugation (He et al., 2012; Hetz et al., 2006), native SDS-PAGE (Hetz et al., 2006; Liu et al., 2002) and direct observation of fluorescent-IRE1α cluster formation (Kimata et al., 2007; Li et al., 2010a), and is shown to be critical for full IRE1 activation. However, it is likely that dimer rather than the oligomer is the basic functional unit, as loss of foci formation only delays but does not block the downstream UPR signaling (He et al., 2012).

Besides misfolded protein binding and BIP binding models, lipid content change is another potential mechanism to activate IRE1α and other UPR sensors. The lipid content model has attracted great attention, as UPR has been frequently linked to lipid dysregulation in metabolic diseases such as obesity, diabetes and atherosclerosis (Fu et

al., 2011; Ozcan et al., 2004; 2006). Manipulation of lipid composition, particularly increasing the lipid saturation level in ER has been shown to activate IRE1, in both yeast and mammalian cells, which can be alleviated by adding various unsaturated lipids (Ariyama et al., 2010; Pineau et al., 2009). The fact that the chemical chaperone 4-phenyl butyrate (4-PBA) attenuates saturated the lipid-induced UPR suggests that misfolded protein accumulation is the direct reason for the UPR activation. Increased saturated fat in the ER likely disrupts calcium homeostasis, impairs functions of calcium-binding chaperones, and thus causes accumulation of misfolded proteins (Fu et al., 2011). A similar mechanism has also been proposed to mediate the cholesterol-induced UPR (Feng et al., 2003). Interestingly, an in vitro study using IRE1α mutant lacking its luminal domain demonstrates that IRE1α activation by ER lipid saturation level can be solely attributed to its transmembrane domain, implicating that IRE1α can directly sense lipid composition on the ER membrane (Volmer et al., 2013).

Fine-tuning of IRE1 activation by interacting protein adaptors

IRE1α activation is a highly regulated process which can be much more complicated than the models presented above. In fact, IRE1α activation can be facilitated or suppressed by multiple ancillary components on the cytosolic side in addition to the ER-derived signals. The repertoire of IRE1α fine-tuning adaptors, collectively named IRE1α interactome, may vary in different tissues and modulate IRE1α activation in tissue- and/or stimulus-specific manners.

Studies in cell culture models reveal several positive IRE1α regulators, such as BH3-only proteins PUMA and BIM (Rodriguez et al., 2012), and BCL-2 family members BAX and BAD (Hetz et al., 2006), physically interacting with IRE1α cytosolic domains. Knockout or knockdown of these cofactors impairs IRE1α activation in response to pharmacological ER stress. Recently, our lab identified the non-muscle myosin heavy chain IIB (NMHCIIB) as a novel IRE1α interacting protein, necessary for IRE1α foci formation and full induction of XBP1s (He et al., 2012). Interaction of NMHCIIB as well as other cytoskeleton related proteins (unpublished data) suggest a possible role for the cytoskeleton system and motor proteins in the regulation of IRE1α under ER stress. Negative regulators of IRE1α have also been identified. An ER-resident protein BAX inhibitor-1 (BI-1) forms a stable complex with IRE1α and suppresses IRE1α-XBP1 pathway in fly and mouse models (Castillo et al., 2011; Lisbona et al., 2009). ERAD component ubiquitin specific protease (USP) 14 binds the cytosolic region of inactive IRE1α, preventing its activation by ER stress (Nagai et al., 2009). Scaffold protein RACK1 (receptor for activated C-kinase) mediates complex formation between IRE1α and protein phosphatase 2A (PP2A), promoting dephosphorylation and inactivation of IRE1α in β cells upon prolonged glucose or ER stress stimulations (Qiu et al., 2010). These inhibitory adaptors together with BIP desensitize or deactivate IRE1α, eliminating unnecessary activation when the stress is mild or removed.

In addition to protein modulators, small compounds may facilitate IRE1α activation as well. A study by the Ron group showed that flavonol quercetin bound to the pocket of the dimer interface formed by yeast Ire1 kinase-RNase domains, potentiated Ire1p RNase

activity in response to ADP (Wiseman et al., 2010). The effect is likely due to enhanced dimerization rather than oligomerization upon compound binding. Even though quercetin is derived from plant, this study opens up the possibility that endogenous mammalian metabolites may interact and activate/potentiate IRE1α under metabolic stresses.

Activation of IRE1 leads to XBP1 splicing and folding capacity induction for adaptation

Activated IRE1 signals ER stress to the nucleus by splicing mRNA of a key UPR transcriptional factor *Xbp1* in metazoans and *HAC1* (*Xbp1* ortholog) in yeast in a spliceosome independent manner. In yeast, the intron of *HAC1* mRNA pairs with 5' UTR forming secondary structure that hinges translation elongation (Rüegsegger et al., 2001). Ire1p RNase domain cleaves both *HAC1u* 5' and 3' splice junctions at the conserved G of the seven-residue stem-loop, to release the 252-nucleotide intron (Sidrauski and Walter, 1997). After removal of the intron, the two adjacent exon fragments are ligated by tRNA ligase Rlg1, yielding a mature *HAC1i* mRNA, which can be translated into a functional transcription factor upregulating the entire yeast UPR transcriptome (Sidrauski et al., 1996).

In metazoans, IRE1α splices 26 nucleotides from the *Xbp1u* mRNA to generate the spliced form - *Xbp1s*, causing a frame shift to avoid the premature stop codon, and producing a stable bZIP transcription factor with DNA binding domain (DBD) and transactivation domain (TAD) (Yoshida et al., 2001). Overall XBP1s positively

influences transcription as an activator. Its activity can be positively or negatively affected by various post-translational modulations. Disruption of PI3K subunits p85α and p85β by insulin signaling promotes interaction between XBP1s and p85α/ p85β. Binding of p85α/β enhances nuclear translocation of XBP1s, and thus increases XBP1s-mediated transcriptional activation (Park et al., 2010; Winnay et al., 2010). On the other hand, XBP1s can be SUMOylated by PIAS2 (protein inhibitor of activated STAT 2). Addition of small ubiquitin-like modifiers (SUMOylation) on two lysine residues of XBP1s transactivation domain downregulates its transcriptional activity (Chen and Qi, 2010). In addition, *Xbp1* mRNA (*Xbp1u*) can be constitutively translated to an incomplete transcription factor lacking the last fraction of TAD. XBP1u has a very short half-life and reduce XBP1s protein level by forming degradation-prone complex with XBP1s (Yoshida et al., 2006).

The major downstream targets of XBP1s include ER-resident chaperones and foldases, lipid synthesis enzymes and ERAD components. These genes synergistically assist folding processes, increase ER capacity and enhance degradation of misfolded protein, together functioning as adaptation to restore ER homeostasis and promote cell survival(Walter and Ron, 2011). However, recent studies also indicate that a high level of XBP1s may be pro-apoptotic and detrimental to cell survival (Allagnat et al., 2010; Zeng et al., 2009).

Activation of IRE1 leads to RIDD

Recent work has uncovered more substrates for IRE1α endonuclease domain. Unlike XBP1, cleavage of these ER associated mRNA by IRE1α doesn't produce functional protein; rather contribute to the reduction of peptide loading into ER. This non-specific decay of ER cargo mRNA termed as regulated IRE1α dependent degradation (RIDD) was fist discovered in drosophila S2 cells, where in response to DTT, a subset of mRNA get degraded by IRE1α endonuclease activity depending on their ER localization and amino acid sequence. (Hollien and Weissman, 2006). Later, similar phenomena were observed in mammalian cells, likely in a cell- or tissue specific manner (Hollien et al., 2009; Lipson et al., 2008; Oikawa et al., 2007; Tirasophon et al., 2000). RIDD has been shown to degrade CD59 in Hela cells (Oikawa et al., 2007), insulin transcript in pancreatic β cells (Lipson et al., 2008) and mRNA of itself as feedback control in COS-1 cells (Tirasophon et al., 2000). A sequence consensus CUGCAG has been proposed as a common substrate recognition and cleavage motif for both *Xbp1* mRNA splicing and RIDD (Oikawa et al., 2010).

Mechanistically, RIDD and *Xbp1* splicing seem to be differentially regulated. Forced activation of IRE1α RNase domain by ATP analogue circumventing ER stress results in only *Xbp1* splicing but not decay of other mRNA substrates (Hollien et al., 2009). The alternate endoribonuclease outcomes may depend on different IRE1α kinase activation modes (Han et al., 2009). Besides ER cargo reduction, RIDD can degrade mRNA for pro-survival chaperones, which complicates the physiological significance of IRE1α

activation, and raises the question whether prolonged IRE1α RNase activity also contributes to apoptosis under stressed conditions (Han et al., 2009).

Activation of IRE1 initiates multiple signaling pathways through its interactome

Interactome of IRE1α not only fine-tunes its activity but also diversify its physiological outputs. Activated IRE1α crosstalks to a variety of kinases involving in alarm signaling pathways such as JNK/ASK1 (Nishitoh et al., 2002; Urano et al., 2000), MAPK kinases p44 (ERK) and p38(Nguyên et al., 2004). Adaptor protein TRAF2 binds IRE1α cytosolic domain coupling IRE1α signaling with ASK1 (apoptosis signal-regulating kinase 1) (Nishitoh et al., 2002) and JNK (cJun-N terminal kinase) activation (Urano et al., 2000). In vitro and vivo evidences suggest versatile outcomes of IRE1α-JNK signaling pathway: JNK activation by IRE1α controls ER-stress induced autophagy and apoptosis in cell model, and suppresses insulin receptor substrate (IRS) to in part mediate insulin resistance in obese animals (Ozcan et al., 2009; 2004; Urano et al., 2000). The IRE1α-TRAF2-ASK1 axis seems to be required for ER-stress caused JNK activation and neuron cell death in polyglutamine aggregation-induced human neurodegenerative disorders (Nishitoh et al., 2002). In addition, IRE1α leads to IκB kinase (IKK) activation, which promotes phosphorylation, disassociation and degradation of NfκB repressor IκB (Hu et al., 2006). Both JNK and IKK-NfκB pathways may promote IRE1α-induced inflammatory responses via upregulating an array of inflammatory genes as an alternative result of IRE1α activation in addition to XBP1s-mediated ER expansion (microarray data in our lab). Besides the above examples, interactomic screening in our and other labs revealed far more interacting proteins with various known or possible functions. The

biological significance of these adaptor proteins requests further investigation, which will enhance our understanding of both mechanistic and physiological aspects of the UPR sensor IRE1α.

1.4.2 PERK PATHWAY

PERK is a metazoan type I transmembrane ER-resident protein with kinase activity on its cytosolic fraction. PERK luminal region shows structural similarity in despite of limited sequence homology to IRE1α. In addition, a BIP binding domain and a dimerization interface are also found in the luminal fragment of PERK (Bertolotti et al., 2000; Ma et al., 2002). Thus it has been proposed that BIP prevents PERK dimerization/oligomerization, and retains monomeric PERK in an inactive status in a similar manner as it desensitizes IRE1α. This hypothesis is supported by the fact that luminal domains of IRE1α and PERK are shown to be inter-switchable without disrupting their sensibility to ER stress (Liu et al., 2000). However, whether PERK luminal dimer also directly binds to misfolded ER protein is still unknown.

Following activation by misfolded proteins are PERK oligomerization and trans-autophosphorylation on its activation loop. Phosphorylation on the loop enhances affinity of PERK with its kinase target eIF2α (Marciniak et al., 2006). Activated PERK regulates protein translation by directly phosphorylating eukaryotic translation initiation factor 2 α (eIF2α) on its serine 51 residue (Harding et al., 1999). Phosphorylation of eIF2α by PERK attenuates global protein translation, to reduce ER burden and promote survival under ER stress conditions (Harding et al., 2000; Scheuner et al., 2001; Yan et al., 2002).

Moreover, phosphorylated eIF2α enhances translation of selective proteins in despite of a general inhibitory effect. The most well characterized protein produced by this mechanism is ATF4 (Activating transcription factor 4), whose 5' UTR contains two extra untranslated open reading frame (uORF). Ribosome scanning starts at the first uORF (uORF1), efficiently proceeds to the inhibitory second uORF (uORF2) and thus preclude translation of ATF4 under non-stressed condition. ER-stress induced phosphorylation on eIF2α delays ribosome re-initiation favoring translation start site at ATF4 over uORF2 after scanning uORF1 (Lu et al., 2004a).

ATF4 results in upregulation of additional transcription factors such as ATF3 (Activating transcription factor 3) and CHOP (C/EBP-homologous protein, also named as GADD153), which together with ATF4 promote expression of genes in the categories of metabolism, inflammation, redox regulation and apoptosis (Jiang et al., 2004; Wek et al., 2006; Whitney et al., 2009) (unpublished data from our lab). Of note, CHOP is a bZIP transcription factor that upregulates pro-apoptotic genes such as carbonic anhydrase VI (CAVI) (Sok et al., 1999), death receptor 5 (DR5) (Yamaguchi and Wang, 2004), Tribbles homolog 3 (TRB2) (Ohoka et al., 2005), and downregulates pro-survival protein BCL2 (Matsumoto et al., 1996; McCullough et al., 2001). It is the first identified and the most well studied pro-death UPR gene under prolonged or severe ER stress.

Activation of PERK-eIF2α pathway can be attenuated at different levels by various mechanisms. eIF2α-ATF3 upregulates GADD34, a substrate-specific regulatory component in a phosphatase complex that dephosphorylates eIF2α as a negative feedback

(Jiang et al., 2004). P58ipk a transcriptional target of XBP1s, interacts with PERK and suppresses its kinase activity during prolonged ER stress (Yan et al., 2002). Signaling pathways triggered by other initiators can also negatively regulate PERK downstream pathways. For example, priming cells with toll-like receptor TLR activators inhibits translation of ATF4, without affecting upstream PERK activation (Woo et al., 2009).

Recent investigations have identified additional PERK targets: PERK phosphorylates NRF2, releases it from sequestration by cytoskeletal anchor, KEAP1 for nuclear translocation. NRF2 functions as a cyto-protective PERK target, as loss of NRF2 impairs cell viability in chronic ER stressed condition(Cullinan et al., 2003). PERK also activates GSK3β (glycogen synthase kinase 3 β) in an eIF2α-independent way to promote degradation of p53, suggesting GSK3β as another direct PERK kinase target (Baltzis et al., 2007). Whether there exist more PERK targets and/or regulatory adaptors remains to be tested. Compared to IRE1α, the relative low level of endogenous PERK expression has been an obstacle for immunoprecipitation-based screening. More efficient immunoprecipitation methods and more sensitive mass-spectrometric tools will greatly assist our understanding of PERK activation and its downstream events.

1.4.3 ATF6 PATHWAY

ATF6 is a type II transmembrane ER stress sensor also added to the UPR family since metazoan cells. Activation of ATF6 depends on regulated intramembranous proteolysis (RIP), a process known to regulate SREBP in cholesterol homeostasis (Ye et al., 2000). The luminal domain of ATF6 is also indispensable for ER stress responses(Chen et al.,

2002a). However, how ATF6 luminal domain senses unfolded proteins is less understood, as its luminal domains shares little homology with its counterparts on IRE1α and PERK. The finding of multiple BIP binding sites provides one explanation of stress sensing: ATF6 is retained in an inactive status in ER by binding of BIP in unchallenged conditions, and translocates to Golgi via transport vesicles upon BIP depletion by misfolded protein (Shen et al., 2002). The ER-to-Golgi transportation is likely directed by two Golgi localization signals (GLSs) on its luminal domain, as ATF6 with only GLS but not BIP binding site is constitutively delivered to Golgi (Shen et al., 2002).

Once in the Golgi apparatus, ATF6 is cleaved by two proteases, site-1 protease (S1P) and site-2 protease (S2P) sequentially to remove its luminal domain and transmembrane anchor respectively (Haze et al., 1999; Ye et al., 2000). The cleavage process releases a 50-kDa N-terminal cytosolic domain of ATF6 (ATF6N) as a b-ZIP Transcription factor. ATF6N migrates into the nucleus and preferentially binds to ER stress-response element (ERSE) featured by the consensus motif CCAAT-N9-CCACG at the promoter regions of the downstream target genes(Yamamoto et al., 2004). One important target for ATF6 is the transcription factor XBP1 (Yoshida et al., 2001), which prefers binding sites with UPR-response element (UPRE, TGACGTGG/A) over ERSE. In addition to their specific binding elements, ATF6 and XBP1s can both interact with ATTGG-N-CCACG, the ERSE-II motif (Yoshida et al., 2001), and together induce ER chaperones and ERAD genes in collaboration with other transcription factors for the recovery of ER homeostasis.

Recent studies have added several ATF6-like ER transmembrane bZIP transcription factors as new members of UPR initiators. Reported novel UPR initiators include Luman, CREBH and OASIS, which share the similar RIP-dependent activation mechanism as ATF6. Luman is stimulated by pharmacological blockage of ER-to-Golgi flux and activates transcription of genes with ERSE consensus (Liang et al., 2006; Raggo et al., 2002). CREBH is a liver-specific transcription factor required for acute phase responses (APR) upon cytokine- and antigen- induced ER stress (Zhang et al., 2006a). OASIS increases BIP and suppresses cell death in astrocytes undergoing ER stress challenge (Kondo et al., 2005). Taken together, the cell type-specific UPR sensors suggest differential UPR pathways optimized for specialized cellular adaptation in response to distinct physiological stimuli.

1.4.4 Physiological and pathological UPR

The unfolded protein response has (UPR) been wildly associated with multiple human diseases such as obesity and diabetes, inflammation, neurodegeneration, and cancer, and is considered to play a causal role in many disease settings. Addressing the mechanisms underlying the UPR activation and its crosstalk with other signaling pathways is of pivot significance for the treatment of these pathological disorders.

UPR in obesity and diabetes

Obesity and diabetes has been an increasing health threat to human society ever since we gradually switch to high-energy food consumption and contemporary life style. The absorption, utilization and synthesis of glucose need to be coordinately regulated by

metabolic tissues such as liver, fat, pancreas, and hypothalamus to achieve glucose homeostasis. Disruption of glucose homeostasis leads to diabetes and damages to various tissues. Abnormality in insulin production, secretion and responsiveness is one of the most prevailing causes for elevated glucose, which can be closely linked to UPR modulation.

In 2004, the study by Hotamisligil group first proposed UPR as the intermediating link to couple obesity and type II diabetes (Ozcan et al., 2004). Ever since then, accumulating evidence has suggested ER stress in metabolic tissues especially liver and adipose tissue as a potential therapeutic target for metabolic disorders. In obese animals, the activation of IRE1α-JNK axis in liver and fat desensitizes insulin receptor by phosphorylating insulin receptor substrate-1 (IRS-1). Loss of XBP1 predisposes mice to high-fat diet induced obesity and glucose intolerance likely due to increased ER stress in metabolic tissues (Ozcan et al., 2004). Oral treatment of chemical chaperones attenuates ER stress in these tissues, and restores insulin sensitivity and glucose homeostasis in ob/ob mice (Ozcan et al., 2006). Interestingly, partial loss of IRE1α-XBP1 downstream target GRP78 protect mice against diet-induced obesity and insulin resistance, which may be due to compensatory ER capacity expansion under adaptive UPR (Ye et al., 2010).

Wolcott-Rallison syndrome (WRS) is an early onset type I diabetic diseases commonly treated with insulin supplementation. Genetic mapping suggests that mutations on PERK gene may be responsible for the manifestations of WRS (Delépine et al., 2000). PERK-eIF2α is required for translational control, protecting pancreatic β cells against heavy ER

burden caused by fast insulin production in large quantity. Several mouse models support the role of PERK-eIF2α pathway in pancreatic development and degeneration: Ser51Ala eIF2α mutant mice die after birth with pancreatic β cell deficiency (Hetz et al., 2006; Scheuner et al., 2001), while PERK-/- mice are born with normal pancreas, but later exhibit gradual pancreatic β cells loss and progressive diabetes (Harding et al., 2001; Zhang et al., 2002). At cellular and molecular level, PERK deficiency causes a remarkable suppression of insulin mRNA, resulting in significant insulin level drop in both pancreas and serum of PERK-deficient animals (Zhang et al., 2006b). Meanwhile, loss of PERK impairs ER protein trafficking and exportation, which leads to enlarged ER and retention of proinsulin (Gupta et al., 2010).

Although the translational regulation by PERK-eIF2α is essential for the ER homeostasis and β cell survival, its prolonged activation under pathological ER stress may cause oxidative stress and cell apoptosis through CHOP induction. Investigations of Chop-/- mice on diabetic backgrounds suggest that compensatory insulin production induces ER stress and PERK-eIF2α-CHOP pathway, which may contribute to the β cell loss at the late stage of type II diabetes (Song et al., 2008). Development of pancreatic β cell and optimal insulin secretion also require IRE1α target XBP1. β cell-specific XBP1 knockout reduces islet area, blocks pro-insulin process and causes hyperglycemia and glucose intolerance. IRE1α is hyperactivated as compensatory feedback for XBP1 deficiency, and cleaves β cell mRNA including *Insulin* mRNA, to partially mediate the insulin insufficiency in β cell-specific XBP1 knockout mice (Lee et al., 2011).

Later studies also reveal significant contribution of UPR into the maintenance of balanced hepatic gluconeogenesis and lipid synthesis. Translational control by PERK-eIF2α pathway is required for perinatal gluconeogenesis. Neonates containing Ser51Ala eIF2α mutant fail to induce hepatic gluconeogenesis gene PEPCK and die from hypoglycemia (Kim et al., 2008; Ron and Walter, 2007; Scheuner et al., 2001). Meanwhile, XBP1 protein is upregulated by carbohydrate consumption to promote key genes in lipogenesis (Lee et al., 2008). Hepatic XBP1 deficiency results in hypocholesterolemia and hypotriglyceridemia (Lee et al., 2008). Contrast to the phenotype in XBP1 deficient mice, liver-specific IRE1α knockout mice develop hepatosteatosis, which can be further aggravated by pharmacological ER stress (Zhang et al., 2011). Phosphorylation of eIF2α promotes lipogenic genes in vitro, whereas attenuation of eIF2α in vivo reduces adipogenic genes in liver, enhances glucose homeostasis and prevents hepatosteatosis (Oyadomari et al., 2008). This finding together with the PERK activation observed in obese mouse liver suggests PERK-eIF2α as the alternative mechanism mediating hepatosteatosis and type II diabetes in addition to the IRE1α-XBP1 pathway (Iwawaki et al., 2004; Ozcan et al., 2004).

In the central nerve system, hypothalamus controls the appetite in response to adipocyte or gut hormones. Leptin is an adipokine acting on a subset of hypothalamic neurons to suppress food intake and increase energy expenditure. UPR activation have been observed in hypothalamus in obese animals, and is associated with diet-induced leptin insensitivity. Genetic or pharmacological manipulation that enhances ER capacity

significantly attenuates ER stress and increases leptin sensitivity in the hypothalamus (Ozcan et al., 2009; Zhang et al., 2008).

UPR in immunity

UPR pathways, especially the IRE1α-XBP1 branch, regulate multiple developmental or differentiation processes in both adaptive and innate immunity. *Xbp1* mRNA is highly expressed in pre-pro-B cells and plasma cells, tightly regulated by B cell specific activator proteins (Reimold et al., 1996). In the XBP-1/RAG-2-/- chimeric mice, XBP1-/- hematopoietic cells develop to B and T lymphocytes successfully. However, XBP1-/- B cells expressed very low levels of immunoglobulin upon in vitro lipopolysaccharide stimulation, and fail to defend against polyoma virus, a B-cell-dependent antigen. Simply overexpressing XBP1 in wild-type B lymphocytes forced B cell to differentiated into plasma cells, evident by the increased plasma cell surface marker Syndecan-1, suggesting XBP1 is not only required but also sufficient for B cell to plasma cell differentiation (Reimold et al., 2001). *Xbp1* mRNA in activated B cells is upregulated by cytokine IL-4 pathway and transcription factor BLIMP-1, and then spliced by IRE1α for functional protein production (Iwakoshi et al., 2003; Lee et al., 2008; Shaffer et al., 2004). The resulting XBP1s protein boosts transcription of genes involved in ER and Golgi secretory pathways, expanding the ER volume and folding apparatus in anticipation for increasing immunoglobulin synthesis in plasma cells (Shaffer et al., 2004). In addition, $XBP1^{fl/fl}$ CD19+/Cre ($XBP1^{CD19}$) conditional knockout mice are generated to advance our understanding of B cell-specific role of XBP1. $XBP1^{CD19}$ mice are protected from chemical-induced lupus, an autoimmune disease, while having normal antibody-specific

memory B cells after immunization (Todd et al., 2009). Loss of IRE1α, the XBP1 upstream regulator, impairs terminal plasma cell differentiation as expected, whereas surprisingly affects hematopoietic stem cell proliferation and early B cell development. IRE1α deficiency results in B cell developmental defect in bone marrow due to dysregulated VDJ recombination factors RAG1/2 and TdT, suggesting broader downstream events other than XBP1 splicing in a cell type specific manner (Zhang et al., 2005).

It was originally proposed that dramatic increase of immunoglobulin synthesis causes ER stress and initiates IRE1α-XBP1 pathway. However, several recent evidences have challenged this hypothesis: 1. XBP-1 induction is differentiation-dependent and remains normal in the mutant B cells without IgM secretion (Hu et al., 2009). 2. A dynamics study shows sequential waves of chaperone induction and ER expansion prior to immunoglobulin synthesis (van Anken et al., 2003). 3. Development of antibody-secreting B cells are independent of the other two UPR branches, PERK and ATF6 pathways, suggesting these two are not activated due to lack of ER stress (Aragon et al., 2012; Gass et al., 2008; Zhang et al., 2005). These studies implicate an alternative model in which XBP1 is programmed to increase at transcriptional level upon differentiation and spliced with unchanged basal IRE1α activity, while the other pathways remain inactive with no overt ER stress. However, differential activation threshold or specialized regulatory interactome may also explain the different requirement among distinct UPR pathways. A more direct monitoring tool of ER stress level will greatly help to clarify this question.

UPR is critical for not only development of adaptive immune system but also the regulation of innate immunity. TLR2 and TLR4 specifically activate IRE1α-XBP1 but not the other two pathways in macrophages. TLRs-triggered XBP1 activation results in a distinct transcriptional profile compared to ER stress-induced transcriptome, and is required for optimal expression of cytokines such as IL-6, IL-1β, TNF and IFN-β (Martinon et al., 2010; Smith et al., 2008; Zeng et al., 2010). In addition, constitutive XBP1 expression is observed in another innate immune cell type - dendritic cells (DCs) and essential for its survival. Both conventional and plasmacytoid DCs decreased in Chimeric mice lacking XBP1, while overexpression of XBP1 rescued the DC cell loss (Iwakoshi et al., 2007). This essential role of XBP1 in innate immune system is conserved in lower species, as C.elegans with a loss-of-function xbp1 mutant exhibit dilated ER and larval lethality when infected with *Pseudomonas aeruginosa* (Richardson et al., 2010). Interestingly, TLR signaling can also negatively regulate the UPR pathways. Pre-engagement of TLR3 and TLR4 directly suppresses ATF4-CHOP in a TRIF-dependent manner but leaves PERK and eIF2α intact (Woo et al., 2009). Although the detailed mechanism remains unclear, this opposite TLR processes on IRE1α and PERK pathways may evolve to prevent CHOP-induced apoptosis while optimize cytokine production through XBP1 induction.

XBP1 variants have been associated with human inflammatory bowel diseases (IBD) as genetic risk factors. Mice with intestinal epithelial cell (IEC)-specific XBP1 deletion spontaneously develop enteritis and are more susceptible to colitis. The phenotypes originate from the role of XBP1 in Paneth cell homeostasis and epithelium in response to

proinflammatory IBD inducers (Kaser et al., 2008). The gastrointestinal IRE1β is also required to protect mice from weight loss and death under dextran sodium sulfate (DSS)-induced colitis. Significant increase of BIP protein in IRE1β-/- mice suggests high levels of ER stress (Bertolotti et al., 2001). However, whether ER stress is the direct mediator of phenotypic changes in IRE1β-/- requires further investigations.

UPR in neuron diseases

Neuronal degenerative diseases are late onset aging-associated diseases usually coupled with disruption of proteostasis (Balch et al., 2008). Increasing evidence implicates that the impaired ERAD and ER stress are common causes for a number of neuron diseases including Parkinson's disease, Alzheimer's disease, amyotrophic lateral sclerosis (ALS), and Huntington's disease (Cornejo and Hetz, 2013; Duennwald and Lindquist, 2008; Holtz and O'Malley, 2003). However whether UPR promotes pathogenic progress or protects cells against diseases is still an open question. Mouse hippocampal cell HT22 primed with low level of ER stress are resistant to oxidative glutamate toxicity, a process believed to trigger neuronal loss by extracellular glutamate. Mechanistically, this cytoprotection protection is mediated by pre-emptive conditional eIF2α phosphorylation (Lu et al., 2004b). Ectopic expression of the IRE1α downstream target XBP1s attenuates dopaminergic neuron cell death and protects mice against chemical-induced Parkinson's disease (Sado et al., 2009). The protective role of XBP1 is also supported by studies of the Alzheimer's disease using taupathies or Aβ-overexpressing fly models (Casas-Tinto et al., 2011; Loewen and Feany, 2010).

On the contrary, neuron-specific XBP1 deletion enhances the degradation of $SOD1^{mut}$ aggregation by lysosome-mediated autophagy pathway, and protects mice against ALS (Hetz et al., 2009). In addition, the IRE1α-ASK1 pathway has been shown to mediate neuron cell death in both SOD1 mutation-related ALS and polyglutamine-induced Huntington's disease (Nishitoh et al., 2002; 2008). Pharmacological ER suppressors have been proposed as potential treatment for ALS (Vaccaro et al., 2013). The controversial results point to a complicated relation between ER stress/UPR and neuron diseases. The UPR pathway may influence clinical outcomes of neuron degeneration in a disease-specific way.

Unlike most neuron diseases originating from genetic or environmental disadvantages, Prion disease is a unique case of neuron dysfunction caused by infectious misfolded protein that transforms normal PrP^{C} to non-degradable pathogenic PrP^{Sc}. Several studies using model systems report ER chaperone induction in prion disease, suggesting occurrence of ER stress and UPR (Hetz et al., 2003; 2005). However, upstream ER stress markers such as phosphorylated PERK and eIF2α are not detected in human prion specimen, and only increase slightly in prion-infected mice (Unterberger et al., 2006). Mice specifically lacking brain XBP1 show normal stress responses upon prion infection and similar levels of neural loss and survival curve compared to WT controls, which rules out the role of XBP1 in prion disease (Hetz et al., 2008). It would be interesting to examine prion infection and pathology in genetic mouse models with deficiency of individual UPR components for a comprehensive picture of the UPR in prion disease.

UPR in cancer

Carcinogenetic progression allows cells escape growth restrictions for fast and unlimited proliferation. The high energy and oxygen demanding for rapid cell growth requires various intracellular and extracellular adaptive changes. One of the growth challenges for tumor cells is to adapt protein synthesis with decreasing environmental disadvantages such as energy deprivation and hypoxia. A Large portion of ER proteins bears glycosylation, which can be affected by carbohydrate insufficiency. Low ATP levels under energy deprivation also limits the chaperone function and thus impairs ER folding capacity. In addition, hypoxia induces oxidative stress, which is another source of ER stress.

It is not surprising that increasing evidence shows abnormal upregulation of UPR or at least partial UPR pathways in tumor cells. The distal pro-survival UPR components – ER chaperones are frequently upregulated in various types of cancer. Induction of chaperones such as GRP78 and GRP94 was detected in human gastric tumor (Song et al., 2001), lung cancer(Tsai et al., 2013), fibroarcoma (Jamora et al., 1996), malignant breast cancer (Fernandez et al., 2000), hepatocarinoma (Shuda et al., 2003) and esophageal adenocarcinomas (Chen et al., 2002b). The master transcription factor XBP1s responsible for ER stress-mediated chaperone induction at the transcription level is found in breast cancer (Gomez et al., 2007; Lacroix and Leclercq, 2004) and lymphoma (Davies et al., 2003; Maestre et al., 2009). Studies also report proximal UPR activation at the sensor level in cancer cells. IRE1α plays a key role in angiogenesis and tumor growth in human glioma (Drogat et al., 2007), while PERK activation by constitutive activated BCR-ABL

tyrosine kinase mediates drug resistance, and thus protects chronic myeloid leukemia against imatinib treatment (Kusio-Kobialka et al., 2012). However, direct evidence is lacking to demonstrate whether the prevalent chaperone induction in tumors is always initiated by ER stress.

Efforts have been made to identify therapeutic drugs targeting to the protective UPR, such as proteasome inhibitors that suppress IRE1α activity and XBP1 production and cause myeloma cell apoptosis (Lee et al., 2003). Furthermore, UPR-targeted drugs can also be used in combination with immunotherapy. Epidermal growth factor (EGF) fused with cytotoxin SubA binds specifically to EGFR (Epidermal growth factor receptor) positive tumor and selectively cleaves GRP78 in glioma. Injection of the fusion protein delays tumor growth in xenograft mice, while the reagent per se can be well tolerated by the animals (Prabhu et al., 2012).

Interestingly, although mild and prolonged UPR are thought to be protective for tumor growth and survival, several therapeutic drugs promote tumor-toxicity by upregulating apoptotic UPR. Nitric oxide-induced glioma cell death is abolished by siRNA knock down of IRE1α (Kim et al., 2010). Fenretinide and bortezomib activate eIF2α-ATF4 signaling pathway which is indispensable for drug effects on neuroblastoma and melanoma cell lines (Armstrong et al., 2010). A recent high throughput screen selected a small molecular that specifically activated the apoptotic branch of the UPR (Flaherty et al., 2012). However what the mechanistic basis differentiates physiological outcomes upon UPR activation (adaptive v.s. apoptotic) in given tumor types remains a mystery.

Quantitative and comprehensive measurement of the UPR activation is needed to pave the foundation for our understanding of UPR pathways in cancer.

1.5 RESEARCH AIMS AND DISSERTATION ORGANIZATION

Countless studies report that the UPR causally associate with the pathogenesis of multiple human conformational diseases and thus are proposed as potential therapeutic targets for medicine development. However, different measuring methods can reach contradictory conclusions on ER stress levels and sources of the UPR activating signals. One of the major unsolved questions resulting in this dilemma is that the broad UPR downstream targets may be initiated not only by ER stress but also by crosstalk from other signaling pathways. In addition, individual UPR branches may have different sensitivity to ER misfolded protein accumulation at the sensor level. How to accurately define and quantitatively measure ER stress and UPR activation levels appears to be an obstacle for deeper understanding of the UPR in human diseases.

Multiple genes are transcriptionally upregulated by UPR transcription factors such as XBP1s, ATF4 and ATF6. Q-PCR has been wildly used to measure the steady-state mRNA levels of these UPR factors, including but not limited to *Bip, p58ipk, Chop, Erdj4*, and *Pdia6*. Commercially available antibodies also provide the convenience to detect the protein levels of these chaperones. However, there are several drawbacks for using UPR downstream targets: first of all, their activation is not none or all. Situations in which only a subset of the UPR transcriptome is upregulated are not uncommon. Conclusions solely based on downstream targets may be misleading depending on the

genes of choices, while microarray may not be experimentally feasible for every specimen. Secondly, the UPR downstream targets are distal outcomes and hardly reflect the levels of ER stress quantitatively. Last but not the least, other signaling pathways unrelated to ER stress or UPR have been shown to induce the UPR targets, such as CHOP induction by insulin and growth factors(Brewer et al., 1997; Miyata et al., 2008), or ATF4 via TLR signaling (Woo et al., 2009). Thus, the downstream targets are not suitable as the sole UPR marker, and better to be displayed with other measurement.

Xbp1 splicing by IRE1α has been another popular hallmark for the UPR activation. PCR products using primers designed around the splicing site are run on a high percentage agarose gel. Loss of 26 nucleotides fastens the migration of spliced *Xbp1s* mRNA and results in the separation from the unspliced form *Xbp1u* (Lin et al., 2007). Alternatively, enzyme digestion can be applied after PCR, as splicing deletes a digestion site for Pst I restriction enzyme on the human and mouse *Xbp1* mRNA. Electrophoresis of digested PCR products yields a large band of *Xbp1s* and two smaller bands of *Xbp1u*, making the separation more obvious (Established by the David Ron lab). The splicing appears to be a good marker more closely related to the occurrence of ER stress, except that it is hard to collect enough mRNA from certain tissues.

The Miura lab generated a transgenic mouse model for in vivo monitoring of ER stress (Iwawaki et al., 2004). The mice express an XBP-1-venus (green fluorescent protein) fusion protein in all tissues, which can be spliced by IRE1α RNase domain upon ER stress. The spliced indicator mRNA produces a florescent fusion protein, indicating the

ER stress levels in different tissues. This model can be of great use to investigate tissue specific ER stress under various physiological and pathological challenges. However, it is restricted for laboratory studies but not for clinical diagnosis.

We believe that the most direct method to determine ER stress is at the UPR sensor level. Phosphorylation and oligomerization are the two events closely coupled with IRE1α and PERK activation. IRE1α oligomerization can be observed as foci under fluorescence microscope. But this process requires overexpression of GFP-tagged protein, which may not fully reflect endogenous situations. Antibodies are available for site-specific phosphorylation of IRE1α and PERK, even though we found the one for IRE1α doesn't always work for endogenous protein. The phospho (Thr980)-PERK antibody from Cell Signaling Technology works very well. However PERK is shown as a smear under severe ER stress triggered by pharmacological reagents, thapsigargin and tunicamycin, suggesting more than one site being phosphorylated. We know little about the ER stress level, which the Thr980 phosphorylation is corresponding to. Slow migration of IRE1α and PERK on SDS-PAGE gels is often used to detect ER stress when phospho-antibodies are not available. However the migration can be too mild to detect, especially under mild physiological ER stress conditions. Thus, developing sensitive and quantitative methods is critical to enhance our understanding of ER stress and UPR in both in vitro and in vivo settings.

This thesis dissertation is centered on the investigation of the physiological ER quality control system, particularly the UPR. Chapter 1 introduces the ER homeostasis, ER stress,

ER quality control machineries such as ERAD and UPR, UPR activation and its significance in conformational diseases. Chapter 2 focuses on the development of a Phos-tag based method to quantitatively detect mild physiological UPR at sensor level in cell culture and mouse models. This method is based on alkoxide-bridged dinuclear metal (Zn^{2+} or Mn^{2+}) embedded in the pockets of acrylamide-pendant Phos-tag molecule (Fig. 1.2). The positively charged metals interact with negatively charged phosphate groups and delay the mobility of phosphorylated proteins (Kinoshita et al. 2006). Salt concentration in the buffer may affect the process of electrophoresis and cause band distortion between adjacent lanes. Therefore, cytosolic HSP90 (Heat Shock Protein 90), which has constant levels of phosphorylation under non-stressed and ER stress conditions, is used to reveal the basal position of each lane. A crosstalk between UPR and metabolic pathways is revealed by using this method and presented in Chapter 3. Chapter 4 presents a conditional ERAD deficient mouse model generated to investigate the tissue-specific influence of ER stress and physiological UPR. Contrast to original expectation, I identify an ER stress-independent role of ERAD in B lymphocyte development. Finally, Chapter 5 summarizes the dissertation research and discusses possible future directions. Chapter 2 and Chapter 3 have been published as on the PLoS ONE (2010) and the Journal of Biological Chemistry (2013) respectively. Chapter 4 will be continued by other lab members and published in the future. In addition to the above projects, I also take advantage of the Phos-tag based method to explore various mechanistic and physiological aspects of the UPR, which results in many interesting insights. These findings are organized into three appendixes: Appendix A discusses proteostasis boundary reset by transcriptional upregulation of XBP1 during plasma cell differentiation with no overt

UPR activation. Appendix B reports a novel IRE1α interacting protein FARP1 discovered in a proteomic screen from the lab. Appendix C presents the physiological oscillation of UPR at both sensor and target levels, picturing circadian patterns of UPR in various important organs.

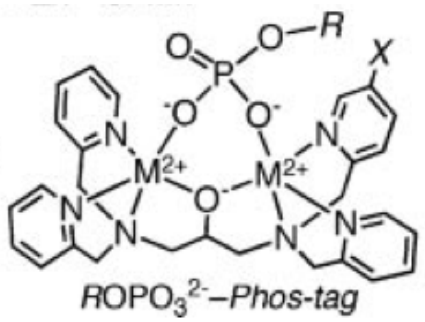

Figure 1.2 Phos-tag molecules and phosphorylated compounds. Phos-tag molecule crosslinks to biotin beads or polyacrylamide gels and reversibly captures phosphorylated compounds, such as phosphorylated proteins.

CHAPTER 2. A PHOS-TAG-BASED APPROACH REVEALS THE EXTENT OF PHYSIOLOGICAL ENDOPLASMIC RETICULUM STRESS

Published as: **Yang, L**., Xue, Z., He, Y., Sun, S., Chen, H., and Qi, L. (2010). A Phos-Tag-Based Approach Reveals the Extent of Physiological Endoplasmic Reticulum Stress. PLoS ONE *5(7): e11621.*

2.1 ABSTRACT

Cellular response to endoplasmic reticulum (ER) stress or unfolded protein response (UPR) is a key defense mechanism associated with many human diseases. Despite its basic and clinical importance, the extent of ER stress inflicted by physiological and pathophysiological conditions remains difficult to quantitate, posing a huge obstacle that has hindered our further understanding of physiological UPR and its future therapeutic potential. Here we have optimized a Phos-tag-based system to detect the activation status of two proximal UPR sensors at the ER membrane. This method allowed for a quantitative assessment of the level of stress in the ER. Our data revealed quantitatively the extent of tissue-specific basal ER stress as well as ER stress caused by the accumulation of misfolded proteins and the fasting-refeeding cycle. Our study may pave the foundation for future studies on physiological UPR, aid in the diagnosis of ER-associated diseases and improve and facilitate therapeutic strategies targeting UPR in vivo.

2.2 INTRODUCTION

ER homeostasis is tightly monitored by ER-to-nucleus signaling cascades termed UPR (Ron and Walter, 2007). Recent studies have linked ER stress and UPR activation to many human diseases including heart complications, neurodegenerative disorders, and metabolic syndrome (Kim et al., 2008; Ron and Walter, 2007). Indeed, chemical chaperones and antioxidants aiming to reduce ER stress and UPR activation have been shown to be effective in mouse models of obesity and type-1 diabetes (Back et al., 2009; Basseri et al., 2009; Malhotra et al., 2008). Despite recent advances, our understanding of UPR activation under physiological conditions is still at its infancy, largely due to the lack of sensitive experimental systems that can detect mild UPR sensor activation.

The underlying mechanisms of UPR signaling and activation induced by chemical drugs such as thapsigargin (Tg) are becoming increasingly well-characterized (Ron and Walter, 2007). Upon ER stress, two key ER-resident transmembrane sensors, inositol-requiring enzyme 1 (IRE1α) and PKR-like ER-kinase (PERK) undergo dimerization or oligomerization and trans-autophosphorylation via their C-terminal kinase domains, leading to their activation (Kim et al., 2008; Ron and Walter, 2007). Phosphorylation of IRE1α and PERK has been challenging, if not impossible, to detect under physiological conditions. The mobility-shift of IRE1α shown in many studies is very subtle and, as demonstrated in this study, may be inaccurate and misleading. In addition, commercially-available phospho-specific antibodies (e.g. P-Ser724A IRE1α and P-Thr980 PERK) do not reflect the overall phosphorylation status of the proteins. Finally, use of these

antibodies, if successful, raises the question as to whether Ser724 of IRE1α or Thr980 of PERK is indeed phosphorylated under various physiological and disease conditions.

Alternatively, many studies have used downstream effectors such as X-box binding protein 1 (XBP1) mRNA splicing, phosphorylation of eukaryotic translation initiation factor 2α (eIF2α), C/EBP homologous protein (CHOP) and various genes involved in protein folding and ER-associated degradation (ERAD) as surrogate markers for UPR activation. This method, albeit convenient, may be confounded by the possibility of integrating signals not directly related to stress in the ER. For example, the PERK pathway of the UPR is part of the integrated stress response that consists of three other eIF2α kinases (Ron and Walter, 2007). Activation of any of these kinases leads to eIF2α phosphorylation and induction of ATF4 and CHOP (Ron and Walter, 2007). A recent study also showed that ATF4 and CHOP can be regulated translationally in a PERK-independent manner via the TLR signaling pathways (Woo et al., 2009). Furthermore, UPR target genes such as CHOP and ER chaperones can be induced by other signals, such as insulin and cytokines/growth factors (Brewer et al., 1997; Miyata et al., 2008). Thus, downstream UPR targets alone are not best suited for accurate assessment and evaluation of UPR status, especially under physiological and disease settings.

Our previous study utilized the Phos-tag-based system (Kinoshita et al., 2006) to detect IRE1α phosphorylation mainly in Tg-treated culture cells (Sha et al., 2009). Here we have further modified the system to maximize the resolution of phosphorylation and extended the system to detect PERK phosphorylation. Strikingly, our system allows for

increased sensitivity in detecting UPR activation and more importantly, accurate quantitation of ER stress. This powerful tool allows us to quantitatively measure the extent of UPR or ER stress induced by various physiological conditions, including (a) the accumulation of misfolded proteins in HEK293T cells, (b) the basal feeding conditions in various adult tissues and (c) the fasting- feeding cycle in the pancreas. Our data reveal that many tissues and cell types constitutively display mild ER stress and more intriguingly, various acute physiological challenges increase ER stress by 2–3 fold over basal levels.

2.3 MATERIALS AND METHODS

Cells and reagents

HEK293T and MEFs as described in (Sha et al., 2009) were maintained in DMEM supplemented with 10% FBS (Hyclone) and 1% penicillin/streptomycin. Tg (EMD Calbiochem) and stock CHX (Sigma) were dissolved in DMSO and ethanol, respectively. Cells were treated with Tg at indicated concentrations for the indicated times and immediately snap-frozen in liquid nitrogen. Phos-tag was purchased from NARD Institute (Japan).

Protein lysates, Western blot and Phos-tag gels

Whole cell or nuclear extraction was performed as we previously described (Chen and Qi, 2010; Sha et al., 2009). Lysate protein concentrations were measured using the Bradford assay (Biorad) and normalized to 0.5~2 μg/μl using SDS sample buffer. Samples were boiled for 5 min prior to loading onto a SDS-PAGE gel. 15–30 μg of

whole cell lysates or 1–10 μg of nuclear extracts were used in a mini SDS-PAGE. Phos-tag gel was modified from our previous report (Sha et al., 2009) with the following running conditions: 100 V for 3 h for IRE1α using 25 μM Phos-tag and 15 mA for 15 min followed by 5 mA for 9.5 h for PERK using 3.5 μM Phos-tag. To achieve optimal results, we always run IRE1α and PERK on separate gels using the following conditions. Membranes were routinely strip- reprobed for 2–4 times. The IRE1α blot in the Phos-tag gel was routinely reprobed with HSP90 (90 kDa vs. 110 kDa IRE1α) as a position control.

Importantly, for both regular and phos-tag gels, gel-running was stopped when the 75 kDa maker ran off the gel and same amounts of lysates were loaded. Therefore, the difference in separating the phosphorylated from the non-phosphorylated species between Phos-tag and regular gels was mainly attributable to the effect of Phos-tag incorporated.

Antibodies for Western blot

GRP78 (goat, 1:1,000), XBP1 (XBP1u/s-specific, rabbit, 1:1,000), CHOP (mouse, 1:500) and HSP90 (rabbit, 1:5,000) were purchased from Santa Cruz; p-eIF2α, eIF2α, IRE1α and (p)-PERK (rabbit) antibodies were purchased from Cell Signaling and used at 1:1,000–2,000. Primary antibodies were diluted in 5% milk/TBST or 2% BSA/TBST and incubated with PVDF membrane overnight at 4°C. Secondary antibodies were goat anti-rabbit IgG HRP, goat anti-mouse IgG HRP (Biorad) and donkey anti-goat IgG HRP (Jackson ImmunoResearch), all of which were used at 1:10,000.

Mice and tissues

Wildtype C57BL/6 mice were purchased from the Jackson Laboratory or bred in our mouse facility. For some experiments, mice were injected with 40 μg CHX per g body weight (dissolved in 100 μl PBS) for 2 h before they were dissected. Epididymal white adipose tissues (WAT) and pancreas were harvested, snap-frozen in liquid nitrogen and stored at -80°C. All animal procedures have been described previously (Qi et al., 2006; 2009) and were approved by the Cornell IACUC (#2007-0051).

Plasmids and transfection

NHK, wildtype and dominant negative E305Q/E578Q p97 (p97-QQ) plasmids were gifts from Qiaoming Long and Fenghua Hu (Cornell University), respectively. HEK293T were transfected with plasmids using polyethylenimine (PEI, Sigma) as we recently described (Chen and Qi, 2010). Cells were snap-frozen in liquid nitrogen 24 h post-transfection followed by Western blot.

Phosphatase treatment

100 μg cell lysates or tissue lysates were incubated with 2.5 μl calf intestinal phosphatase (CIP) or 0.5 μl λ phosphatase (λPPase, New England BioLabs- NEB) in 1X NEB buffer 3 (100 mM NaCl, 50 mM Tris-HCl, 10 mM MgCl2, 1 mM DTT) or 1X PMP buffer (50 mM HEPES, 100 mM NaCl, 2 mM DTT, 0.01% Brij35, NEB) with 1 mM $MnCl_2$ at 37 or 30°C for 45 or 30 min, respectively. Reaction was stopped by adding 5X SDS sample buffer, and the mixture were incubated at 90°C for 5 min.

RNA extraction and Q-PCR

Total mRNA extractions were carried out using a combination of Trizol and RNeasy kit (Qiagen) for pancreas. RNAs were reverse transcribed using Superscript III kit (Invitrogen). For Q- PCR, cDNA was analyzed using the SYBR Green PCR system on the Roche 480 LightCycler (Roche). Reactions using samples with no RT and water were included as negative controls to ensure the specificity of the Q-PCR reaction. All Q-PCR data were normalized to ribosomal l32 gene in the corresponding sample. Primer sequences are listed in Supplementary material Table 2.1.

	Gene	Forward	Reverse
Q-PCR	*Chop*	TATCTCATCCCCAGGAAACG	GGGCACTGACCACTCTGTTT
	Erdj4	CTTAGGTGTGCCAAAGTCTGC	GGCATCCGAGAGTGTTTCATA
	Grp78	TGTGGTACCCACCAAGAAGTC	TTCAGCTGTCACTCGGAGAAT
	Atf4	CGAGATGAGCTTCCTGAACAGC	GGAAAAGGCATCCTCCTTGC
	P58ipk	GTGGCATCCAGATAATTTCCAG	GAGTTCCAACTTCTGTGGAAGG
	L32	GAGCAACAAGAAAACCAAGCA	TGCACACAAGCCATCTACTCA
	Xbp1t, total	ACATCTTCCCATGGACTCTG	TAGGTCCTTCTGGGTAGACC
	Xbp1s, spliced	GAGTCCGCAGCAGGTG	GTGTCAGAGTCCATGGGA

Image quantification

Quantification was performed using the NIH ImageJ software where band densities were calculated and subtracted from the background. Data are represented as mean ± SEM from several independent samples or experiments.

Statistical analysis

Results are expressed as mean ± SEM. Comparisons between groups were made by unpaired two-tailed Student t-test. $P<0.05$ was considered as statistically significant. All experiments were repeated at least twice.

2.4 RESULTS

2.4.1 Visualization of sensor phosphorylation and quantitation of ER stress

We optimized the separation of phosphorylated IRE1α and PERK proteins in a Phos-tag-based Western blot (see Methods section and Figure 2.1). The mobility change of IRE1α and PERK was reversed by phosphatase treatment (Figure 2.2A). Strikingly, IRE1α and PERK hyperphosphorylation patterns were distinct (Figure 2.2A), reflecting various levels of phosphorylation upon activation. Dramatically, p-IRE1α exhibited one discrete slow-migrating band in the Phos-tag gels, a feature that allows for quantitation of the percent of p-IRE1α out of total protein (see below). Upon treatment with Tg, the percent of phosphorylated IRE1α out of total IRE1α protein increased from 30 min post-treatment, peaked around 4 h and slightly decreased at 8–17 h, with nearly 30, 100 and 80% IRE1α phosphorylated, respectively (Figure 2.2B–C). Similarly, PERK hyperphosphorylation increased at 30 min, peaked at 4 h and decreased after 8–17 h. In both cases, the dynamic patterns of IRE1α and PERK phosphorylation were either not discernible or less impressive in regular gels or using the phospho-specific antibody (Figure 1B and D).

The temporal dynamic patterns of IRE1α and PERK phosphorylation as shown above indicate that hyperphosphorylation of UPR sensors correlates with the amount of stress in the ER. Further supporting this notion, hyperphosphorylation of IRE1α and PERK increased with Tg concentrations, peaking and subsequently plateauing at 38 nM Tg upon 4 h treatment (Figure 1E). Demonstrating the sensitivity and quantitative nature of our method, ~15% of IRE1α protein was phosphorylated upon 4 nM Tg treatment and

increased to ~50% under 9 nM Tg (Figure 2.2E–F). In contrast, IRE1α phosphorylation was not visible using a regular gel system and phosphorylation of PERK was also much less impressive (Figure 2.2E). Thus, our method achieves both accuracy and sensitivity in detecting ER stress and UPR activation. We then went on to characterize the extent of ER stress under three physiological conditions.

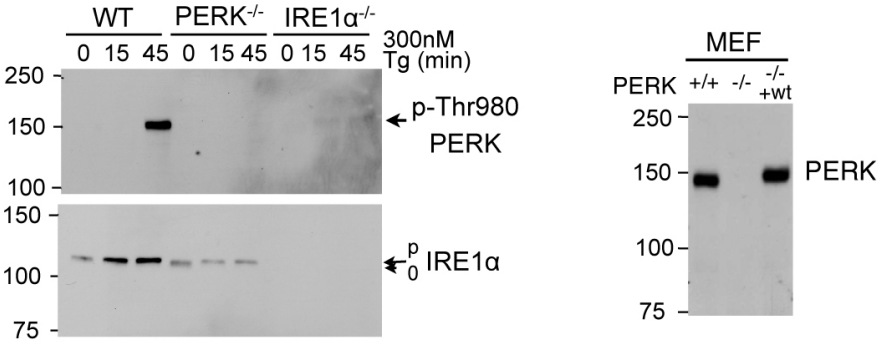

Fig. 2.1 Immunoblots of p-Thr980 PERK, IRE1α (left) and total PERK (right) in different MEFs treated with or without Tg. (left) IRE1α-/- and PERK-/- MEFs were used; (right) wildtype (+/+), PERK-/- (-/-) and PERK-/- MEFs rescued with wildtype PERK (-/- + wt).

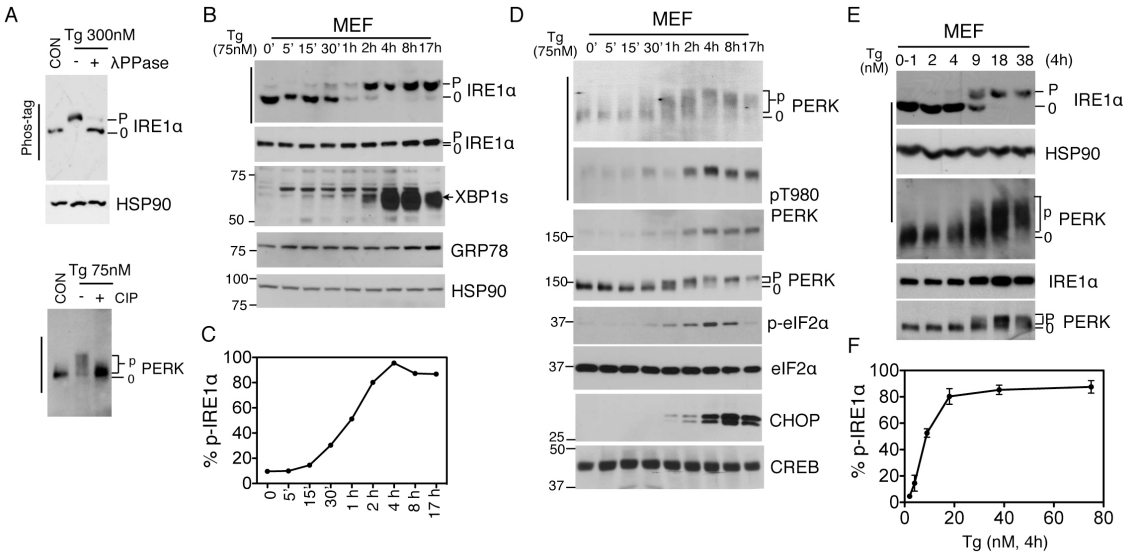

Figure 2.2 Visualization and quantitation of ER stress under pharmacological stress. (A) Immunoblots of IRE1α (upper) and PERK (lower) proteins in Tg-treated MEFs treated with or without λPPase or CIP. (B and D) Immunoblots of IRE1α (B) and PERK (D) using the Phos-tag vs. regular gels. MEFs were treated with 75 nM Tg at indicated period of time. (C) Quantitation of percent of phosphorylated IRE1α in total IRE1α protein in Phos-tag gels shown in B. (E) Immunoblots of IRE1α and PERK in wildtype MEFs treated with Tg at indicated concentrations for 4 h. (F) Quantitation of percent of phosphorylated IRE1α in total IRE1α protein in Phos-tag gels in E. HSP90 and CREB, loading controls. Phos-tag gels are indicated with a bar at the left-hand side. ‘‘0’’ refers to the non- or hypophosphorylated forms of the protein whereas ‘‘p’’ refers to the phosphorylated forms of the protein.

2.4.2 Accumulation of misfolded proteins induces mild ER stress

Although ER stress was initially characterized as induced by accumulation of unfolded proteins (Cox et al., 1993; Kozutsumi et al., 1988; Mori et al., 1993), it remains impossible to quantitate the levels of stress inflicted by accumulation of misfolded proteins in the ER. To this end, we ectopically expressed the terminally-misfolded a1-antitrypsin (AT) genetic variant-null Hong Kong (NHK) (Figure 2.3A), a frequently mutated allele in human a1 AT deficiency (Sifers et al., 1988) or the dominant-negative mutant of p97 (p97- QQ) (Figure 2.3C), a member of the AAA-ATPase protein family involved in ERAD (Ye et al., 2001). In both cases, IRE1α and PERK were phosphorylated when compared to cells overexpressing control or wildtype proteins (Figure 2.3A and C), indicating the specificity of sensor activation in response to misfolded proteins. Interestingly, IRE1α phosphorylation nearly tripled in both cases reaching 20–30% (Figure 2.3B–D). Similar observations were obtained in Sel1L-deficient MEFs (not shown), in which ERAD is defective (Francisco et al., 2010). Thus, our data revealed quantitatively the extent of ER stress induced by accumulation of misfolded proteins in the ER, a finding that was impossible using regular systems under similar running conditions (Figure 2.3A and C).

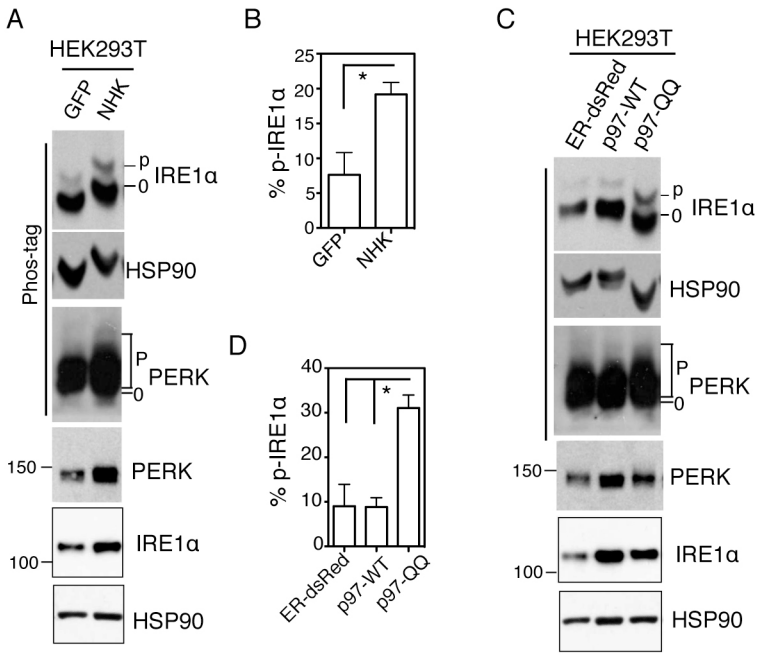

Figure 2.3 Accumulation of misfolded proteins induces mild ER stress. (A and C) Immunoblots of IRE1α and PERK in HEK293T cells transfected with the indicated plasmids for 24 h. NHK, the unfolded form of a1-antitrypsin; p97-QQ, dominant negative form of p97-WT. ER-dsRed and GFP, negative control plasmids. HSP90, a position and loading control. (B and D) Quantitation of percent of phosphorylated IRE1α in total IRE1α protein in Phos-tag gels shown in A, C. Values are mean ± SEM *, $P<0.05$ using unpaired two-tailed Student's t-test. Representative data from at least three independent experiments shown.

2.4.3 Many tissues exhibit basal ER stress under feeding conditions

We then analyzed the levels of basal ER stress in various tissues from adult mice under 2h refeeding after 20h fasting. Intriguingly, many tissues exhibited slower electrophoretic mobility of IRE1α and PERK proteins (Figure 2.4A and 2.5A). The mobility shift of IRE1α and PERK was specific for phosphorylation as it was reversed by phosphatase treatment (Figure 2.4B and 2.5B); importantly, this was caused by signals from the ER as it was attenuated by I.P. injecting the mice with a protein translation inhibitor, cycloheximide (CHX) (Figure 2.4C). Quantitatively, phosphorylated IRE1α accounted for over 40% of total IRE1α protein in the pancreas and ~10% in most of the other tissues (Figure 2.4D). Our data is in line with an early finding in which the XBP1-GFP reporter mice exhibited basal UPR primarily in the pancreas (Iwawaki et al., 2004). Pointing to the complexity of tissue-specific UPR, IRE1α exhibited multiple slower migrating bands and PERK was beyond the detection limit in skeletal muscle (Figure 2.4A and 2.5A). The nature of these slower migrating bands in the IRE1α blot was not due to phosphorylation as they were resistant to phosphatase treatment (Figure 2.5C).

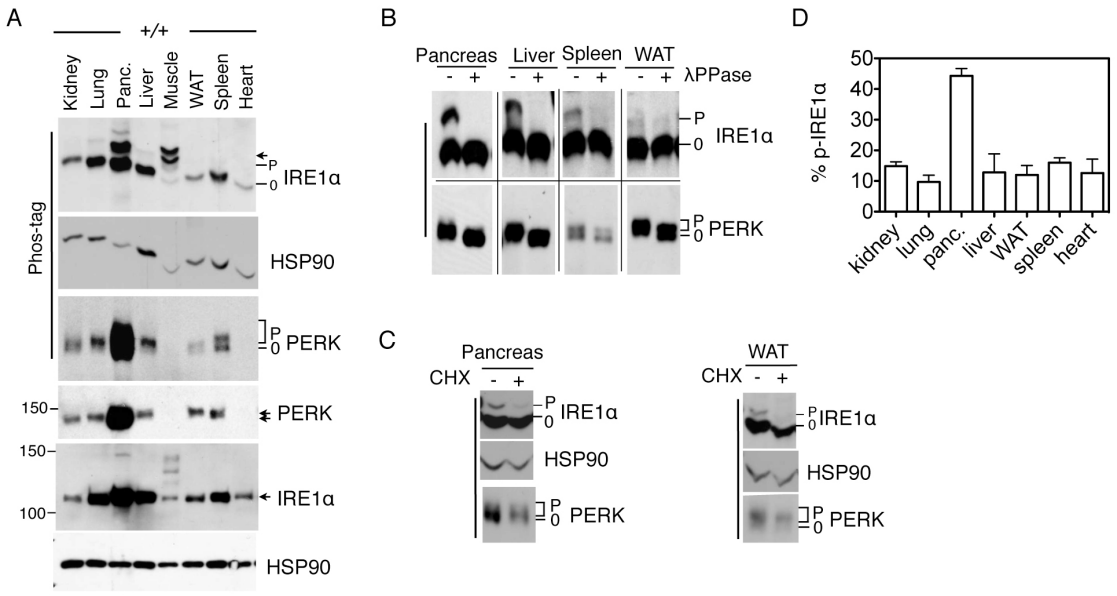

Figure 2.4. Many tissues exhibit basal ER stress under feeding conditions. (A) Immunoblots of IRE1α and PERK in various tissues of wildtype mice. WAT, white adipose tissues; Panc, pancreas; Muscle, gastrocnemius. HSP90, a position and loading control. (B–C) Immunoblots of IRE1α and PERK in tissue lysates treated with λPPase (B) or in pancreatic and WAT lysates prepared from mice injected with CHX (C). (D) Quantitation of percent of phosphorylated IRE1α in total IRE1α protein in various tissues shown in A. Values are mean ± SEM. Representatives of at least two independent experiments shown.

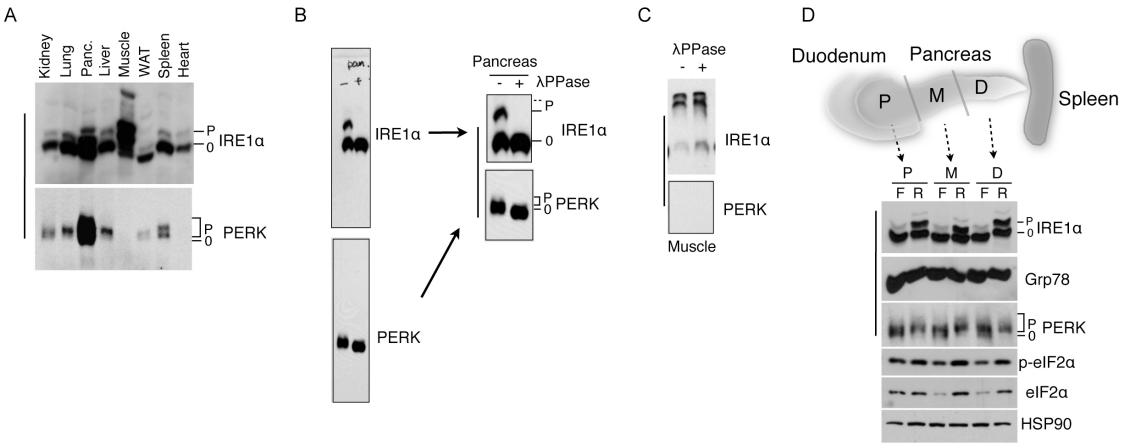

Figure 2.5 (A) Immunoblots of IRE1α (top) and PERK (bottom) in various tissues of wildtype mice under feeding conditions, an independent experiment from the one shown in Fig. 2.4 A. WAT, white adipose tissues; Panc, pancreas; Muscle, gastrocnemius. (B) Original Phos-tag whole-gel images for the data shown in Fig. 2.4B. Note the specificity of the antibody and the complete reverse of phosphorylation upon phosphatase treatment. (C) Immunoblots of IRE1α and PERK in muscle lysates treated with λPPase. The multiple bands of IRE1α in the muscle are not due to hyperphosphorylation and PERK protein levels are beyond detection limit. (D) Immunoblots of IRE1α and PERK in lysates extracted from different regions of the pancreas of 13-week-old wildtype mice under the 20 h-fasting (F) and 2 h-refeeding (R) conditions. The position of the pancreas is relative to the duodenum (proximal, middle or distal) - see the diagram on top. HSP90, a loading control. Phos-tag gels are indicated with a bar at the left-hand side.

2.4.4 Refeeding induces mild ER stress in the pancreas

We then conducted an in-depth analysis of UPR activation during the fasting-refeeding process in the pancreas (20 hr fasting followed by 2 hr feeding). Indeed, refeeding significantly increased phosphorylation of both IRE1α and PERK (percent of p-IRE1α under fasting vs. refeeding: 8.7±4.3% vs. 29.5±5.4%; $P<0.05$) (Figure 2.6A–B). This effect was independent of the region of the pancreas sampled (Figure 2.5D). Supporting the importance of our method in analyzing mild physiological UPR, similar running conditions in regular gels resulted in a much less impressive mobility-shift for PERK (Figure 2.6A). This mild PERK phosphorylation was undetectable using the phospho-PERK antibody (Figure 2.6A). In addition, although comparing to IRE1α from fasted animal tissues, IRE1α did exhibit a slightly slower mobility shift upon refeeding in regular gels after prolonged gel running conditions, this shift did not reflect the overall phosphorylation status of IRE1α as revealed by the Phos-tag gel (Figure 2.6A). Furthermore, phosphorylation of IRE1α, an immediate downstream effector of PERK, did not change (Figure 2.6A). Finally, while some UPR targets such as CHOP, ERDJ4 and P58IPK were induced upon refeeding (Figure 2.6C), both the mRNA and protein levels of Grp78, an ER chaperone, were not altered (Figure 2.6A and C). Thus, our data demonstrated that the fasting- feeding cycle acutely stimulates mild UPR activation in the pancreas.

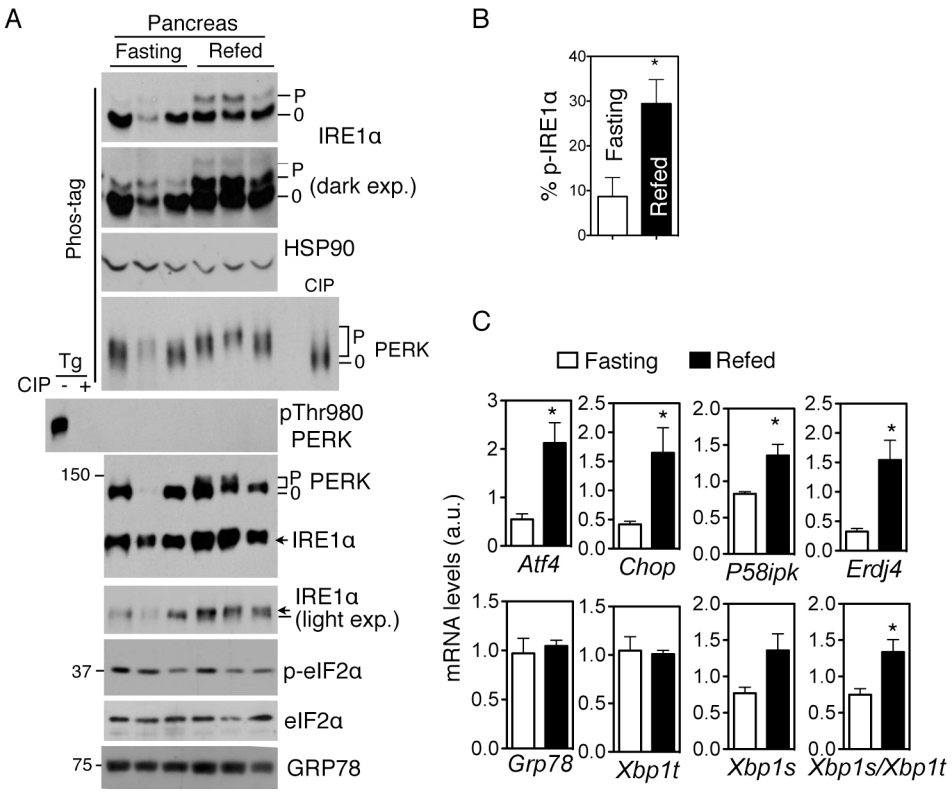

Figure 2.6. Fasting-refeeding induces mild ER stress in pancreas. (A) Immunoblots of lysates from the pancreas of wildtype mice either fasted or fasted followed by 2 h refeeding (refed). For the PERK blot, a mixture of all 6 samples treated with CIP were included as a control. For the p-PERK blot, Tg-treated MEF cell lysates with or without CIP treatment were included as a control. HSP90, a loading control. (B) Quantitation of the percent of phosphorylated IRE1α in pancreas under fasting and refeeding conditions shown in A (N = 4 mice per cohort). (C) Q-PCR analyses of UPR genes in the pancreas under either fasting or refeeding. Values are mean ± SEM. *Xbp1t*, total *Xbp1*; *Xbp1s/Xbp1t*, splicing efficiency. N = 3–4 mice. *, P<0.05 using unpaired two-tailed Student's t-test. Representatives of at least two independent experiments shown.

2.5 DISCUSSION

In summary, we have optimized a sensitive and simple Phos-tag-based system to quantitatively assess ER stress and UPR activation with the following major advantages: First, dynamic ranges of PERK and IRE1α phosphorylation can be more sensitively visualized compared to regular SDS-PAGE gels; this is particularly important for physiological UPR where ER stress can be so mild that traditional methods may no longer be accurate or reliable. Second, the major breakthrough of our method lies in the unique pattern of IRE1α phosphorylation in the Phos-tag gel, which allows for a quantitative assessment of ER stress. To our knowledge, this is the first demonstration of quantitation of ER stress under physiological or pathological settings (e.g. the fasting-refeeding cycle or the accumulation of misfolded proteins). Finally, in comparison to using commercially-available phospho-specific antibodies (e.g. P-Ser724A IRE1α and P-Thr980 PERK), our method not only provides a complete view of the overall phosphorylation status of IRE1α and PERK proteins, but also circumvents the issue of whether these specific residues are indeed phosphorylated under certain physiological conditions.

Our data reveal that many tissues and cell types display constitutive basal UPR activity, presumably to counter misfolded proteins passing through the ER. This observation is in line with an early report demonstrating that under physiological conditions removal of these misfolded proteins in yeast requires coordinated action of UPR and ERAD (Travers et al., 2000). Taking it one step further, our data show that a fraction of mammalian IRE1α and PERK is constitutively active in many tissues, with ~10% IRE1α being

phosphorylated and activated. This low level of IRE1α activation and ER stress in many tissues may provide a plausible explanation for the inability of an earlier study to detect basal UPR in the XBP1s-GFP reporter mice (Iwawaki et al., 2004). We believe that this basal UPR activity, especially the IRE1α-XBP1 branch, is critical in maintaining ER homeostasis and providing quality control as supported by the embryonic lethality of IRE1α and XBP1- deficient mice (Masaki et al., 1999; Reimold et al., 2000; Ron and Walter, 2007; Wu and Kaufman, 2006; Zhang et al., 2005). It is noteworthy that in skeletal muscles, IRE1α exhibited multiple non-phosphorylated bands while PERK protein is beyond the detection limit. As the IRE1α-XBP1 pathway is active in adult skeletal muscles (Iwawaki et al., 2004), the role of UPR in myocytes is an interesting question as it may offer new insights into physiological UPR.

As exocrine pancreatic acinar cells account for over 80% of the pancreatic mass, pancreatic ER stress observed under the fasting- feeding cycle likely reflects the acute elevation of protein synthesis in acinar cells in response to food intake (Morisset and Webster, 1972). Indeed, mice with XBP1 or PERK deficiency exhibit defective development of exocrine pancreas (Harding et al., 2001; Lee et al., 2005; Zhang et al., 2002), suggesting an indispensable role for UPR in countering the fluctuating stress associated with food intake. While UPR is mildly active under fasting presumably to attenuate protein synthesis as previously suggested (Zhang et al., 2002), our data showed a 3-fold increase of IRE1α phosphorylation, i.e. UPR, to enhance ER homeostasis in preparation for an upcoming wave of protein synthesis. Our results are in line with earlier observations demonstrating that ER in pancreatic acinar cells becomes dilated within 2–4

h refeeding (Slot and Geuze, 1979; Slot et al., 1979). Nonetheless, it is quite surprising that ER stress in pancreatic cells fluctuates with the fasting-feeding cycle because acute mild UPR would expectedly reset proteostasis upon each fasting-feeding cycle, leading to the expansion of the proteostasis network and adaptation (Powers et al., 2009). Hence, we postulate that the proteostasis network in acinar cells is very flexible in order to respond to many variables in the feeding process. The same is likely to be true for pancreatic islet cells.

There are several potential applications for our method in both basic and clinical research. First, our method may help elucidate the activation mechanisms for IRE1α and PERK. The effect of critical residues or inter-/intra-molecular interactions on sensor activation as well as branch-specific activation of non-canonical UPR pathways can now be accurately measured and quantitated. Second, our method may aid in the diagnosis of UPR-associated diseases by providing a more sensitive tool for detecting ER stress. The knowledge of the extent of ER stress in a given tissue of a patient may help assess disease progression. Finally, our method may assist in drug development and design. The efficacy of drugs such as chemical chaperones or antioxidants on ER stress can be quantitatively measured based on sensor activation, circumventing the complications associated with crosstalk among various pathways.

As ER stress is being implicated in an increasing number of physiological processes as well as human diseases such as cancer, liver diseases, neurodegeneration and type-1 diabetes (Kim et al., 2008; Ron and Walter, 2007), new strategies and approaches

enabling a comprehensive understanding of UPR in physiological and disease settings are urgently needed to facilitate drug design targeting UPR in conformational diseases (Kim et al., 2008). The ability to directly visualize and quantitate UPR activation is an important step towards gaining novel insights into physiological UPR and improving therapeutic strategies targeting UPR in vivo.

2.6 ACKNOWLEDGMENTS

We thank Drs. Qiaoming Long and Fenghua Hu for plasmids; Sylvia Allen for excellent care and supply of the mice; Drs. Scott Emr, Fenghua Hu, Martha Stipanuk and Marcus Smolka (Cornell University) for critical reading of the manuscript; and other members of the Qi laboratory for helpful discussions and technical assistance. A patent has been filed regarding methods to quantitate ER stress.

CHAPTER 3. PHENFORMIN ACTIVATES UNFOLDED PROTEIN RESPONSE IN AN AMP-ACTIVATED PROTEIN KINASE (AMPK)-DEPENDENT MANNER

Published as: **Yang, L**., Sha, H., Davisson, R.L., and Qi, L. (2013). Phenformin Activates the Unfolded Protein Response in an AMP-activated Protein Kinase (AMPK)-dependent Manner. J Biol Chem *288*, 13631–13638.

3.1 ABSTRACT

Activation of unfolded protein response (UPR) is associated with the disruption of endoplasmic reticulum (ER) homeostasis and has been implicated in the pathogenesis of many human metabolic diseases, including obesity and type-2 diabetes. However, the nature of the signals activating UPR under these conditions remains largely unknown. Using a method that we recently optimized to directly measure UPR sensor activation, here we screen the effect of various metabolic drugs on UPR activation and show that an antidiabetic drug phenformin activates UPR sensors IRE1α and PERK via both ER-dependent and -independent manners. Mechanistically, AMPK activation is required but not sufficient to initiate phenformin-mediated IRE1α and PERK activation, suggesting the involvement of additional factor(s). Interestingly, activation of the IRE1α, but not the PERK pathway, is partially responsible for the cytotoxic effect of phenformin. Together, our data show the existence of a noncanonical UPR whose activation requires cytosolic kinase AMPK, adding another layer of complexity to UPR activation under metabolic stress.

3.2 INTRODUCTION

Alteration of ER homeostasis initiates signaling pathways, which allow for the communication between ER and other cellular organelles, collectively termed unfolded protein response (UPR). Activation of UPR has been associated, causally in some instances, with various physiological and pathological conditions such as cancer, obesity, type-1 diabetes and cardiovascular diseases (Sha et al., 2011; Wang and Kaufman, 2012). The expansion of ER folding capacity and the reduction of nascent peptide load by UPR assist the recovery and reset of ER homeostasis. However, UPR can act as a double-edged sword as prolonged UPR activation may induce apoptosis (Walter and Ron, 2011).

Upon accumulation of misfolded proteins in the ER lumen, canonical UPR in mammals is initiated by the activation of three major ER- transmembrane sensors IRE1α, PERK and ATF6 (Walter and Ron, 2011). Under ER stressed conditions, binding of misfolded proteins and/or the dissociation of chaperone GRP78 results in IRE1α dimerization, trans-autophosphorylation, oligomerization with the help of actin cytoskeleton (He et al., 2012) and the activation of its RNase activity (Korennykh et al., 2009; Shamu and Walter, 1996). Activated IRE1α splices 26 nucleotides from the Xbp1 mRNA to generate Xbp1s (spliced) transcript, which encodes a transcription factor XBP1s responsible for the induction of various ER chaperones (He et al., 2010; Liou et al., 1990). The activation mechanism for PERK may be similar to that of IRE1α since their luminal domains are inter-changeable (Liu et al., 2000). However, unlike IRE1α, PERK has only a kinase domain, which trans-autophosphorylates itself and phosphorylates eukaryotic translation initiation factor 2α (eIF2α) upon activation (Harding et al., 1999). Phosphorylation of

eIF2α attenuates global translation while paradoxically increases the expression of ATF4 and CHOP (Lu et al., 2004a). Unlike IRE1α and PERK, ATF6 translocates to the Golgi and undergoes proteolysis to release its N-terminal domain, which encodes an active transcription factor. N-terminal ATF6 may be responsible for the upregulation of genes involved in protein folding, trafficking and degradation (Chen et al., 2002a).

Many of the mechanistic insights into UPR activation were garnered from the use of pharmacological drugs, such as dithiotheitol (DTT) that blocks disulfide bond formation (Tatu et al., 1993), thapsigargin (Tg) that inhibits ER calcium pump (Thastrup et al., 1990) and tunicamycin (Tm) that impairs ER protein glycosylation (Dennis et al., 1999). Physiologically, UPR has been detected in various metabolic status changes such as in obese liver and adipose tissues (Ozcan et al., 2004) and in refeeding pancreas (Yang et al., 2010). Interestingly, glucagon-induced IRE1α activation is dependent on protein kinase A (PKA), supporting the possibility of direct regulation of UPR by cytosolic metabolic pathways (Mao et al., 2011). However, how metabolic stress activates UPR is poorly understood.

To address whether and how metabolic signals crosstalk with UPR pathways and facilitate UPR activation, we take advantage of a recently developed Phos-tag-based method. This method allows for visual assessment and quantitative detection of UPR activation at the sensor level (Qi et al., 2011; Sha et al., 2009; Yang et al., 2010). We tested the effect of several metabolic drugs to mimic physiological energy deprivation conditions on UPR. To our surprise, among all the tested drugs, only the hypoglycemic

agent phenformin potently activated IRE1α and PERK pathways. In addition, overexpression of chaperone GRP78 attenuated phenformin- mediated UPR activation while translational inhibition had no effect. Mechanistically, phenformin-induced UPR required kinase activities of both UPR sensors as well as AMPK, but not liver kinase B1 (LKB1). Interestingly, an AMPK agonist AICAR was not sufficient to activate UPR, suggesting the involvement of additional factor(s) in phenformin-mediated UPR activation. Thus, our study implicates the requirement of AMPK in phenformin-mediated UPR activation and provides a framework for further studies to understand the crosstalk between metabolic signals and UPR activation.

3.3 MATERIALS AND METHODS

Cell lines

HepG2, 266-6, 3T3-L1, MEFs, and phoenix cells were maintained in DMEM supplemented with 10% FBS and 1% penicillin/streptomycin. PERK null (PERK-/-) and WT control MEFs were gifts from Dr. Douglas Cavener, Penn State University. AMPKα1α2-/- and AMPK+/+, LKB1-/- and LKB1+/+ MEFs (gifts from Dr. Reuben Shaw, Salk Institute) were previously described (Gwinn et al., 2008). IRE1α-/- MEFs stably expressing WT and mutant IRE1α were generated as previously described (Xue et al., 2011). XBP1i- or luciferase RNAi (CONi)- expressing 3T3L1 cells were previously described (Sha et al., 2009).

Reagents

Tunicamycin (Tm) and thapsigargin (Tg) (EMD Calbiochem, Billerica, MA) were dissolved in DMSO and used at 5 μg/ml and 75~300 nM, respectively. AICAR ((5-aminoimidazole-4-carboxamide ribonucleotide, Toronto Research Center, Toronto, Ontario, Canada) was used at 2 mM. Phenformin, 2-deoxy- D-glucose (2DG), rotenone and rapamycin (Sigma Aldrich, St. Louis, MO) were used at 5 mM, 2 mM, 1 μM and 80 μM, respectively. CHX from EMD Calbiochem was dissolved in ethanol and used at 50 μg/ml. Selection drugs puromycin and G418 were purchased from Sigma and EMD Calbiochem, respectively. Phos-tag was purchased from the NARD Institute (Amagasaki, Japan).

Drug treatment

10^6 cells were plated in 6-well plates in culture medium and incubated overnight. Before experiments, medium was changed to serum-free DMEM supplemented with 0.05% BSA and 1% penicillin/streptomycin. Half an hour later, drugs were added for the indicated time. For CHX treatment, cells were pre-treated with 50 μg/ml CHX for 30 min and throughout the drug treatment. At the end of experiments, cells were snap-frozen in liquid nitrogen before analysis.

Plasmids

WT and K618A mouse PERK cDNA (gifts from Dr. David Ron) (Harding et al., 1999) were subcloned into the pBabe-puro vector. WT human IRE1α cDNA in the pMSCV retroviral vector was provided by Dr. Claudio Hetz (University of Chile) (Hetz et al., 2006). pMSCV-K599A IRE1α was generated by mutagenesis (Xue et al., 2011).

Stable cell line generation

PERK-/- MEFs stably expressing pBabe-WT and mutant PERK, and 3T3-L1 fibroblasts stably expressing PERKi and its control (CONi) were generated using retroviral transduction as previously described (Sha et al., 2009). pSuper- neo vectors (Dr. Lee Kraus, UT Southwestern Medical Center) encoding CONi (gatatgggctgaatacaaa) or PERKi (agtggaaagctgaggtata) were used for retroviral transduction and stable cell line generation.

Adenoviral infection

HepG2 cells in 12-well plates were infected with 5 μl of 10^{12} particles/ml adenoviruses encoding LacZ or GRP78 (Young et al., 2012). After overnight incubation, cells were incubated in DMEM with 0.05% BSA and 1% penicillin/streptomycin for 0.5h and then treated with mock, Tg, Tm or phenformin.

Western blot

Cell nuclear fractionation, whole cell lysate preparation and Western blot analysis were performed as described (Sha et al., 2009). Phosphatase treatment of whole cell lysates and Phos-tag gel was performed as described (Qi et al., 2011; Yang et al., 2010). Quantification of Western blots was done using the ChemiDoc XRS+ system with ImageLab software (Biorad, Hercules, CA) or by ImageJ.

Antibodies

GRP78(goat, 1:1000), ATF4 (rabbit, 1:1,500), CHOP10 (mouse, 1:500), XBP1 (rabbit, 1:1,000) and HSP90 (rabbit, 1:5,000) were purchased from Santa Cruz (Santa Cruz, CA).

(p-T172) AMPK (rabbit, 1:1,000), (p-S79) ACC (rabbit, 1:1,000), (p-S51) eIF2α (rabbit, 1:1,000), IRE1α (rabbit, 1:1,000), (p-T980) PERK (rabbit, 1:1,000), and (p-S240/244) S6 (rabbit, 1:1,000) antibodies were purchased from Cell Signaling (Beverly, MA); CREB antibody (rabbit, 1:6,000) was from Dr. Marc Montminy (Salk Institute). Secondary antibodies were goat anti-rabbit and anti-mouse IgG HRP and donkey anti-goat HRP used at 1:10,000 (Biorad).

Quantitative PCR (qPCR) and RT-PCR

Total mRNA extractions were carried out using Trizol- based protocol (Molecular Research Center, Inc.) and reverse transcribed using Superscript III kit (Invitrogen, Calsbad, CA). qPCR was performed with primers described in (Yang et al., 2010). RT-PCR analysis of spliced and unspliced Xbp1 was performed as described (Sha et al., 2009). RT-PCR products were separated by electroporesis on a 2% agarose gel (Invitrogen) containing ethidium bromide and visualized using Bio-Rad ChemiDoc XRS+ system.

Survival assay

2-5x10^4 3T3-L1 fibroblasts stably expressing control RNAi, XBP1i or PERKi were plated in each well of a 24-well plate, incubated for overnight and treated with 5 mM phenformin for the indicated time. Cells were snap-frozen in liquid nitrogen and thawed at room temperature (25°C). DNA content was measured using CyQuant kit (Invitrogen) per supplier's protocol as an indication of relative cell numbers.

Statistical analysis

All experiments have been repeated at least twice. Results are expressed as mean ± s.e.m. Comparisons between groups were made by unpaired two-tailed Student t-test, except that in the cell survival assay ANOVA was used. $P<0.05$ was considered as statistically significant.

3.4 RESULTS

3.4.1 Phenformin induces IRE1α and PERK phosphorylation

To study the link between metabolic pathways and UPR, we tested the effect of various metabolic drugs on UPR sensor activation in hepatoma cell line HepG2. Several drugs with capacity to affect cellular metabolic state were selected, such as inhibitors of mitochondrial electron transport phenformin (Davidoff, 1968) and rotenone (CHANCE et al., 1963), a nonmetabolizable glucose analog 2DG that blocks glycolysis (SOLS and CRANE, 1954), and an inhibitor of mTOR complex rapamycin (Brown et al., 1994). Following 2 h treatment, whole cell lysates were prepared and separated on Phos-tag-containing or regular SDS-PAGE gels to visualize IRE1α and PERK phosphorylation, respectively. The slower- migrating bands of IRE1α and PERK represent their phosphorylated forms as they are sensitive to phosphatase treatment (Fig. 3.1A). Detailed characterization of UPR activation using the Phos- tag-based methods has been previously described (Qi et al., 2011; Sha et al., 2009; Yang et al., 2010). Of note, we were not able to assess the activation of the ATF6 pathway due to the lack of a reliable antibody for endogenous ATF6 proteins.

As expected, most metabolic drugs affected cellular metabolic state within the 2-hour treatment as reflected by the decreased phosphorylation of ribosomal protein S6 (Fig. 3.1B). However, only phenformin, a derivative of biguanides, significantly elevated IRE1α and PERK phosphorylation, to a level comparable to that of classical ER stressor such as Tg or Tm (Fig. 3.1C-D, and data not shown). The effect of phenformin on UPR sensors was not merely due to the inhibition of mitochondrial electron transport as rotenone, another mitochondrial respiration inhibitor, had the opposite effect on IRE1α phosphorylation (Fig. 3.1C-D).

To further characterize the nature of phenformin- mediated activation of IRE1α and PERK, we performed the following two experiments to attenuate ER stress. First, cells were pre-treated with a protein translation inhibitor CHX. As expected, inhibition of protein translation greatly reduced both basal and Tg-induced IRE1α and PERK phosphorylation (Fig. 3.1C-D). By contrast, phenformin-mediated IRE1α and PERK activation remained unaffected by CHX (Fig. 3.1C-D).

Second, we infected HepG2 cells with an adenovirus encoding the ER chaperone GRP78, which is known to increase ER folding capacity and thereby alleviate UPR activation (Wang et al., 1996; Young et al., 2012). Overexpression of GRP78 significantly attenuated phenformin-mediated IRE1α and PERK phosphorylation compared to the controls (Fig. 3.1E-F). The effect of GRP78 on Tg-induced ER stress in HepG2 cells was modest likely due to the expression level of GRP78, as more dramatic effect of GRP78 was observed in HEK293T cells where viral infection was more efficient (Fig. 3.1G).

Thus, we conclude that the accumulation of unfolded/misfolded proteins at least in part responsible for phenformin-mediated UPR activation.

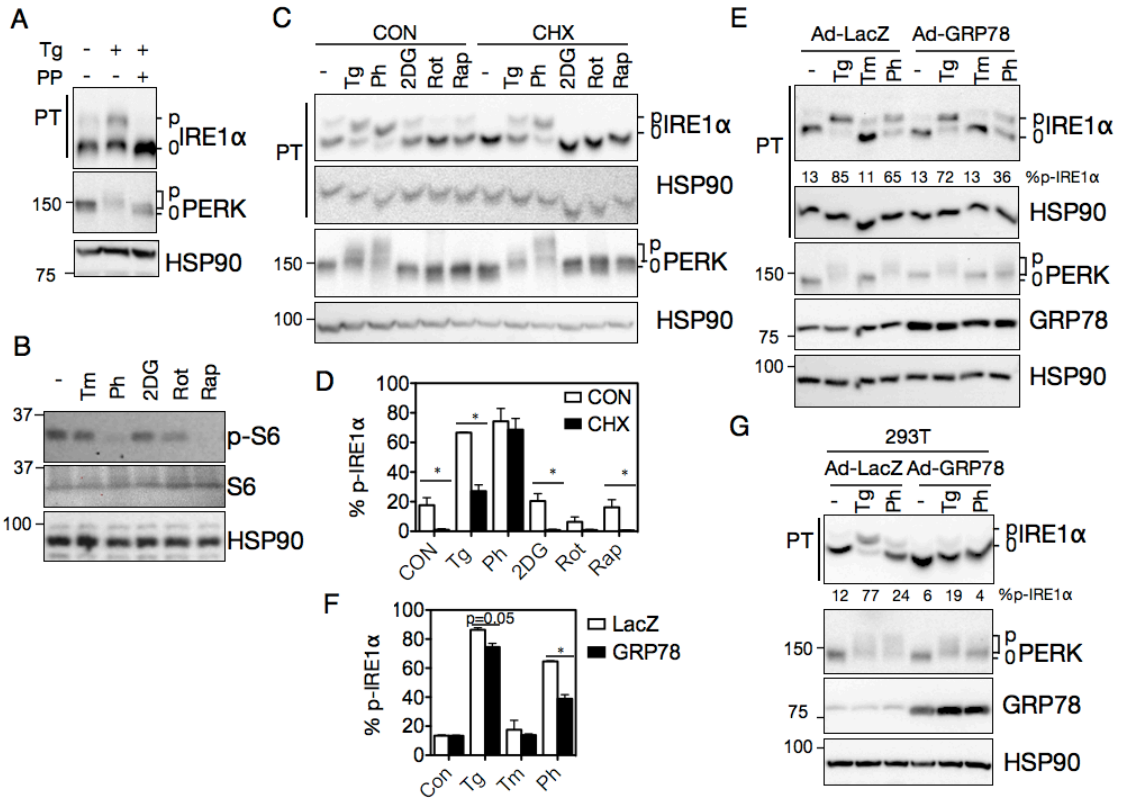

Figure 3.1 Phenformin treatment activates UPR sensors IRE1α and PERK. (A) Phos-tag (PT) analysis of IRE1α and Western blot analysis of PERK in HepG2 cells treated with 75 nM thapsigargin (Tg) for 2 h. Whole cell lysates were treated with or without λ phosphatase (PP). HSP90, a loading control. (B) Western blot analysis of (p-)S6 in HepG2 cells treated with phenformin (Ph, 5 mM), 2-deoxy-D-glucose (2DG, 2 mM), rotenone (Rot, 1 μM), or rapamycin (Rap, 80 μM) and tunicamycin (Tm, 5 μg/ml) for 2 h. (C) Western blot analysis of IRE1α and PERK in HepG2 cells treated with various drugs as in A and B. In the cycloheximide (CHX) group, HepG2 cells were pre-treated with 50 μg/ml CHX for 30 min and throughout the drug treatments. (D) Quantitation of the percent of phosphorylated IRE1α in total IRE1α (hereafter referred to as %IRE1α) in (C). (E-F) Western blot analysis of IRE1α and PERK in HepG2 (E) and HEK293T cells

(F) infected with adenoviruses overexpressing LacZ or GRP78 followed by drug treatment; and quantitation of two independent experiments of E shown in (F). Data are representative of at least two independent experiments. Values as mean ± s.e.m with three repeats. Statistical analysis was done by t-test (*, $p<0.05$).

3.4.2 Phenformin-mediated IRE1α and PERK activation is a general phenomenon

To determine whether this is a general phenomenon, we examined in detail the effect of phenformin on UPR in various cell types. In MEFs, phenformin treatment increased AMPK phosphorylation and decreased S6 phosphorylation as expected (Fig. 3.2A). Consistently with the data in HepG2 cells shown in Fig. 1, phenformin induced IRE1α phosphorylation (Fig. 3.2A) and *Xbp1* mRNA splicing (Fig. 3.2B). Similarly, phenformin increased PERK and eIF2α phosphorylation and CHOP protein levels (Fig. 3.2C). Moreover, the activation of IRE1α and PERK pathways was supported by the increased transcript levels of UPR target genes, including Grp78, Erdj4, Chop and Gadd34 (Fig. 3.2D). Similar observations were obtained in pancreatic acinar 266-6 cells (Fig. 3.2E), β cell line INS-1 and macrophage cell line RAW (not shown). Thus, our data show that phenformin- induced UPR activation is a general phenomenon regardless of cell types.

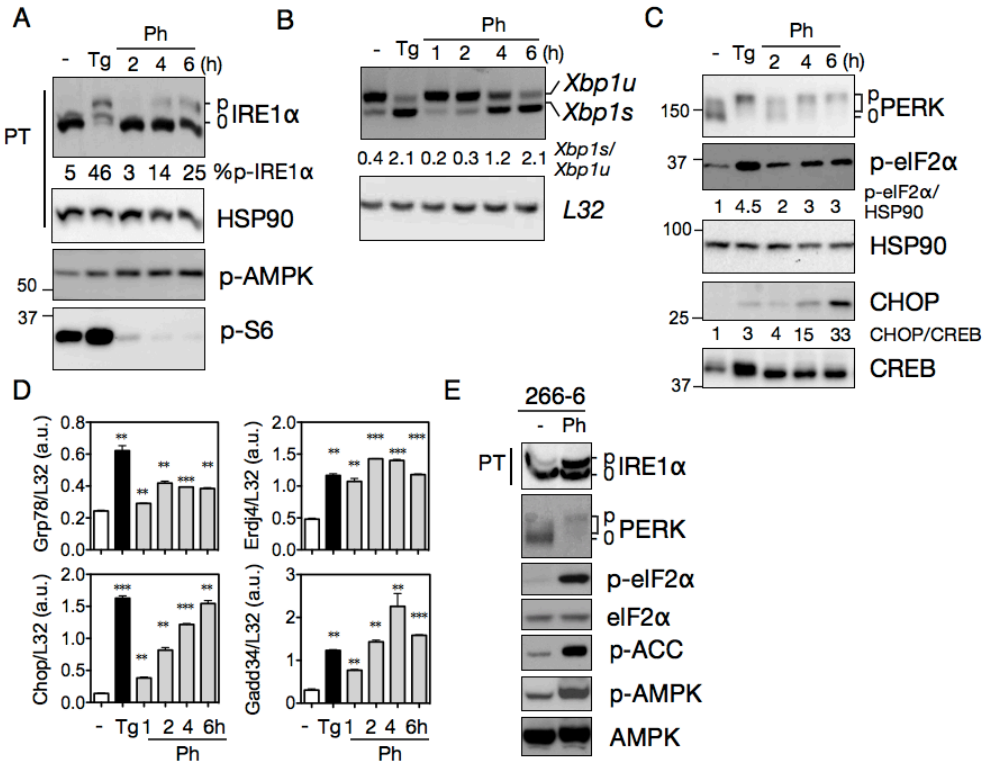

Figure 3.2 Phenformin effect on UPR activation is a general phenomenon. (A) Western blot analysis of IRE1α in MEFs treated with 75 nM Tg for 2 h or 5 mM Ph at the indicated times. (B) RT-PCR analysis of *Xbp1* mRNA splicing in MEFs treated as in (A). Ribosomal gene *L32*, a loading control. (C) Immunoblots of the PERK pathway in MEFs treated as in (A). (D) qPCR analysis of UPR targets in MEFs treated as in (A). mRNA levels of each gene were normalized to L32. (E) Western blot analysis of IRE1α and PERK in pancreatic acinar cell 266-6 treated with 5 mM Ph for 2h. HSP90 and CREB, loading controls. Data are representative of three independent experiments. Quantitation from one experiment shown below the gel. Statistical analysis was done by t-test comparing each treatment with non-treated control (*, $p<0.05$. **, $p<0.01$. *** $p<0.001$)

3.4.3 AMPK is required for phenformin-mediated IRE1α and PERK activation

Phenformin effect is partially mediated by AMPK (Zhou et al., 2001). We next asked whether AMPK is required for the phenformin-mediated UPR activation. To this end, we examined UPR activation in AMPK-/- MEFs lacking both AMPKα1 and α2 catalytic domains. Indeed, the activation of the IRE1α pathway, including IRE1α phosphorylation and *Xbp1* mRNA splicing, was completely abolished by the loss of AMPK (Fig. 3.3A-B). This was not due to intrinsic defects of UPR activation in AMPK-/- cells as Tg-induced IRE1α activation was not blocked (Fig. 3.3A-B). At the mRNA level, AMPK deficiency blocked phenformin- but not Tg- induced Erdj4 expression (Fig. 3.3C). Similarly, activation of the PERK pathway by phenformin, but not Tg, were significantly reduced in AMPK-/- MEFs as shown by Thr980 PERK phosphorylation (Fig. 3.3D) and induction of CHOP at both mRNA and protein levels (Fig. 3.3C and 3.3E). Of note, lack of phosphorylation of ACC, a direct AMPK target, in AMPK-/- MEFs in response to phenformin confirmed the complete loss of AMPK activity (Fig. 3.3D). Thus, our data suggest that AMPK is required for phenformin-mediated IRE1α and PERK activation.

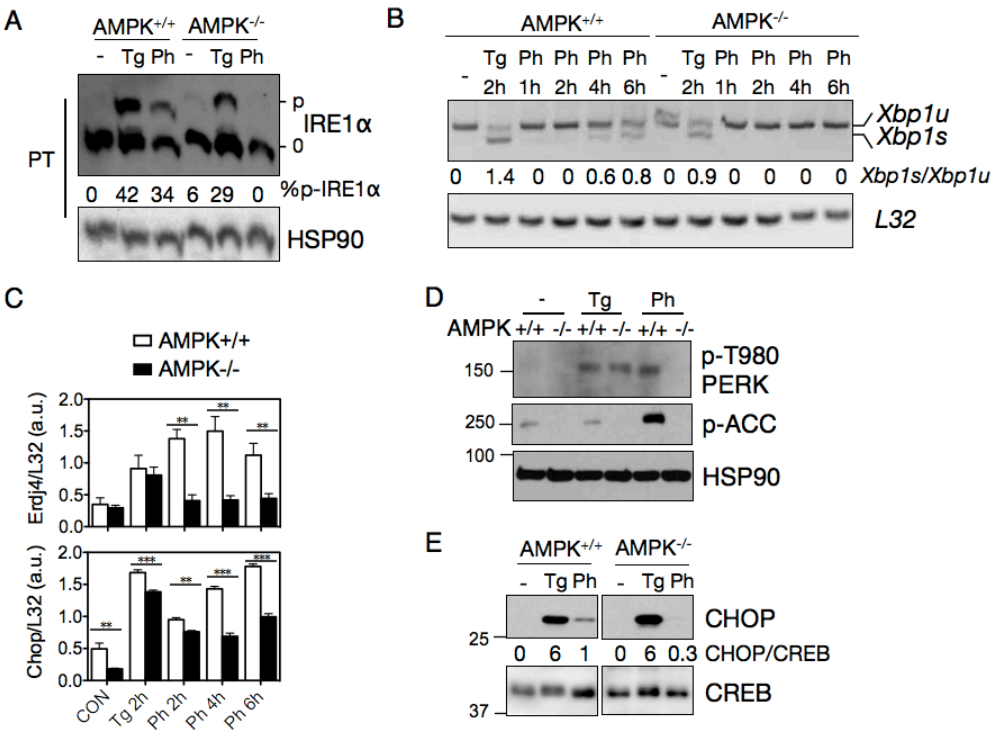

Figure 3.3 AMPK is required for phenformin-mediated UPR activation. (A) Western blot analysis of IRE1α in AMPK-/- or WT MEFs treated with 75 nM Tg or 5mM Ph for 6 h. (B) RT-PCR analysis of *Xbp1* mRNA splicing in AMPK+/+ and AMPK-/- MEFs treated with 75 nM Tg and 5 mM Ph for the indicated times. (C) qPCR analysis of mRNA level changes of Erdj4 and Chop in AMPK+/+ and AMPK-/- MEFs treated as in (B). (D-E) Western blot analysis of the PERK pathway, p-T980 PERK (D) and CHOP (E), in AMPK+/+ and AMPK-/- MEFs treated as in (A). HSP90 and CREB, loading controls. Data are representative of three independent experiments. Quantitation from one experiment shown below the gel. Statistical analysis was done by t-test between AMPK+/+ and AMPK-/- MEFs for each treatment (*, $p<0.05$. **, $p<0.01$. *** $p<0.001$).

3.4.4 LKB1 is dispensable for phenformin effect

LKB1 is an upstream kinase of AMPK in some settings (Hawley et al., 2003; Lizcano et al., 2004). We next asked whether LKB1 is required in phenformin-mediated UPR activation. Comparable levels of IRE1α and PERK hyperphosphorylation were observed in LKB1-/- and wildtype cells treated with phenformin (Fig. 3.4A). This was further supported by the similar induction of CHOP protein (Fig. 3.4A). Thus, LKB1 is dispensable for phenformin-mediated UPR activation. Indeed, phenformin-induced ACC phosphorylation did not require LKB1 (Fig. 3.4B), suggesting the presence of other AMPK upstream kinase(s).

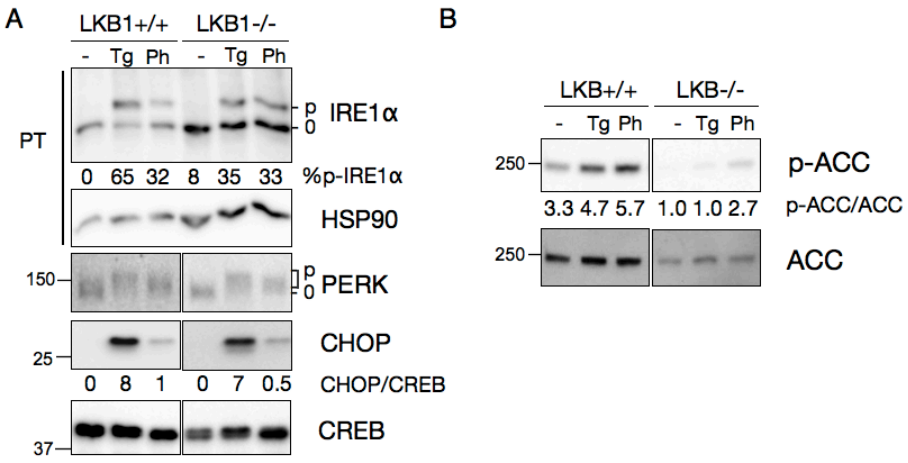

Figure 3.4 LKB1 is dispensable for phenformin-mediated UPR activation. (A) Western blot analysis of IRE1α and PERK pathways in LKB1+/+ and LKB1-/- MEFs treated with 75 nM Tg or 5mM Ph for 6 h. (B) Immunoblots of (p)-ACC in LKB1+/+ and LKB1-/- MEFs treated with drugs for 8 h. HSP90 and CREB, loading controls. Data are representative of three independent experiments. Quantitation from one experiment shown below the gel. Of note, the blots shown in this figure were derived from the same exposure of the same gels with the irrelevant lanes cut off.

3.4.5 AMPK activation is not sufficient to activate IRE1α and PERK

We are next asked whether AMPK is sufficient to induce UPR using another AMPK agonist AICAR (Sullivan et al., 1994). Treatment of AICAR expectedly increased AMPK phosphorylation at Thr172 and decreased S6 phosphorylation (Fig. 3.5A). However, no increase of IRE1α and PERK phosphorylation was observed even with prolonged treatment (Fig. 3.5B), arguing that AMPK activation was not sufficient to promote IRE1α and PERK activation. Rather, we noticed that IRE1α phosphorylation was decreased with time, suggesting that AMPK activation alone may downregulate ER stress, likely through the inhibition of protein translation (reduced p-S6). This observation is consistent with previous reports showing that AMPK activation alone alleviates ER stress in various cell types (Dong et al., 2010; Gomez et al., 2008; Lee et al., 2012; Lu et al., 2012; Mayer and Belsham, 2010; Terai et al., 2005).

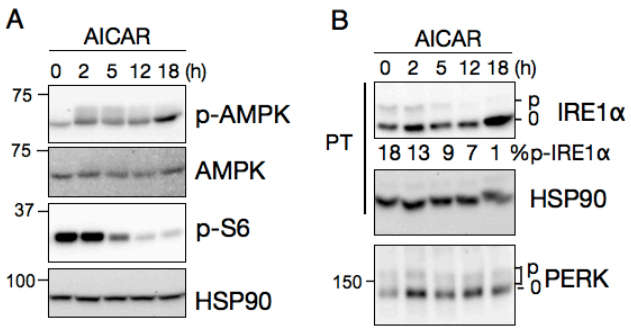

Figure 3.5 AMPK activation is not sufficient to activate UPR. Western blot analysis of (p-) AMPK and (p)-S6 (A) and IRE1α and PERK (B) in WT MEFs treated with 2 mM AICAR for the indicated times. Note the suppressive effect of AICAR on IRE1α activation in B. Data are representative of three independent experiments. Quantitation from one experiment shown below the gel. HSP90, the loading control.

3.4.6 Kinase activities of both IRE1α and PERK are indispensable for their activation by phenformin

In canonical UPR, kinase activities of IRE1α and PERK are required for the transautophosphorylation and activation. To test the involvement of kinase activities of IRE1α and PERK in phenformin-mediated activation, we generated PERK knockout (PERK-/-) MEFs stably expressing empty vector pBabe, WT PERK or kinase-dead K618A PERK (Bertolotti et al., 2000), and measured phenformin-induced phosphorylation. The kinase-dead K618A mutation specifically prevented PERK from auto-phosphorylation and activating downstream targets ATF4 and CHOP under both Tg and phenformin treatment (Fig. 3.6A). Similarly, only WT but not kinase-dead K599A IRE1α was responsive to phenformin treatment (Fig. 3.6B). In conclusion, intact IRE1α and PERK kinase domains are required for the phenformin effect, suggesting that phenformin effect is mediated through the kinase activities of IRE1α and PERK.

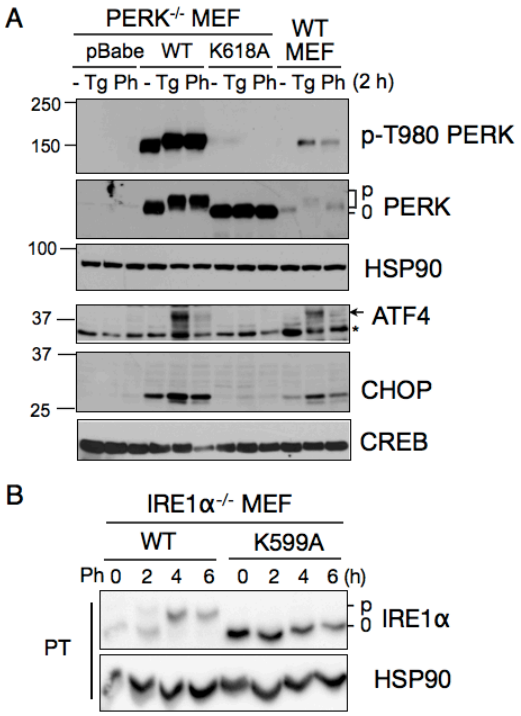

Figure 3.6 Kinase activities of IRE1α and PERK are required for the phenformin effect. (A) Western blot analysis of the PERK pathway in PERK-/- MEFs stably expressing empty vector, WT or K618A kinase-dead PERK treated with 300 nM Tg and 5mM Ph for 2 h. Wild type MEFs as control. ATF4 and CHOP were detected using nuclear extracts of the same cells. (B) Western blot analysis of IRE1α phosphorylation in IRE1α-/- MEFs stably expressing WT or K599A IRE1α treated with phenformin (5 mM) for the indicated times. HSP90, loading/position controls. CREB, a loading control for nuclear fraction. Data are representative of at least two independent experiments.

3.4.7 Activation of IRE1α-XBP1 pathway partially mediates the cytotoxicity of phenformin

Prolonged treatment of phenformin has cytotoxicity as its potential side effect (Heishi et al., 2008). As UPR is a key determinant of cell fate, we next asked whether IRE1α and PERK activation accounted, at least in part, for the cytotoxicity of phenformin. To this end, we generated 3T3-L1 fibroblasts stably expressing RNAi against PERK (PERKi) or the major target of IRE1α XBP1 (XBP1i) (Fig. 3.7A-B). Cell survival upon prolonged phenformin treatment was revealed by the CyQuant assay measuring the amount of DNA as the indicator of cell numbers. Cell numbers started to decline after 7h phenformin treatment in CONi cells while cells expressing XBP1i showed slower cell loss rate (Fig. 3.7A). On the other hand, knockdown of PERK had no significant effects on cell survival compared to the control group (Fig. 3.7B). Thus, the IRE1α-XBP1 pathway, but not PERK, is in part responsible for the cytotoxicity of phenformin.

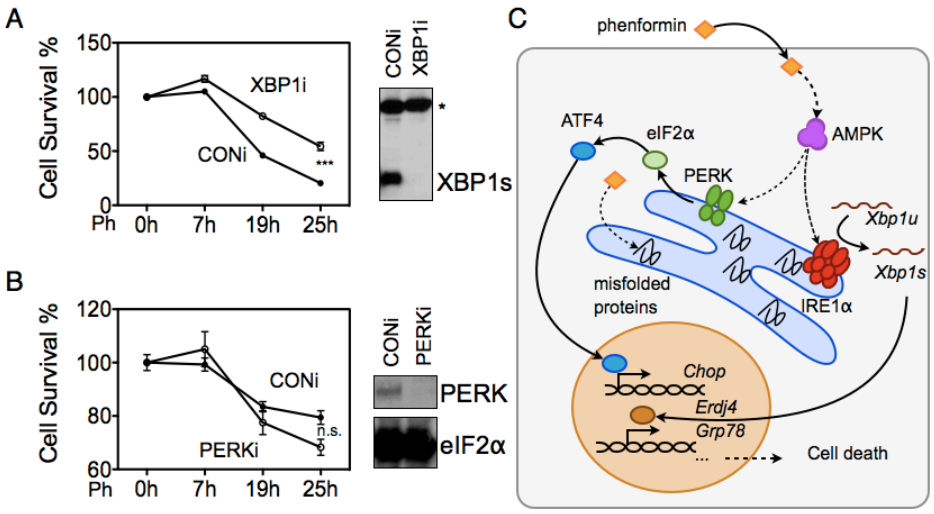

Figure 3.7 Activation of the IRE1α pathway in part mediates the cytotoxicity of phenformin and the model. (A-B) Cell survival assay in 3T3-L1 cells stably expressing CONi, XBP1i (A) or PERKi (B) treated with 5 mM Ph for the indicated times with immunoblots showing the levels of XBP1s and PERK on left. In (A), Western blot analysis of XBP1s were done using nuclear extracts of cells treated with 300 nM thapsigargin for 3 h as XBP1s protein levels at basal condition was very low. Values as mean ± s.e.m with three repeats. Statistical analysis was done by ANOVA (***, $p<0.001$). (C) Schematic model for the phenformin-induced IRE1α and PERK activation. Phenformin treatment leads to AMPK activation, which together with signals from the ER activates UPR. Upregulation of the IRE1α target XBP1s, but not the PERK pathway, in part accounts for the cytotoxicity of phenformin.

3.5 DISCUSSION

Our study demonstrates the phenformin-induced UPR activation in an AMPK-dependent manner. The downstream outcomes of this phenformin- induced UPR highly resemble those of the UPR triggered by traditional ER stress inducers, including the activation of downstream canonical events of IRE1α and PERK pathways, such as the requirement of kinase activities of IRE1α and PERK, Xbp1 splicing, eIF2α phosphorylation and induction of ER chaperones. However, the activation mechanism appears to be distinct: The phenformin-mediated UPR activation is resistant to cycloheximide treatment and requires the cytosolic energy sensor AMPK. Based on these findings, we conclude that activation of UPR sensors can be facilitated by metabolic signals from outside of the ER lumen under metabolic challenges.

In addition to the activation mechanism, our data show that phenformin-mediated UPR activation may be responsible for the cytotoxic effect of phenformin. It has been shown that IRE1α and PERK pathways differentially regulate cell survival in response to ER stress (Wang and Kaufman, 2012). While the PERK pathway promotes cell death in part via CHOP-mediated induction of pro-apoptotic genes such as Bim (Puthalakath et al., 2007), the IRE1α-XBP1 pathway may promote cell survival via the induction of ER folding capacity (Hetz, 2012; Lin et al., 2007; 2009). On the other hand, several recent reports showed that high levels of XBP1s can also be pro-apoptotic (Allagnat et al., 2010; Zeng et al., 2009). Here, our data showed an improved cell survival rate in XBP1-deficient cells treated with phenformin while no difference in PERK-deficient cells, suggesting that the IRE1α-XBP1 pathway is pro- apoptotic in this context. In line with

our study, in a previous report, another biguanide derivative metformin selectively upregulating PERK pathway results in no cell apoptosis (Quentin et al., 2011). Thus, the role of UPR branches in cell fate decision is likely to be cell type- and context-specific.

Phenformin has been removed from the anti- diabetic drug market due to its liver-toxicity and potency for inducing lactic acidosis while its analog metformin remains on the market (Assan et al., 1975). Recently, phenformin starts to re-attract interests for its greater anti-tumor efficacy than metformin in mouse models (Appleyard et al., 2012). Enhanced cell cycle inhibitor p21 has been suggested as one of the mechanisms underlying the inhibition of cell proliferation and induction of apoptosis in phenformin-treated cancer cells (Caraci et al., 2003). However, the detailed mechanisms of its cytotoxicity are still not fully understood. Our data suggest UPR as a potential mechanism for the cell fate determination of phenformin. Whether the liver toxicity or the anti-cancer effect of phenformin is mediated by the IRE1α-XBP1 pathway requires further investigations using in vivo models.

Several recent studies have shed light on the emerging crosstalks between UPR and metabolic signaling pathways such as AMPK or mTOR pathways (Appenzeller-Herzog and Hall, 2012). For example, a recent study showed that the RNase activity of IRE1α may be required for nitric-oxide-mediated activation of AMPK (Meares et al., 2011), while UPR activation downregulates the mTOR pathway to enhance autophagy, presumably to provide amino acids by degradation of unnecessary proteins (Qin et al., 2010). Conversely, AMPK activation reduces translation and attenuates ER stress and

UPR (Dong et al., 2010; Gomez et al., 2008; Lee et al., 2012; Lu et al., 2012; Mayer and Belsham, 2010; Terai et al., 2005), similar to our observation. Nonetheless, our data showed that phenformin activates UPR in an AMPK-dependent manner and AMPK deficiency completely abolishes the phenformin-induced UPR while having no effect on Tg-induced UPR. Thus, these new data suggest that AMPK is required but not sufficient to activate UPR. We speculate that additional phenformin-responsive factor(s) may be required in this process (Fig. 3.7C). We speculate that signals from inside the ER may act as the additional factor, exert synergistic effect with AMPK to activate UPR sensors under phenformin treatment as overexpression of GRP78 attenuated the phenformin effect on UPR. Possible mechanisms include the interruption of folding, maturation and secretion of ER proteins.

Our study reveals the complexity of mammalian UPR activation, which seems to be tightly regulated by multiple signaling pathways in addition to stress in the ER. We recently showed the involvement of non-muscle myosin II ad actin cytoskeleton in the activation of IRE1α in response to ER stress (He et al. 2012). Thus, together with this study, we postulate that UPR sensors not only sense the ER environment, but also are able to integrate cytosolic signals such as actin cytoskeleton and metabolic status.
The challenge that lies ahead is to determine the nature of physiological signals triggering ER stress and activating UPR as well as quantitating the amount of ER stress under physiological setting. We recently demonstrated the importance and efficacy of a Phos-tag-based approach to quantitating and visualizing ER stress (Qi et al., 2011; Sha et al., 2009; Yang et al., 2010). This approach takes advantage that IRE1α is separated into two

bands on a Phos-tag gel, with the slower-migrating band representing the phosphorylated form which tightly correlates with IRE1α and UPR activation. Many laboratories have successfully used this approach to detect IRE1α activation under more physiological conditions in various cell and tissue types. With the aid of this method, this study reports a case of UPR activation facilitated by metabolic signals in the cytosol. Understanding of the alternate modes of UPR activation will be pivotal and instrumental for the development of therapeutic strategies that modulate ER stress and homeostasis in human health and diseases.

3.6 ACKNOWLEDGEMENT

We thank Drs. Douglas Cavener (Penn State University), Claudio Hetz (University of Chile), Lee Kraus (UT Southwestern Medical Center), Marc Montminy (Salk Institute), David Ron (University of Cambridge), and Reuben Shaw (Salk Institute) for reagents. We also thank Dr. Stipanuk (Cornell University) and the Qi lab members for helpful discussions. L.Y. was supported in part by the American Heart Association Founders Affiliate Predoctoral Fellowship 12PRE9400033. This work was supported by NIH R01DK082582, R21AA020351 and American Diabetes Association 7-08-JF-46 and 1-12-CD-04 (to L.Q.).

CHAPTER 4. SEL1L, A CORE ERAD COMPONENT MAINTAINS THE PRE-BCR CHECKPOINT AND IS INDISPENSIBLE FOR B CELL DEVELOPMENT

4.1 ABSTRACT

B cell development relies heavily on signaling pathways mediated by various surface receptors, which are synthesized in ER (endoplasmic reticulum). However the importance of ER homeostasis and ER quality control system in B cell development is under-appreciated. To dissect the role of ERAD, the housekeeping ER quality control machinery, in this process, we generated a conditional knockout mouse model in which SEL1L, a key ERAD component, is selectively deleted in B cell linage. Loss of SEL1L resulted in B cell developmental defect and systemic B cell reduction. No ER stress or UPR activation was detected in B precursors, which ruled out UPR-mediated apoptosis as a causal factor for B cell loss. Remarkably, we observed unusual ER accumulation of a preBCR subunit VpreB, which may mediate the reduction of surface preBCR expression, impair the signaling pathways in differentiation and proliferation, and ultimately influence B cell maturation. In summary, our study of SEL1L null B cells reveals a novel role of ERAD in B lymphocyte checkpoint maintenance, establishing the significance of ER quality control in the delicate developmental control process.

4.2 INTRODUCTION

The terminally misfolded ER proteins are eliminated by machineries organized on the ER membrane, which are collectively termed as ER-associated degradation (ERAD) pathway. Depending on the topology (luminal protein or transmembrane protein) and the location of lesion (in the luminal, transmembrane or cytosolic domains), substrates can be sorted by adaptors for different ERAD pathways (Smith et al., 2011). Distinct ERAD pathways are defined by specific E3 ubiquitination complexes including Hrd1p and Doa10p in yeast, and many more in metazoans, such as HRD1, GP78, TRC8, RMA1 and TEB4.

The most well characterized E3 core organizer is the HRD1/SEL1L complex, which is evolutionally conserved from yeast to mammals. At the center of this complex is the ubiquintin ligase HRD1, a six transmembrane protein with a catalytic ring domain in the cytosolic side(Kikkert et al., 2004). HRD1 receives ubiquitin units from E2 ubiquintin-conjugating enzymes and passes the ubiquitin chains onto the ERAD substrates retro-translocated from ER for further degradation by cytosolic proteasome (Kikkert et al., 2004; Mueller et al., 2008). Another critical component in HRD1 E3 complex is the central adaptor SEL1L (Mueller et al., 2006). SEL1L is a interaction hub protein featured by multiple tetratricopeptide repeats on its luminal domain, a single transmembrane segment and a small cytosolic proline-rich tail (Biunno et al., 2006) (Mittl and Schneider-Brachert, 2007). SEL1L has been proposed to nucleate the whole E3 complex (Christianson et al., 2012; Mueller et al., 2006; 2008), maintaining complex

stability(Gardner et al., 2000)while serving as the loading dock for substrate-binding lectins such as mammalian OS-9 and XTP3-B (Christianson et al., 2008).

The indispensable housekeeping function of HRD1/SEL1L ERAD pathway has been indicated by the overt ER stress and the embryonic lethality observed in animals lacking of HRD1 or SEL1L (Francisco et al., 2010; Yagishita et al., 2005). However, the embryonic lethality hinders our understanding of the tissue-specific physiological functions of HRD1/SEL1L ERAD pathway. In this project, we are particularly interested in the role of ERAD in B cell development, a process that requires a high ER capacity. During B cell development, ER produces a large amount of surface receptors, such as SCF receptor cKIT, cytokine interleukin-7 (IL-7) receptor (IL-7R) and premature B cell receptor (preBCR), to communicate with the bone marrow microenvironment, providing important survival and differentiation signals, (Herzog et al., 2009; Nagasawa, 2006).

preBCR (premature B cell receptor) is a key checkpoint expressed specifically at precursor-B cell (pre-B) stage, critical for the transition from pre-B to immature B stage (Herzog et al., 2009). preBCR is a tetramer consisted of a pair of Igμ heavy chains and two surrogate light chains, with more structural complexity compared to the other dimer receptors such as IL-7R (Interleukin 7 receptor) or cKIT (stem cell factor receptor) (Nishimoto et al., 1991). The surrogate light chains (the non-variable light chain-like structure) are composed by non-variable peptides VpreB and λ5, and are required for membrane expression and downstream signaling of preBCR (Papavasiliou et al., 1996). Upon preBCR activation, Src-family protein tyrosine kinases such as LYN and SYK

phosphorylate preBCR-associated adaptors Igα and Igβ. Phosphorylated adaptors in turn recruit Src-tyrosine kinases for differentiation signaling transduction (Flaswinkel and Reth, 1994). Another target of Src-tyrosine kinases is the co-receptor CD19, which activates the PI3K-AKT pathway for proliferation (Aiba et al., 2008). In addition, IL-7R senses IL-7 secreted by the stromal cells activates AKT in an ERK-dependent manner to enhance proliferation synergistically with preBCR derived signals (Milne and Paige, 2006). preBCR and IL-7R-controlled differentiation and proliferation, and thus serve as the checkpoints to ensure suitable environment and functional heavy chain before further development.

Of note, assembly of both conventional and premature BCR is under tight control by the ER folding machinery (Hendershot, 1990; Minegishi et al., 1999). A considerable amount of unassembled Igμ is retained in ER by BIP (Cohen et al., 2013; Hendershot, 1990; Hsu and Betenbaugh, 1997) and delivered to ERAD for degradation upon prolonged ER retention (Fagioli and Sitia, 2001). In fact, only a small percentage of preBCR complexes can exit ER even after successful assembly (Brouns et al., 1996). This restricted transportation implies a positive selection for functional preBCR as quality control. However, how ER machinery contributes to this quality control is poorly understood and often taken for granted.

To understand the physiological importance of ERAD and ER homeostasis in B cells, we generated a conditional ERAD knockout mouse model. Our data show that loss of the key ERAD component SEL1L severely impairs B cell development before the immature

B cell stage. In contrast to our expectation, this phenotype is not the result of ER stress-induced apoptosis. Rather, we observed dysregulation of the pre-BCR signaling pathway, which may be the direct cause of developmental blockage. An unusual intracellular accumulation of surrogate light chain VpreB due to loss of SEL1L, likely disrupts normal preBCR assembly, leads to decreased surface expression of other pre-BCR components, and may be the fundamental reason for the phenotypic defects. From these observations, we derive the hypothesis that ERAD contributes to the regulation of preBCR production and maintains the essential checkpoint for B cell development.

4.3 MATERIALS AND METHODS

Mice

Agouti mice on C57BL/6N background with two loxP cassettes flanking the 6th exon of SEL1L (Sel1L f/f) were backcrossed with C57B6/L mice for 6 generations for a pure C57B6/L background. The resulted C57B6/L Sel1L f/f mice and C57B6/L CD19-Cre mice from Jackson laboratory (B6.129P2(C)-Cd19tm1(cre)Cgn/J) were used to generate the animals for experiments. Adult (8-20 weeks) Sel1L f/f; CRE+/- offspring is used as B cell specific knockout (BKO), while Sel1L f/f; CRE-/- littermates of similar ages as wild type control (WT). Genotyping was performed with PCR primers as the following: Sel1L F: 5'-CTGACTGAGGAAGGGTCTC-3' and R: 5'-GCTAAAAACATTACAAAGGGGCA-3' (325 bp as wild-type allele, 286 bp as floxed allele). CD19-CRE (oIMR 1084: GCG GTC TGG CAG TAA AAA CTA TC/ oIMR1085: GTG AAA CAG CAT TGC TGT CAC TT) and CD19-wt (oIMR1589: CCT CTC CCT

GTC TCC TTC CT/1590: TGG TCT GAG ACA TTG ACA ATC A) primer sets are purchased from Jackson laboratory.

Flow cytometry

Flow cytometry was performed as previously described in (Xia et al., 2011). BD permeablization and fixation kit was used for intracellular staining. Fluorochrome antibodies against B220 (RA3-6B2), CD43 (1B11), CD19 (6D5), CD138 (281-2), VpreB (R3), cKIT (ACK2), IL-7Rα (A7R34), Igα, Igβ (HM79-12), IgM (RMM-1), IgD (11-26c.2a), BP-1 (6C3), HAS (M1/69), CD4 (GK1.5), CD8 (YTS169), CD5 (53-7.3), CD11b (M1/70), CD45 (30-F11) and BrdU-FITC (PRB-1) and isotype control antibodies were purchased from Biolegend. Igμ was from Jackson Immunoresearch. Antibodies (except BrdU-FITC) were used at 1:150 - 1:200 dilution for surface staining and 1:100 dilution for total staining in 50 μl system. BrdU-FITC was used at 1:20 dilution.

Splenic B cell purification (negative selection)

B-cell purification from spleens was carried out using the BD IMagTM Cell Separation System (BD Biosciences). Spleens were gently pushed through 70 μm nylon mesh (Fisher Scientific 22363548) to yield single cell suspension. Red blood cells were lysed on ice for 1 min in ACK lysis buffer (0.15 M NH_4Cl ,1 mM $KHCO_3$,0.1 mM Na_2EDTA, pH 7.2). After two washes with 10 ml PBS (137mM NaCl, 2.7mM KCl, 4.3mM Na_2HPO_4, 1.4mM KH_2PO_4, pH 7.4), 10^8 splenocytes were incubated with 5 μl biotin-conjugated anti mouse CD3 antibody and 3 μl biotin-conjugated anti mouse CD11b antibody (UCSF Monoclonal Antibody Core Facility, 0.5 mg/ml) with a total volume of

100 µl at 4°C for 20 min followed by incubation with 60 µl Streptavidin Particles Plus (BD Biosciences 557812) with a total volume of 300 µl at 4°C for 20 min. Then cells were transferred to a 12 × 75 mm tube which was inserted into a Cell Separation Magnet Apparatus (BD Biosciences) for 5 min. Cells from the flow-through, i.e. the CD3- and CD11b-negative portion, were collected, washed with PBS and then resuspended in 1 ml DMEM culture medium. Of note, CD3 antibody targets T cells while CD11b antibody recognizes monocytes, macrophages, eosinophils, granulocytes and NK cells. Purity was determined using flow cytometry.

Bone marrow CD19+ B cell purification (positive selection)

Bone marrow cells were flushed out from freshly harvested bones by PBS with 10% FBS and 1% penicillin/streptavidin, and filtered through 70 µm nylon mesh (Fisher Scientific 22363548) to yield single cell suspension. 2-3x10^8 cells were incubated with 30 µl anti-CD19-biotin in 500ul PBS/10%FBS/1%PS for 20 min at 4°C, followed by incubation with 70 µl Streptavidin Particles Plus (BD Biosciences 557812) with a total volume of 200 µl at 4°C for 20 min. CD19+ cells are enriched by 7 min incubation in Cell Separation Magnet Apparatus (BD Biosciences) twice and were snap frozen in liquid nitrogen. Purity was determined using flow cytometry.

B cell differentiation into plasma cells

The procedure was adopted from (Iwakoshi et al., 2003)with some modifications. Briefly, purified B cells were diluted in DMEM containing 10% FBS at a concentration of 5×10^6/ml, cultured in 24-well plate (1 ml per well) and stimulated with 20 µg/ml LPS

(Calbiochem 437627) and 20 ng/ml murine IL-4 (Peprotech 214-14). Cells were collected and snap-frozen in liquid nitrogen for western blots. Proliferating B cells were diluted to 5×10^6/ml with the fresh medium containing IL-4 and LPS every 48 h as described (Iwakoshi et al., 2003).

BrdU incorporation assay

Mice were injected with 20 µl BrdU in PBS (10mM) per g body weight for 2h, which enables incorporation into bone marrow cells. Saline injection was used as control. Bone marrows were flashed out from freshly collected bones. After red blood cell lysis, 10^6 cells were staining against surface CD19 (Biolegend, 1:100 in PBS) at 4°C for 20min. Cells were permeablized and fixed using BD Fixation and Permeabilization kit, followed by incubation in 200 µl DNaseI (50U/ml) at room temperature for 30min. Then cells stained with BrdU-FITC (1:20 in 100 µl BD Permeabilization/Wash Buffer), and incubated at room temperature for 45min before flow cytometry.

Western blot

Cells were lysed in Tris-based lysis buffer (150 mM NaCl, 50 mM Tris, pH7.5, 1 mM EDTA and 1% Triton X-100) supplemented with 1µM DTT and 1x protease inhibitors (Sigma). Supernatant was collected after microcentrifugation at 4°C for 10 min (Yang et al., 2010). Equal amount of supernatant was used for regular western blot on mini SDS-PAGE gels or Phos-tag gels as described in (Yang et al., 2010). Bone marrow cells from 3-4 mice were pooled together for either WT or BKO groups.

Antibodies

GRP78(goat, 1:1000) and HSP90 (rabbit, 1:5,000) were purchased from Santa Cruz (Santa Cruz, CA). p-S51 and total eIF2α (rabbit, 1:1,000), IRE1α (rabbit, 1:1,000), p-S473 and total AKT (rabbit, 1:1,000), p-ERK42/44 (rabbit, 1:2000), p-LYN (rabbit, 1:2000) and CD79A(Igα) (rabbit, 1:1,000) antibodies were purchased from Cell Signaling; SEL1L (rabbit, 1:1000) and CD79B(Igβ) (rabbit, 1:1000) was purchased from Abcam; Calnexin (rabbit, 1:10000) and ERP57 (rabbit, 1:2000) were from Assay Design; HRD1 (rabbit, 1:2000) was from Novus Biologicals. Secondary antibodies were goat anti-rabbit and anti-mouse HRP, and donkey anti-goat HRP used at 1:10,000 (Biorad).

RNA extraction and semiquantitative PCR

Cells from 3-4 mice were pooled together for each group after freshly purified by CD19-biotin beads and magnetic isolation. RNA extraction and cDNA preparation were performed as described previously (Yang et al., 2013). Primer sequences for PCR were adopted from (Maeda et al., 2006; Reynaud et al., 2008; Zhang et al., 2005) and listed as below:

Pax5 F:CGGGTCAGCCATGGTTGTG, R:GTGCTGTCTCTCAAACACG; VpreB1 F:CGTCTGTCCTGCTCATGCTGC, R:ACGGCACAGTAATACACAGCC; Rag1 F:TGCAGACATTCTAGCACTCTGGCC, R:ACATCTGCCTTCACGTCGATCCGG; Ebf1 F:CAAGACAAGAACCCTGAAATG, R:GTAACCTCTGGAAGCCGTAGT; Igα F: TCAGAAGAGGGACGCATTGTG, R:TTCAAGCCCTCATAGGTGTGA; VDJ-Cμ F:CGCGCGGCCGCTGCAGCAGCCTGGGGCTGAG, R:GGAATGGGCACATGCAGATCTC; Igμ F:TGTGTGTACTGTGACTCACAGGGA,

R:AGGGAGACATTGTACAGTGTGGGT; L32 F:GAGCAACAAGAAAACCAAGCA, R:TGCACACAAGCCATCTACTCA.

The PCR conditions are: 94°C for 5min, 94°C for 1min, 58°C for 20sec and 72°C for 30sec repeated for 25 to 30 cycles according to the different abundance of individual template, and followed by 72°C for 10min.

Statistics

Results are expressed as mean ± s.e.m. Comparisons between non-treated group and groups from each time point were made by unpaired two-tailed Student t-test. $P<0.05$ was considered as statistically significant.

4.4 RESULTS

4.4.1 Sel1L BKO mice exhibit systemic B cell reduction.

To study the physiological importance of SEL1L in B cells, we generated B cell-specific Sel1L knockout mice on C57BL/6 background using CD19 promoter, expressing as a commitment marker specifically in B cell lineage (Rickert et al., 1997). Deletion of the 6^{th} exon of Sel1L caused frame-shift and generated a premature stop codon. The resulting truncated SEL1L protein with only a short ER luminal fraction of 232 amino acids was considered non-functional. Therefore, these mice were defined as B cell-specific Sel1L-/- mice (BKO). Genotyping was performed to distinguish WT and BKO animals (Fig. 4.1).

BKO mice were born normally with similar body sizes and weights as WT littermates (Data not shown). The first phenotypic difference we observed in the BKO mice is the

smaller spleen size. Both spleen weights and the ratios between spleen and body weight in BKO mice were significantly lower than those in WT mice (Fig. 4.2 A). To investigate the cellular basis of this phenotype, we analyzed the immune cell composition in WT and BKO spleens by flow cytometry-based immunotyping. The percentage of IgM+IgD+ or B220+IgM+ B cells decreased from 40% to around 10%, while the percentages of CD4+CD8- T cells and CD4-CD8+ T cells doubled in the spleens of BKO mice compared to WT controls (Fig. 4.2B), indicating a loss of B cells and corresponding increase of T cell occupation. The absolute cell numbers per spleen were also calculated for CD4+CD8- and CD4-CD8+ T cells, CD11b+ myeloid cells and IgM+IgD+ B cells. BKO mice showed an 8 fold-reduction of B cell number while having comparable cell numbers for the other immune cell types (Fig. 4.2C). Thus, B cell Sel1L deficiency specifically reduced B cell in spleen leaving other population intact.

Similar decreases of B220+IgM+ B cell percentages and increases of CD4+ or CD8+ T cell percentages were also detected in other peripheral lymph organs such as lymph nodes and blood (Fig. 4.2D). Both numbers and sizes of Peyer's patches in the gut immune system decreased dramatically (Fig. 4.2E and data not shown). The cellular reduction was due to loss of both naïve B cells (B220+CD138-) and activated B cells (B220+CD138+) (Fig. 4.2F). Peyer's patches consisted of two B cell subtypes: bone marrow-generated CD5-B220+ B2 cells and fetal liver-originated CD5+B220+ B1 cells. Immunotyping CD5 indicated that the population shrinkage of B2 cells was the major reason for peyer's patch B cell deficiency (Fig. 4.2F). Taken together, the data indicated a systemic

reduction of B cells in BKO mice, pointing to possible B cell developmental defect in the bone marrow.

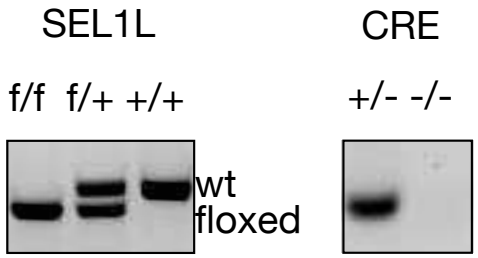

Figure 4.1 Mouse genotyping examples. SEL1Lf/f; CRE+/- and SEL1Lf/f; CRE-/- parents generate SEL1Lf/f; CRE+/- (BKO) and SEL1Lf/f; CRE-/- (Wild type) offsprings. On the left panel, PCR product of LoxP flanked SEL1L migrate faster on agarose gel compared to product from wild type allele. On the right panel, only CRE positive mice result in a PCR product of 100bp.

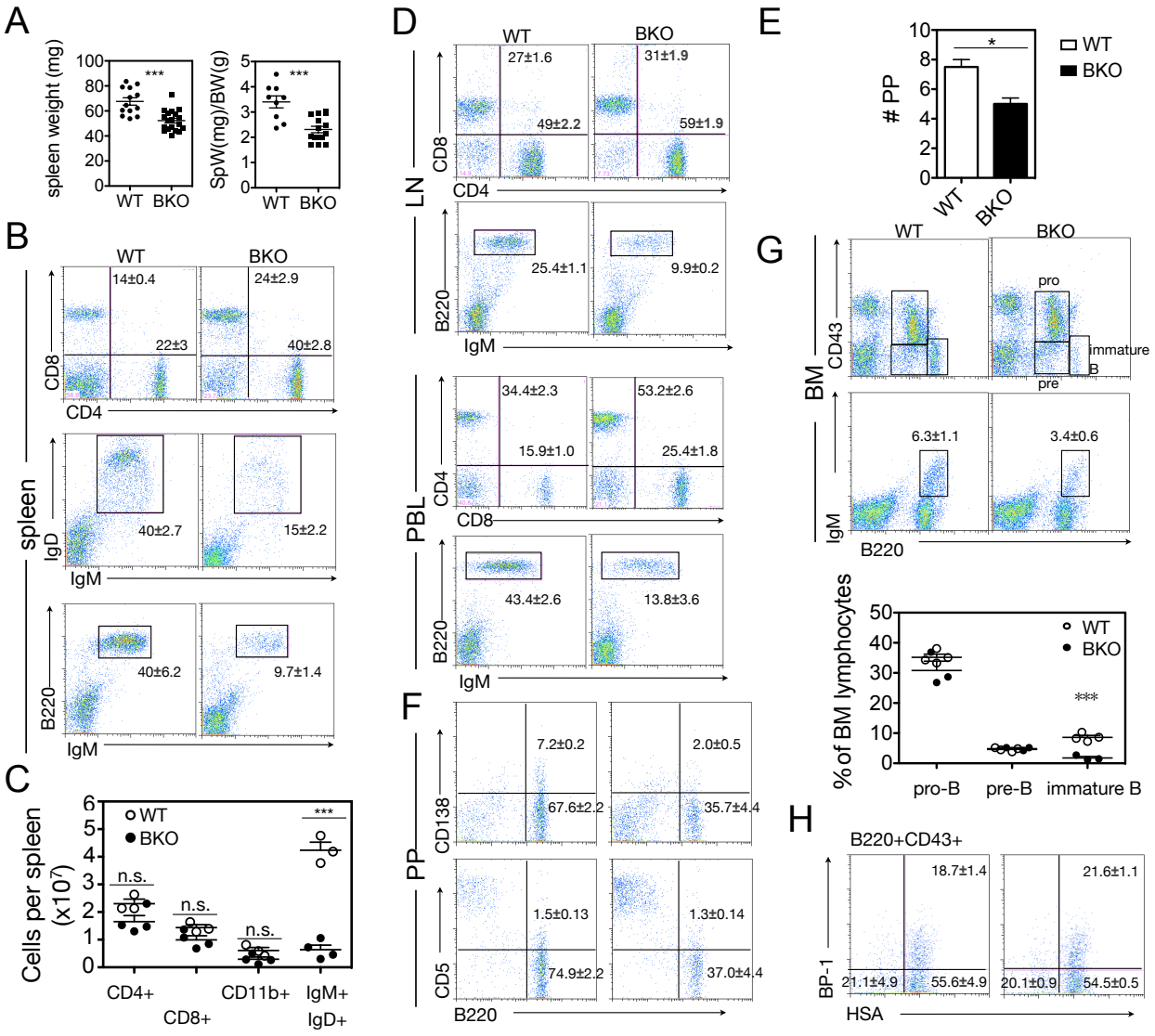

Figure 4.2 Impairment of B cell development in bone marrow leading to decrease of B cellularity in peripheral tissues. (A) Comparison of spleen weight (left) and the ratio between spleen (SpW, mg) and whole body weight (BW, g) (right) in WT and BKO mice. (B) Immunotyping of splenic B and T cell population in WT and BKO mice. Upper: CD4 versus CD8 flow cytometry profiles of T4 (CD4+CD8-) and T8 cells (CD4-CD8+). Middle: IgM versus IgD flow cytometry profiles of mature B cells (IgM+IgD+). Bottom: IgM versus B220 profiles of B cells (B220+IgM+). The numbers indicate the

percentages of each gated population out of total splenocytes. (C) Absolute cell numbers of CD4+ T cell, CD8+ T8, myeloid (CD11b+) and B (IgM+IgD+) cells in WT (open circles) and BKO (solid circles) spleens. (D) CD4 versus CD8 and IgM versus B220 flow cytometry profiles of T cells and B cells in lymph nodes (LN) and peripheral blood (PBL). The numbers indicate the percentages of each gated population out of total cells. (E) The peyer's patch (PP) number per mice. WT (white bar) and BKO (black bar). (F) Upper: B220 versus CD138 immunotyping profiles for activated B cells (plasma cells, B220+CD138+) and naive B cells (B220+CD138-). Bottom: B220 versus CD5 profiles for B2 (B220+CD5-) and B1 (B220+CD5+) B cells. The numbers indicate the percentages of each gated population out of total CD45+ lymphocytes in peyer's patches. (G) Bone marrow immunotyping. Upper: B220 versus CD43 reveals pro-B (B220+CD43+), pre-B (B220+CD43-) and immature B (B220hiCD43-, also contains a small fraction of mature B). Quantification as shown at the bottom of (G). Middle: B220 versus IgM profiles show B cell receptor IgM+ bone marrow B cells (B220+IgM+). The numbers indicate the percentages of B220+IgM+ in gated bone marrow cells. (H) HSA versus BP-1 flow cytometry profiles of gated B220+CD43+ B cell progenitors. Data are representative of two to four independent experiments with n=3-5 mice per group. Quantification is shown as mean ± s.e.m.. *, $p<0.05$. ***, $p<0.001$.

4.4.2 B cell development is defective in BKO bone marrows

Since BKO mice had fewer peripheral B cells, we next examined the B cell development in bone marrows of both groups. The B220+CD43+ B cell progenitors (pro-B) and the B220+CD43- precursors (pre-B) were comparable between BKO and WT mice. However, there was a significant drop for B220hiCD43- immature B cells (Fig. 4.2 G). Immature B is the first population in the development to express complete B cell receptors and can be stained as IgM+. The developmental blockage before immature B cell stage was confirmed by the 50% reduction of B220+IgM+ cells (Fig. 4.2G). B220+CD43+ progenitors can be further divided into three subsets by BP-1 and HSA according to Hardy's standard (Hardy and Hayakawa, 2001; Hardy et al., 1991). Thus, we analyzed the sub-population composition by flow cytometry, but found similar patterns for the three early progenitors between the two genotypes (Fig. 4.2H). Thus, we concluded that SEL1L plays an indispensable role in B cell development. SEL1L deficiency blocks relatively late development before the immature B cell stage.

Interestingly, the residual peripheral B cells remained responsive to antigen stimulation and differentiated into plasma cells normally ex vivo. Same numbers of splenic B cells were purified by negative magnetic purification from either WT or BKO spleens, with the purity of 90% (data not shown), and plated in culture media supplemented with lipopolysaccharide and Interleukin 4 (LPS/IL4). Stimulation of both WT and BKO naïve B cells yielded similar amount of B220+CD138+ plasma cells (Fig. 4.3A). Previous studies indicated the successful recombination rate for CD19-Cre mice was not 100%, which may potentially cause phenotypic leakage in conditional knockout mice (Rickert et

al., 1997). It was possible that the B cell progenitors with unsuccessful CRE-dependent Sel1L deletion managed to develop and partially popularize the peripheral lymph organs. Indeed, we observed same levels of SEL1L protein in purified BKO and WT splenic B cells, confirming that the residual B cells in BKO spleen were in fact “WT” B cells (Fig. 4.3B). If not the conditional knockout leakage, we might expect even more severe B cell loss in BKO mice.

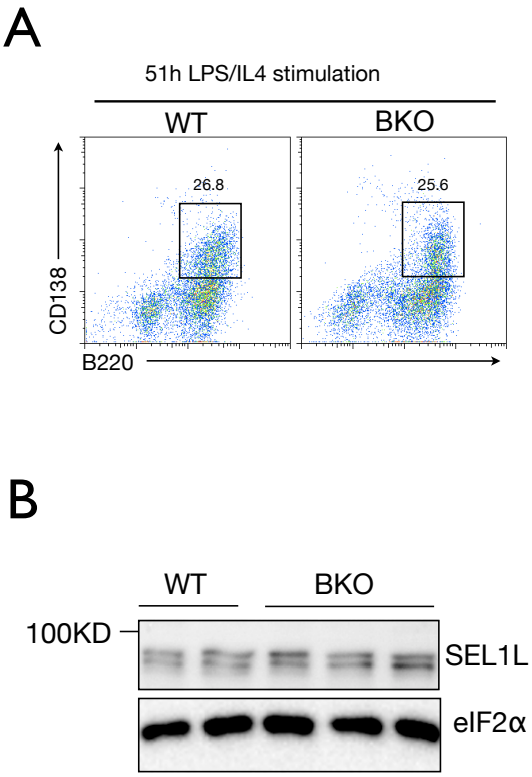

Figure 4.3 The residual B cells in BKO spleen are normal B cells resulted from unsuccessful CRE recombination. (A) After negative purification, same numbers of B cells from WT or BKO spleens were stimulated with 20 μg/ml LPS and 20 ng/ml murine IL-4. B220 versus CD138 flow cytometry profiles show B220+CD138+ plasma cells after 51h stimulation. The numbers represent percentages of plasma cells out of total cells. (B) Western blot against SEL1L in WT and BKO B cells. Each sample contains the same amount of purified splenic B cells from either WT or BKO mice. eIF2α as loading control.

4.4.3 ER stress is not the cause for developmental defect in SEL1L null B cells.

ERAD removes and degrades terminally misfolded peptides from ER, and is required to maintain ER homeostasis. Accumulation of misfolded proteins activates multiple a cascade of stress responses - unfolded protein response (UPR), which not only restore ER homeostasis by enlarging ER folding capacity and reducing nascent peptide loading, but also promote apoptosis under prolonged or severe ER stress (Tabas and Ron, 2011; Walter and Ron, 2011).

In previous studies, loss of SEL1L leads to multiple pathological outcomes including embryonic lethality, pancreas development defect, diet-induced pancreas dysfunction and neuron diseases, presumably mediated by cell death signaling pathways under prolonged ER stress (Francisco et al., 2010; 2011; Kyöstilä et al., 2012; Li et al., 2010b). To investigate the apoptosis level in our case, we examine the phosphatidylserine (PS) externalization levels and plasma membrane integrity by Annexin V and 7AAD respectively. Neither increased cell death (7AAD+Annexin V+) nor early apoptotic cells (7AAD-Annexin V+) was detected in BKO bone marrow B220+ population (Fig. 4.4A). We also performed BrdU proliferation assay and observed even a slight increase of actively duplicating BrdU+ B cells in BKO mice (Fig. 4.4B). Thus, dysregulated apoptosis or proliferation was unlikely the direct development obstacle for BKO B cells.

To test the whether there is overt ER stress in SEL1L-/- B cell precursors, we performed CD19-biotin beads-based magnetic isolation to enrich bone marrow B cell precursors (Fig. 4.5) and screened for UPR markers. SEL1L knockout efficacy was demonstrated

by the dramatic reduction at protein level in CD19+ bone marrow BKO B cells compared to WT B cells (Fig. 4.4C). Remarkably, SEL1L and a UPR sensor IRE1α are only highly expressed in CD19+ cells but not other immune progenitors in the bone marrow, as they are barely detectable in total bone marrow or the flow-through lysates, suggesting a particular high demanding for ER capacity in B cell lineage (Fig. 4.4C). HRD1 protein also decreased in CD19+ cells with SEL1L deficiency (Fig. 4.4C), which is consistent with the previous report that Hrd3p, the yeast SEL1L maintains the stability of hrd1p (Gardner et al., 2000). Surprisingly, we observed no increase of common ER stress markers, including UPR downstream targets phospho-eIF2α, chaperones GRP78 (Fig. 4.4C), ERP57, CXN (Fig. 4.6) and PDI (data not shown). *Xbp1* mRNA splicing by IRE1α activation also remained the same between BKO and WT CD19+ cells (Fig. 4.4D). The Phos-tag gel assay showed no phosphorylated IRE1α band, indicating that the IRE1α was inactive during B cell development (Fig. 4.6). These data together showed that ER homeostasis remained unchanged in despite of ERAD deficiency, and may not be responsible for the B cell developmental defect.

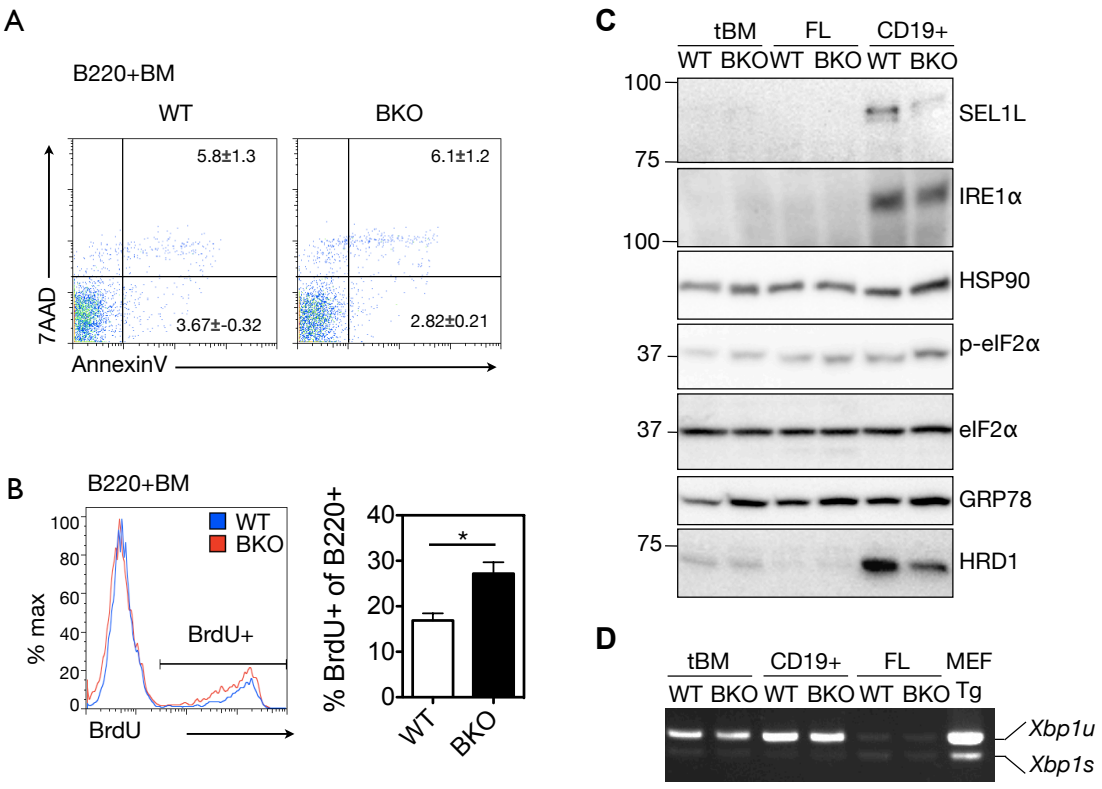

Figure 4.4 No ER stress in BKO mice compared to WT mice. (A) AnnexinV versus 7AAD flow cytometry profiles of B220+ bone marrow B cells. The numbers are percentages of early apoptotic cells (AnnexinV+7AAD-) and dead cells (AnnexinV+7AAD+) out of total bone marrow B cells. (B) Histogram of BrdU incorporation in B220+ bone marrow B cells. Percentage quantification on the right. White bar: WT; Black bar: BKO. *, $p<0.05$. (C) Western blot against SEL1L, HRD1 and UPR components after positive magnetic purification. Whole cell lysates from total bone marrows (tBM), enriched CD19+ B cells (CD19+) and flow-through cells (FL). HSP90, loading control. (D) RT-PCR reveals the *Xbp1* splicing levels in total bone marrows (tBM), enriched CD19+ B cells (CD19+) and flow-through cells (FL). Mouse embryonic fibroblast (MEF) cells treated with 300nM ER stress inducer thapsigargin as positive

control. *Xbp1u*: PCR product from unspliced *Xbp1* mRNA. *Xbp1s*: PCR product from spliced *Xbp1* mRNA. Cells isolated from 3-4 mice were pooled together for each sample group in (C) and (D).

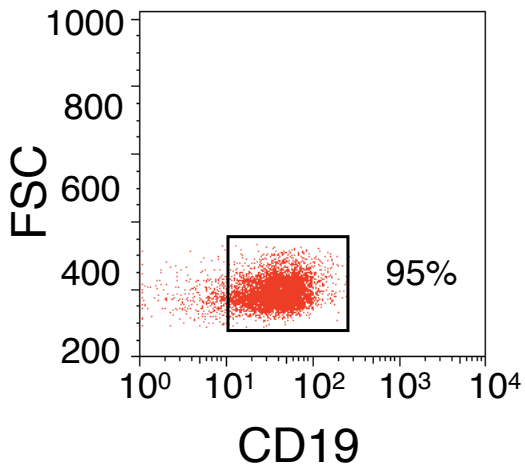

Figure 4.5 Bone marrow CD19+ B cell purification efficiency. Flow cytometry of B cells freshly isolated by positive purification from mouse bone marrow. The number indicates the percentage of CD19+ B cells out of total purified cells.

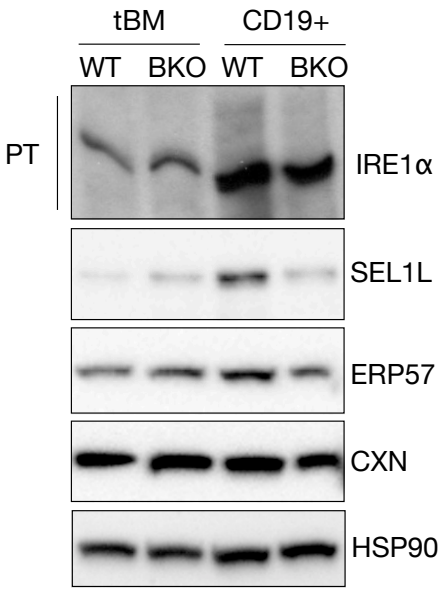

Figure 4.6 Western blots against additional UPR markers. Whole cell lysates from total bone marrows (tBM), and enriched CD19+ B cells (CD19+) were run on Phos-tag gel (PT) or regular SDS-PAGE gels. Cells from 3 mice were pooled for each sample.

4.4.4 Loss of SEL1L leads to dysregulated preBCR signaling pathways

Surface expression of many receptors is crucial for B cell development, as the receptors are responsible for coordinating signals from niche environment with intercellular development events. Particularly, there are two key checkpoints to determine the B cell differentiation before the immature B cell stages. One of them is IL-7R receptor maintaining early lymphocyte expansion (Peschon et al., 1994). The other is the preBCR mediated signaling pathways for differentiation and proliferation. Disruption of either checkpoint strongly impairs maturation of B cells in bone marrows, a phenotype highly reminiscent of the observation in our mice. An immunotyping screen was performed at the two checkpoint receptors as well as cKIT, the receptor for stem cell growth factor (SCF), which also plays indispensable role in B cell development. The data showed unchanged IL-7R α chain (IL-7Rα), and surrogate light chain VpreB on the surface of B220+ cells in WT and BKO mice. Heavy chain Igμ and adaptor protein Igβ, two preBCR and BCR components showed about 50% decreases on B220+ cells and almost 80% reduction on B220hi cells, while common adaptor Igα also dropped from 1.8% to 0.8% (Fig. 4.7A).

As SEL1L participates in ER protein degradation, we also investigated total proteins of above-mentioned receptors at both surface and intracellular levels. The most striking difference was the 4-fold increase of total VpreB (Fig. 4.7B). The induction was mostly attributed to intracellular accumulation, as very few VpreB was detected on the plasma membrane (Fig. 4.7A). IL7R level was also higher in BKO, but to a much less extent (~50% increase). On the contrary, Igα, Igβ, and Igμ all decreased, with more dramatic

reduction for Igβ and Igμ. The percentages of cKIT+ cells were quite small and showed no difference between two genotypes. Together, the surface and total staining indicated that SEL1L deficiency has the greatest influence on the surface production of preBCR receptors. Of note, transcriptional expression of surrogate light chains starts at pro-B and can be detected intracellularly (Wang et al., 1998). The preBCR abnormality in SEL1L BKO mice became obvious as early as the B220+CD43+ progenitor stage (Fig. 4.8).

The preBCR defect was also confirmed at the downstream signaling pathway. CD19+ bone marrow B cells were separated into three fractions via positive purification. Same amount of lysate from total bone marrow, CD19- flow-through and enriched CD19+ cells were run on the SDS PAGE gels (Fig. 4.9A). Consistent with the flow cytometry data, intensity of Igβ and Igμ bands were much weaker in BKO CD19+ cells. The flow through showed some Igμ heavy, suggesting residual CD19+ cells in this fraction after purification. However, the general efficiency was satisfactory as no Igβ was detected in FL. Src-family protein tyrosine kinase LYN is one of the immediate preBCR effector interacting with the cytosolic domains of adaptors Igα and Igβ (Gauld and Cambier, 2004). LYN-/- mice also exhibits decreased peripheral B cells (Chan et al., 1997). Compared to WT, BKO B cell progenitors have less phosphorylated LYN, the active form of LYN, and reduced phospho-AKT and phospho-ERK, supporting the idea of impaired preBCR signaling pathways. Interestingly, total AKT also decreased in BKO, the reason of which remained unknown (Fig. 4.9A).

In addition, we performed RT-PCR and detected reduced mRNA levels of RAG1, a key recombinase required for functional light chain synthesis, and less VDJ-Cu products (Fig. 4.9B). preBCR signaling induces downregulation and subsequential re-expression of RAG recombinases. Re-expression of RAGs is critical for light chain gene rearrangement and BCR production. Thus, the low surface expression of BCR (IgM) (Fig. 4.2G lower panel) suggests lack of light chain recombination, which may be the direct cause blocking the transitions from pre-B to immature B. The mRNA levels of other B development genes such as B cell transcription factors PAX and EBF1, adaptor Igα, immunoglobulin heavy chain Igμ, and surrogate light chain VpreB remained unchanged in BKO cells. Of note, the unchanged VpreB mRNA levels demonstrated that the cellular accumulation of VpreB protein was not due to the transcriptional induction.

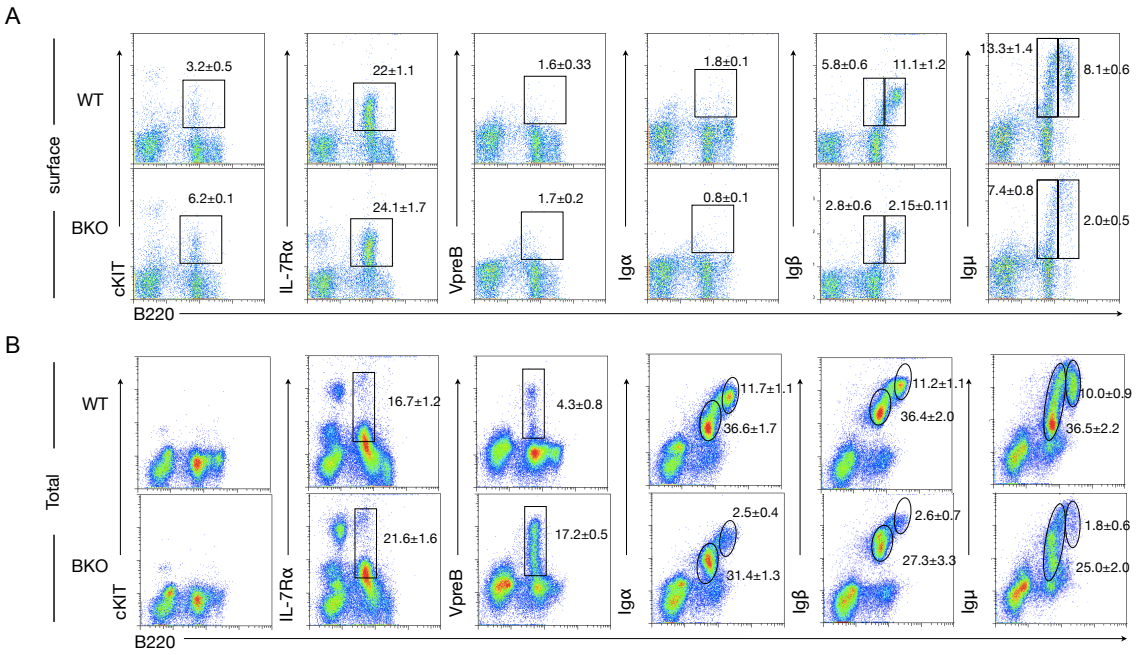

Figure 4.7 Loss of SEL1L leads to dysregulated preBCR signaling pathways. (A) Flow cytometric profiles showing B220 versus surface levels of receptor components cKIT, IL-7Rα, VpreB, Igα, Igβ or Igμ in bone marrow B cells on WT and BKO bone marrow cells. (B) Flow cytometric profiles showing B220 versus total (surface and intracellular) levels of receptor components cKIT, IL-7Rα, VpreB, Igα, Igβ or Igμ in bone marrow B cells on WT and BKO bone marrow cells. The numbers are percentage of gated cells, as mean ± s.e.m..

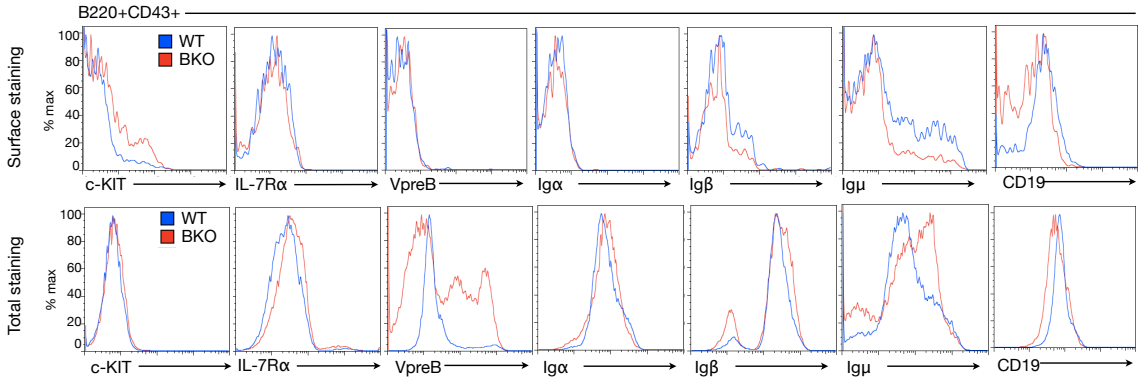

Figure 4.8 surface expressions of receptors that are critical for B cell development on early B cell progenitors. Overlaying histograms showing surface (upper) and total (bottom) staining of receptor components cKIT, IL-7Rα, VpreB, Igα, Igβ, Igμ and CD19 on B220+CD43+ pro-B cells from WT (blue) or BKO (red) mice. x axis represents different levels of each receptor components (from left to right: low to high). y axis represents the % of the highest numbers, and the curves show the relative population distribution with different levels of each receptor components.

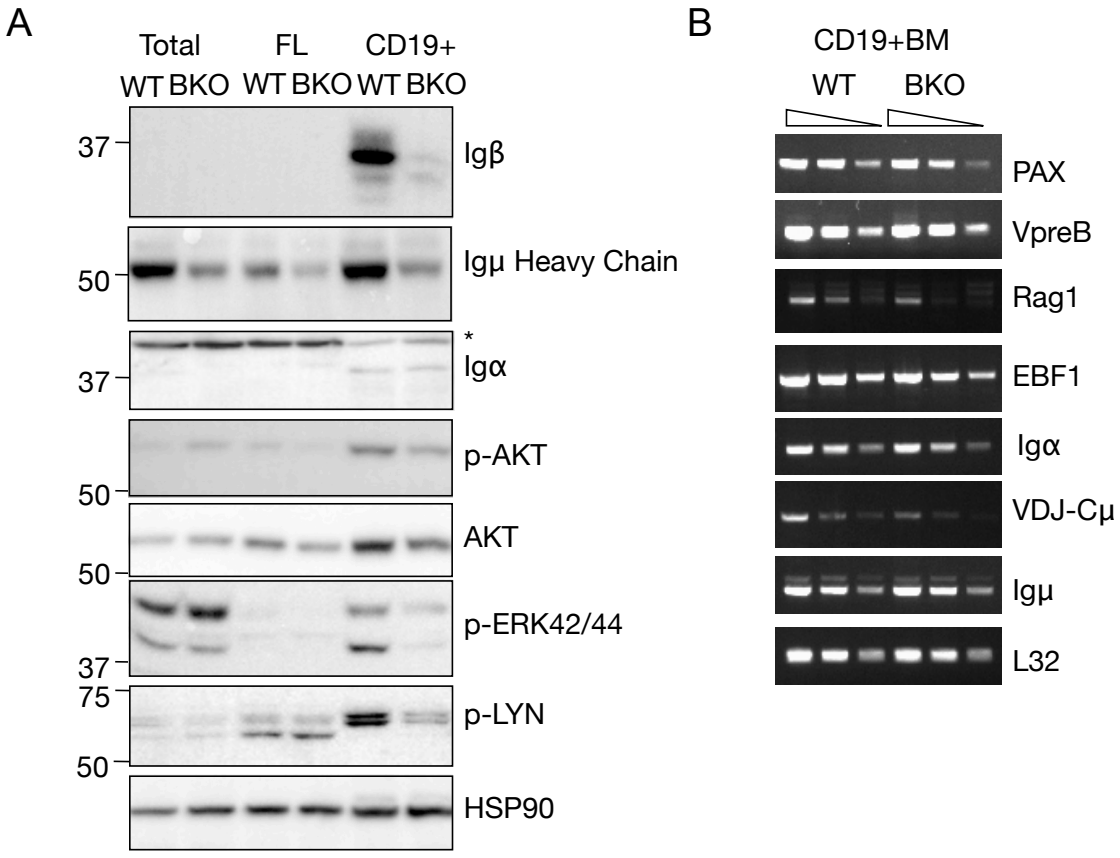

Figure 4.9 preBCR downstream signaling pathways are impaired in BKO. (A) Western blot against preBCR components (Igα, Igβ, Igμ) and downstream signaling effectors (phospho-AKT, phospho-ERK, phospho-LYN) after positive magnetic purification. Whole cell lysates from total bone marrows (tBM), enriched CD19+ B cells (CD19+) and flow-through cells (FL). HSP90, loading control. *: non-specific bands. (B) Semiquantitative PCR of cDNA from freshly isolated WT and BKO CD19+ bone marrow B cells (CD19+BM).Wedges indicate 1:3 serial dilution of cDNA. Data are representative of at least two independent experiments.

4.5 DISCUSSION

preBCR is the key checkpoint signaling guiding B cell precursors to the next stage for an immature B cell repertoire. This positive selection by functional preBCR serves as quality control ensuring functional heavy chain before light chain production. Our study of Sel1L in B cell reveals an unexpected and remarkable role of ERAD in B cell development. ERAD pathway facilitated by core adaptor SEL1L may degrade surrogate light chain VpreB to delicately control the normal surface expression of preBCR and maintains normal preBCR signaling pathways, which is critical for B cell development.

SEL1L was first linked to development in a C.elegans study as a suppressor of Notch signaling pathway (Sundaram and Greenwald, 1993) and was later shown to facilitate and organize ERAD complex for protein degradation (Mueller et al., 2006; 2008). The phenotype in our study is more closely related to SEL1L's role in ERAD rather its suppression of Notch signaling. There are four Notch isoforms – Notch1-4. Notch4 is barely detected in lymphocytes (Saito et al., 2003), while Notch2 expression is particularly restricted in mature B cells. Targeted Notch2 deletion impairs marginal zone B cell formation but has no influence on the early development in the bone marrows (Saito et al., 2003). The expression patterns of Notch1 and Notch3 in B cell lineage are similar, with the highest level in pro-B stage (Saito et al., 2003). Transcriptional repression of Notch 1 is a prerequisite for B cell linage commitment, likely mediated by an early B-lineage commitment factor Pax5 (Souabni et al., 2002). However, we detected even lower Notch1 mRNA level in BKO B cells, which is almost beyond detection (Data

not shown). Thus, Notch1 induction may not be the underlying mechanism bridging the SEL1L deficiency to the B cell developmental defects.

On the other hand, the components of preBCR are highly misfolding-prone. Complicated regulation is necessary for its correct folding, assembly and surface expression. Coordinated folding of surrogate light chain is tightly controlled by the split immunoglobulin domain between VpreB and λ5, while λ5 contains a unique region as an intramolecular chaperone to prevent aberrant folding before paired with VpreB (Minegishi et al., 1999). Paired surrogate light chain escorts Igμ to the plasma membrane to enable the association with heterodimer Igα/Igβ for full preBCR complex. Loss of preBCR due to surrogate light chain deficiency significantly impairs pre-B cell expansion (Mundt et al., 2001; Shimizu et al., 2002). Interestingly, compared to BCR, a larger fraction of preBCR fail to exit ER for surface localization even after assembly, which is likely attributed to the intrinsic property of surrogate light chain (Brouns et al., 1996). Unlike conventional light chain, surrogate light chain promotes low levels of Igμ maturation and high level of ER retention, indicated by the accumulation of EndoH sensitive deglycosylated forms of Igμ (Fang et al., 2001). As no overt ER stress was detected in our case, it is highly likely that the overwhelmed VpreB specifically holds Igμ in the ER and prevents migration of preBCR to Golgi for further modification. It seems that a quantitative balance between VpreB and the rest of the components is of comparable importance as the presence of VpreB per se. However, future studies are in need to dissect the detailed mechanism by which VpreB accumulation blocks preBCR surface expression.

One of the remaining questions is the role of HRD1 in VpreB quantity control. SEL1L mainly associates with HRD1 among all the ERAD E3 ubiquitin ligases; and SEL1L and HRD1 share similar the substrate profiles (Christianson et al., 2012). In addition, misfolded client proteins can be categorized as ERAD-L (lumen), ERAD-M (membrane) and ERAD-C (cytosol), based on their topology and lesion location. VpreB is a soluble ER luminal substrate belonging to the ERAD-L pathway, which is dominantly mediated by HRD1 specific ERAD (Bernasconi et al., 2010). Taken together, HRD1 is the top-1 candidate E3 ligase for VpreB degradation. However, only SEL1L but not HRD1 null mice showed retarded growth besides embryonic lethality, suggesting an HRD1-independent function of SEL1L at the development stage (Francisco et al., 2010; Yagishita et al., 2005). It would be interesting to examine the immune system in HRD1 knockout mice to confirm whether it is the E3 ligase responsible for VpreB degradation.

Another intriguing question raised by this study is whether SEL1L and quantity control are also required for other (earlier or later) stages in B cell life history. Our inducible SEL1L knockout mice showed even earlier B cell maturation blockage starting at pro-B, while the mechanism is still under investigation (Data not shown). In addition, the differentiation from naïve B cells to plasma cells stimulates class-switch and production of humongous secretory immunoglobulin such as IgA, IgD, IgE, and IgG, which may require elevated folding capacity as well as degradation machinery. We indeed observed increased SEL1L at both mRNA and protein levels in B cells activated by LPS/IL4. A plasma cell-specific SEL1L conditional knockout model will provide us more

mechanistic and physiological insights into the role of SEL1L protein and ERAD in the control of immunoglobulin production and function.

Taken together, our study for the first time establishes a novel role of ER degradation machinery in the maintenance of B cell development checkpoints. Sel1L related ERAD pathway contributes to not only quality but also quantitative control of preBCR checkpoint complex. Most previous studies of B cell development have only focused on the receptor-initiated signaling network and transcriptional switch of key differentiation. However, animals with dysregulated maintenance machinery phenotypically can copy those in deficiency of B cell specific receptors or transcription factors, indicating that regulation of checkpoint receptor and checkpoint receptor per se are of comparable physiological importance. Our model of ERAD-dependent VpreB quantitative provides another posttranslational regulation mechanism of checkpoint maintenance. More mechanistic studies are required to enhance our understanding of the significance of ER homeostasis in lymphocyte development.

4.6 ACKNOWLEDGEMENT

We thank Drs. Beiyan Zhou (Texas A&M University) and Julia Felippe (Cornell University) for helpful discussions.

L.Y. conceived and designed the experiments and performed most of the experiments. Y.J and H.K performed some of the experiments. L.Y. and Y.J analyzed the data. Q.L. provided sel1l f/f mice. L.Y. wrote the paper.

CHAPTER 5. SUMMARY AND FUTURE DIRECTIONS

Previous studies using pharmacologically induced ER stress models gain us precious knowledge on the mechanisms and molecular outcomes of the UPR activation. On the other hand, increasing in vivo investigations report participation of ER stress and UPR under various physiological or physiological stimuli, even though the conclusions can sometimes be inconsistent and even controversial. We believe multiple measuring methods especially those at the sensor level are highly recommended for better understanding of the physiological UPR. In Chapter 2, I developed Phos-tag based SDS-PAGE gels that separate phosphorylated IRE1α and PERK from their non-phosphorylated inactive forms. This method sensitively monitors the IRE1α and PERK activation in cells transfected with misfolded protein, and reveals interesting patterns of basal IRE1α in various mouse tissues and its activation in pancreas in response to fast-refeeding. In addition, it can be used for quantitation of the ER stress levels, evident by the IRE1α phosphorylation changes corresponding to the time or concentration increases of thapsigargin treatment.

Chapter 3 and Appendix A and C showed several application of this new measuring tool. Together with the detection of downstream events, Phos-tag gel allows us to identify a novel crosstalk between AMPK and the UPR sensors in a screen of metabolic drugs. In the screen, the anti-diabetic reagent phenformin stimulates IRE1α and PERK as well as their downstream targets in both AMPK- and ER stress-dependent manners. However, activation of AMPK is not sufficient to trigger IRE1α and PERK activation. The nature

of the crosstalk remains mysterious. One possibility is that AMPK directly phosphorylates IRE1α and PERK, leading to structural changes and enhanced activities. However, we didn't detect any interaction in co-immunoprecipitation assay between AMPK catalytic domain and IRE1α/PERK. Alternatively, AMPK may modulate other signaling pathways, which may elevate the ER stress levels. In vitro phosphorylation of kinase-dead IRE1α/PERK by AMPK may be needed to test the hypothesis of direct modulation. Impairment of IRE1α-XBP1 pathway protects cells against phenformin toxicity, suggesting the potential physiological significance of the UPR activation in anti-cancer biguanide treatment.

In the case of Chapter 2, examinations on both proximal and distal parts of the UPR reache the same conclusions regarding to the activation status of the UPR. Remarkably, Appendix A shows an interesting situation in which IRE1α phosphorylation disagrees with XBP1 protein and chaperone induction. B cell to plasma cell differentiation was thought to be ER-stress dependent given the induction of XBP1 and chaperones. However, our study for the first time clearly indicates constant IRE1α phosphorylation and decreased PERK phosphorylation through out the differentiation process, even after dramatic XBP1 protein increase is observed. This evidence strongly argues against the stress response model of plasma cell ER expansion while supporting the anticipation model in which programed Xbp1 transcriptional induction enhances the ER capacity before immunoglobulin synthesis. Another example of inconsistency is presented in Appendix C. *Xbp1* mRNA oscillates with constant IRE1 α phosphorylation in the heart, while mRNA expression profiles of the XBP1 targets *Grp78* and *Erdj4* mRNA exhibit

circadian rhythm in liver and WAT without circadian oscillation of *Xbp1s*. This preliminary data also point to the complexity of the in vivo physiological UPR compared to those in in vitro cell culture models.

Chapter 4 was designed to study the possible role of chronic ER stress in B cell development. Defective ERAD machinery is a common cause of misfolded protein accumulation and leads to several conformational diseases. Thus we generated B cell-specific SEL1L-knockout mice, expecting disruption of ER homeostasis and impaired B cell development. Indeed, we observed systemic loss of B cells and defective B cell genesis in bone marrow in mice lacking of SEL1L. To our surprise, no ER stress is detected at both upstream and downstream levels of the UPR, as indicated by both our method and traditional measurements. Current progress suggests the abnormal accumulation of the preBCR component VpreB as the direct cause of developmental blockage. Accumulated VpreB may disrupt normal assembly and/or modification of the key development receptor preBCR, and thus blocks signaling for differentiation. More studies are warranted to dissect the detailed mechanisms by which the ERAD modulates the pre-B cell checkpoints and B cell genesis. The investigation of the ERAD will also add to our understanding of the intimate relation between ER and tissue functions.

Besides investigating the physiological significance of UPR, I also carried on a mechanistic study on a novel IRE1α interacting protein, FARP1. Unfortunately, data showed no functional importance of FARP1 in IRE1α and PERK activation, even though the physical interaction was confirmed (Appendix B).

Taken together, my thesis dissertation reports the development and application of a Phos-tag based method for better understanding the physiological ER quality control machineries, especially the UPR. However, many interesting questions are raised from the dissertation such as the unexpected discovery in Chapter 3. More efforts to characterize the role of ERAD at different stages of B cell development are required for thorough understanding of the ER protein quantity and/or quality control in B lymphocyte maturation. First of all, in vitro mechanistic studies will help us better understand how the SEL1L complex interacts, modifies and degrades the surrogate light chains, as well as how the surrogate light chain accumulation affects the preBCR complex assembly. Secondly, It would be interesting to compare the HRD1 CD19-CRE mice with our SEL1L deficient animal. The possibility of different immunotyping results in the two models remains. In another word, even though the phenotype we observe in $SEL1L^{CD19\text{-}CRE}$ is highly likely to originate from disruption of HRD1 E3 complex, an HRD1-independent SEL1L function is still not impossible. An HRD1 conditional knockout mouse model would reveal the standing of HRD1 in the picture of B cell development. Last but not the least, based on another preliminary study, the role of SEL1L in B cell development is not restricted in the pre-B stage. Inducible whole body SEL1L knockout greatly affects pro-B cell population, although we have no clue for the underlying mechanism yet. In addition, surrogate light chains are rapidly replaced by conventional light chains, which generate the mature BCR before the naïve B cell stage. Thus, we hypothesize that there is similar requirement for SEL1L for quality/quantity control of mature BCR in naïve B cells. To this end, ex vivo B cell-to-plasma cell differentiation needs to be analyzed using Tamoxifen-driven conditional Sel1l deletion in

B cells. I anticipate that the induced SEL1L loss would greatly impair plasma cell differentiation. Besides the inducible knockout mouse model, specific SEL1L deletion in plasma cell will be another valuable tool for both physiological and mechanistic studies. B cell activation upon antigen immunization as well as BCR (light chain, particularly) modification, localization, secretion and degradation should also be closely examined. Accumulation of conventional light chains might occur, affecting expression and secretion of antibodies.

APPENDIX A. TRANSCRIPTION UPREGULATION OF XBP1 RESETS PROTEOSTASIS BOUNDARY DURING PLASMA CELL DIFFERENTIATION WITH NO OVERT UPR ACTIVATION

A.1 INTRODUCTION

Homeostasis in the endoplasmic reticulum (ER) is tightly monitored by the ER-to-nucleus signaling cascades, called unfolded protein response (UPR) (Ron and Walter, 2007). B cell differentiation into immunoglobulin (Ig)-secreting plasma cells has been long considered to be the best example of UPR activation under physiological settings (Iwakoshi et al., 2003; Reimold et al., 2001; Todd et al., 2008; Zhang et al., 2005). Plasma cells produce large amounts of secreted IgM and IgG whereas naïve B cells express the membrane-bound IgM at a much lower level. Cells or mice deficient in IRE1α or XBP1 exhibit severe defects in ER homeostasis and plasma cell formation (Iwakoshi et al., 2003; Reimold et al., 2001; Zhang et al., 2005). Intriguingly, unlike the IRE1α-XBP1 branch, the PERK branch of UPR is dispensable for B cell differentiation (Gass et al., 2008; Ma et al., 2009), leading to the speculations of either a selective activation (Rutkowski and Kaufman, 2007) or repression (Ma et al., 2009; Wu and Kaufman, 2006) of UPR branches. Here our data show that ER homeostasis was not breached by massive Ig biosynthesis in differentiating B cells, but was rather progressively reset to a new homeostasis through XBP1s transcriptional activity prior to the oncoming waves of antibody load. Thus, in contrast to the current dogma, overt UPR

activation is bypassed during B cell differentiation to antibody-secreting plasma cells, representing a novel scenario for physiological processes associated with changes in demands of protein synthesis and folding in the ER.

A.2 MATERIALS AND METHODS

Animals

Wildtype C57BL/6 mice were either purchased from the Jackson Laboratory or bred in the Cornell Weill Mouse Facility. 8-12 mice at age of 6-8 weeks were used in every B cell differentiation experiment.

Magnetic beads purification (negative selection)

B-cell purification from spleens was carried out using the BD IMagTM Cell Separation System (BD Biosciences). Spleens were gently pushed through 70 µm nylon mesh (Fisher Scientific 22363548) to yield single cell suspension. Red blood cells were lysed on ice for 1 min in ACK lysis buffer (0.15 M NH4Cl ,1 mM KHCO3 ,0.1 mM Na2EDTA, pH 7.2). After two washes with 10 ml PBS (137mM NaCl, 2.7mM KCl, 4.3mM Na2HPO4, 1.4mM KH2PO4, pH 7.4) containing 2% BSA, 10^8 splenocytes were incubated with 5 µl biotin-conjugated anti mouse CD3 antibody and 3 µl biotin-conjugated anti mouse CD11b antibody (UCSF Monoclonal Antibody Core Facility, 0.5 mg/ml) with a total volume of 100 µl at 4°C for 20 min followed by incubation with 60 µl Streptavidin Particles Plus (BD Biosciences 557812) with a total volume of 300 µl at 4°C for 20 min. Cells were transferred to a 12 × 75 mm tube which was inserted into a Cell Separation Magnet Apparatus (BD Biosciences) for 5 min. Cells from the flow-

through, i.e. the CD3- and CD11b-negative portion, were collected, washed with PBS and then resuspended in 1 ml DMEM culture medium. Purity was determined using flow cytometry. Normally over 90% cells were B220+ cells (Fig. A1). Of note, CD3 antibody targets T cells while CD11b antibody recognizes monocytes, macrophages, eosinophils, granulocytes and NK cells.

B cell differentiation into plasma cells

The procedure was adopted from (Iwakoshi et al., 2003; Shaffer et al., 2004) with some modifications. Briefly, purified B cells were diluted in DMEM containing 10% FBS at a concentration of 5×10^6/ml, cultured in 24-well plate (1 ml per well) and stimulated with 20 μg/ml LPS (Calbiochem 437627) and 20 ng/ml murine IL-4 (Peprotech 214-14). Cells were collected and snap-frozen in liquid nitrogen at different time points. Proliferating B cells were diluted to 5×10^6/ml with the fresh medium containing IL-4 and LPS every 48 h as described (Iwakoshi et al., 2003).

Protein lysates

Cells were lysed in Tris-based lysis buffer (150 mM NaCl, 50 mM Tris, pH7.5, 1 mM EDTA and 1% Triton X-100) supplemented with 1 μM DTT and 1x protease inhibitors (Sigma). Supernatant was collected after microcentrifugation at 4°C for 10 min.

Nuclear-cytosolic fractionation

Nuclear extraction for cells were performed as we previously described (Sha et al., 2009).

Western blot and Phos-tag gels

Bradford assay (BioRad) was used to measure protein concentrations of whole cell lysate or nuclear extraction. 15-30 μg of whole cell lysates or 5-10 μg of nuclear extracts were used for regular western blot on mini SDS-PAGE gels. Phosphorylated IRE1α were separated from non-phosphorylated proteins using Phos-tag gels as previously described (Yang et al., 2010).

Antibodies

XBP1 (XBP1u/s-specific, rabbit, 1:1,000), and HSP90 (rabbit, 1:5,000) were purchased from Santa Cruz; p-eIF2α, IRE1α and PERK (rabbit) antibodies were purchased from Cell Signaling and used at 1:1,000–2,000. CREB antibody (rabbit, 1:6,000) was from Dr. Marc Montminy (Salk Institute). Primary antibodies were diluted in 5% milk/TBST or 2% BSA/TBST and incubated with PVDF membrane overnight at 4°C. Secondary antibodies were goat anti-rabbit IgG HRP (Jackson ImmunoResearch) used at 1:10,000.

RNA extraction, Q-PCR and RT-PCR

RNA extraction and Q-PCR were performed as described previously (Sha et al., 2009). All Q-PCR data were normalized to ribosomal l32 gene in the corresponding sample. Primer sequences as listed below: L32 F: 5'-GAGCAACAAGAAAACCAAGCA-3', R: 5'-TGCACACAAGCCATCTACTCA-3'; Xbp1 F: 5'-ACATCTTCCCATGGACTCTG-3', R: 5'-TAGGTCCTTCTGGGTAGACC-3'; Sel1L F: 5'-TGGGTTTTCTCTCTCTCCTCTG-3', R: 5'-CCTTTGTTCCGGTTACTTCTTG-3'; P58ipk F: 5'-GTGGCATCCAGATAATTTCCAG-3', R: 5'-

GAGTTCCAACTTCTGTGGAAGG-3'; Grp94 F:5'-CTCAGAAGACGCAGAAGACTCA -3', R: 5'-AAAACTTCACATTCCCTCTCCA-3'; Myc F:5'-TGAGCCCCTAGTGCTGCAT-3', R: 5'-TCAATTTCTTCCTCATCTTCTTGCT-3'; Blimp-1 F: 5'-GGGAAACCCAAGAGCCTTAC-3', R: 5'-GCTTGCTAGCATGTGTGGAA-3'; Chop F: 5'-TATCTCATCCCCAGGAAACG-3', R: 5'-GGGCACTGACCACTCTGTTT-3'; Gadd34 F: 5'-AGGACCCCGAGATTCCTCTA-3', R: 5'-CCTGGAATCAGGGGTAAGGT-3'.

RT-PCR analysis of spliced and unspliced Xbp1 was performed as described (Sha et al., 2009)

Measurement of ER/Golgi size

To measure ER/Golgi size, $2x10^5$ B cells at different stages of differentiation were collected and incubated in 200µl of culture medium containing 0.4 µg/ml Brefeldin A BODIPY (Invitrogen) for 30 min at 4°C. Then cells were washed once and suspended in 200 µl PBS for immediate flow cytometry analysis.

Measurement of intracellular IgG levels

For intracellular staining, stimulated B cells were collected as indicated and incubated in 200 µl of 70% ethanol for 20 min at 40°C. Following three washes with PBS, cells were kept in 1% formaldehyde until all time points were collected. Cells were washed three times with PBS, incubated with 20 µl of antibodies diluted at optimal concentrations for 45 min at 4°C, and resuspended in 400 µl PBS for analysis using the FACSCalibur flow

cytometer (BD Biosciences). Data were analyzed using the CellQuest software (BD Biosciences). Antibodies used for flow cytometry in this study with final concentrations were: 5 µg/ml PE anti-mouse CD45R/B220 antibody (BD Biosciences 103207), 5 µg/ml PE- Rat IgG2b, kappa isotype control (BD Biosciences 553989), and 6 µg/ml FITC-conjugated anti-mouse IgG (Jackson ImmunoResearch 715-095-151). Of note, anti-IgG antibody recognizes both IgG heavy chain and the common light chain shared by other Ig such as IgM expressed in mature B cells.

Statistics

Results are expressed as mean ± s.e.m. Comparisons between non-treated group and groups from each time point were made by unpaired two-tailed Student t-test. $P<0.05$ was considered as statistically significant. All experiments were repeated at least twice and representative data or data on average are shown.

A.3 RESULTS

We purified splenic B220+ B cells (Fig. A1) and differentiated them to plasma cells using standard LPS and IL-4 stimulation (Iwakoshi et al., 2003; Shaffer et al., 2004). In keeping with previous observations (Federovitch et al., 2005; Gass et al., 2002; Iwakoshi et al., 2003; Reimold et al., 2001; van Anken et al., 2003; Zhang et al., 2005), cells progressively exhibited characteristic changes such as enlarged cell size (not shown), reciprocal regulation of Blimp and c-Myc genes (Fig. A2-A). While the induction of total *Xbp1* mRNA occurred early during differentiation starting at 2h (Fig. A2-A), the increase of active XBP1s protein was detected at 16h following LPS/IL-4 treatment (Fig. A2-B).

Q-PCR revealed induction of ER chaperone genes such as well known XBP1-targets *p58ipk, Grp94* and *Sel1l*, but not PERK targets (Fig. A2-C,D). Accordingly, expansion of ER-Golgi mass started at 16 h (Fig. A3-A), an event that is known to be XBP1s-dependent (Shaffer et al., 2004). The extent of ER-Golgi expansion at 16 h of B cell differentiation was comparable to that of MEFs treated with 75 nM thapsigargin (Tg), an ER-stress-inducing drug, for 7 h (Fig. A3-B).

Levels of intracellular Ig significantly increased at around 24 h (Fig. A3-C), preceded by XBP1s protein accumulation and ER-Golgi expansion. Strikingly, no activation of IRE1α was observed during the differentiation, even after 16 h of LPS treatment (Fig. A4-A, B). Of note, LPS per se didn't suppress IRE1α, as tunicamycin (Tm) was able to increase IRE1α phosphorylation in presence of LPS (Fig. A4-C). Further supporting the lack of IRE1α activation, there was no increase in *Xbp1* mRNA splicing during the 16 h and 24 h periods ($P>0.05$) (Fig. A4-D). When both intracellular Ig levels and ER/Golgi mass peaked at 72 h, IRE1α hyperphosphorylation and *Xbp1* mRNA splicing, i.e. IRE1α activation, reached nadir (Fig. A4-B, D). Finally, neither PERK nor its target eIF2α showed increased phosphorylation (Fig. A4-E, F). The inactivation of PERK pathway and the IRE1α phosphorylation status together argue that ER homeostasis has been reset to readily accommodate the protein load in fully differentiated plasma cells without undergoing ER stress.

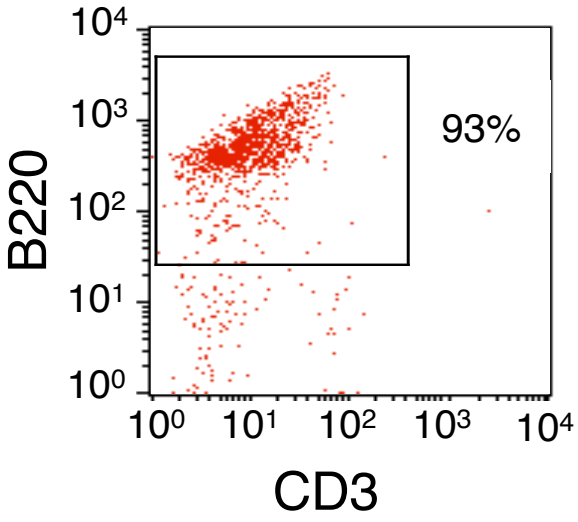

Figure A1 Flow cytometric analysis of purified splenic B cells.

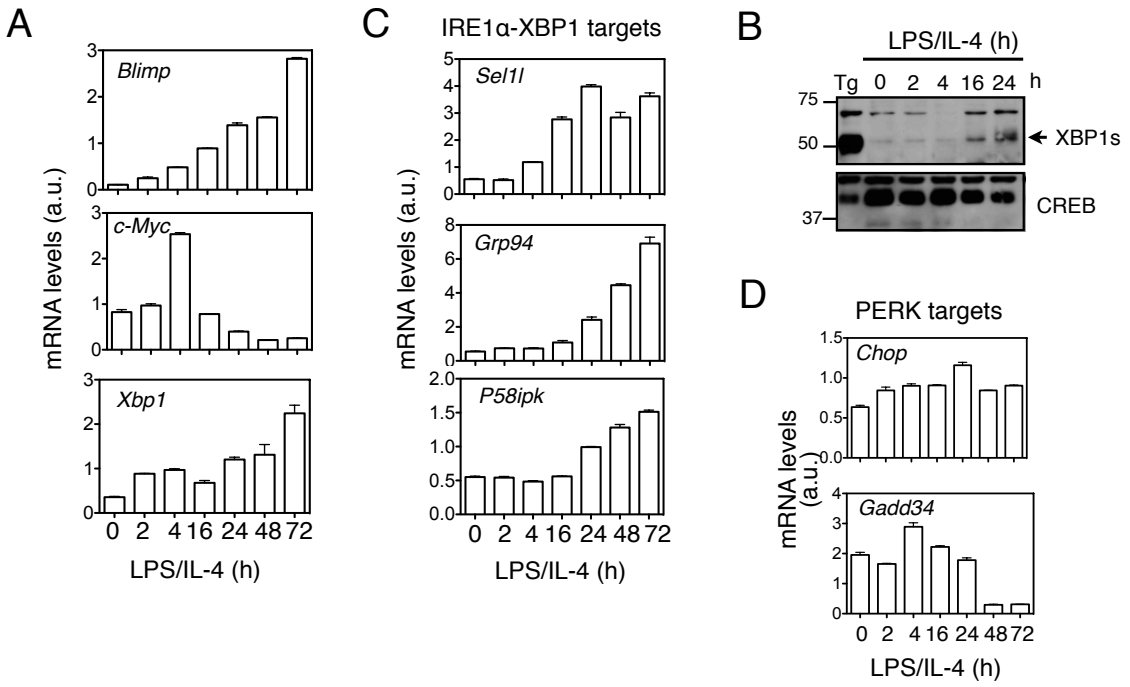

Figure A2 Increases of XBP1s and its targets during B cell to plasma cell differentiation. (A) Q-PCR analyses of *Xbp1* total, *Blimp* and *c-Myc* mRNA in splenic B cells stimulated with LPS and IL-4 at different time points. (B) Immunoblots for XBP1s protein from nuclear extracts of differentiating B cells. CREB, a loading control. Q-PCR analyses was also performed to show the mRNA changes of IRE1α-XBP1 targets (C) and PERK targets (D). Values are mean ± s.e.m. Q-PCR data were normalized to ribosomal L32 gene. a.u.: arbitrary units.

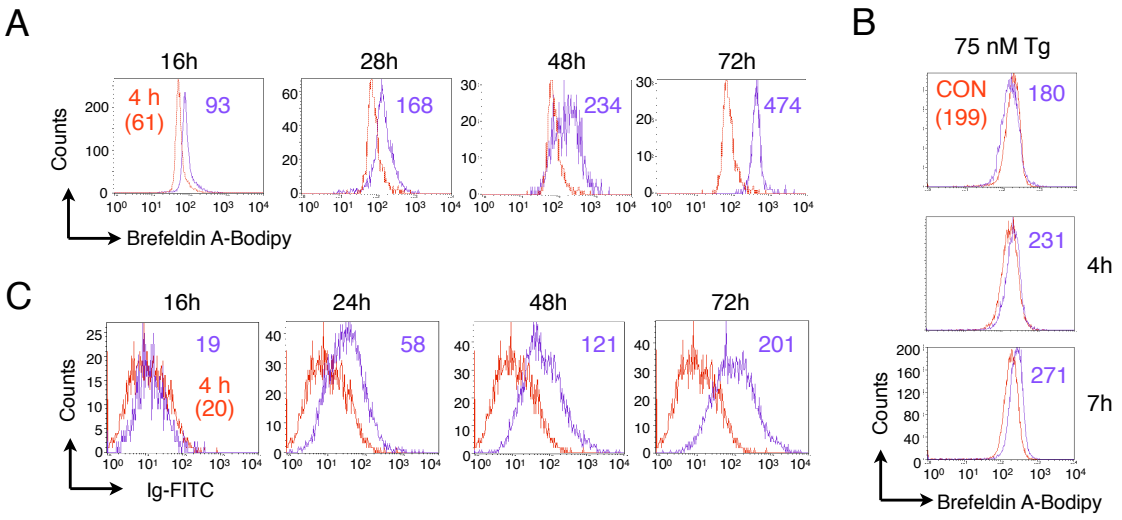

Figure A3 Expansion of ER capacity precedes immunoglobulin synthesis. (A) Flow cytometric analysis of the ER-Golgi mass during B cell differentiation. Cells were stained with ER/Golgi-specific dye brefeldin A-Bodipy. The 4 h time points are used as the control point (to eliminate the possible artifact at 0 h generated in purification procedure) overlaid in red. (B) Flow cytometric analysis of intracellular immunoglobulin (Ig) expression during B cell differentiation, overlaid with 4 h time point. (A-B) are representatives of four independent experiments. Numbers in each histogram of panels A-B refer to the mean channel fluorescence of each peak, i.e. fluorescent intensity. (C) Flow cytometric analysis of the ER-Golgi mass in Tg treated MEF cells. Red line: control, Purple line: treatment.

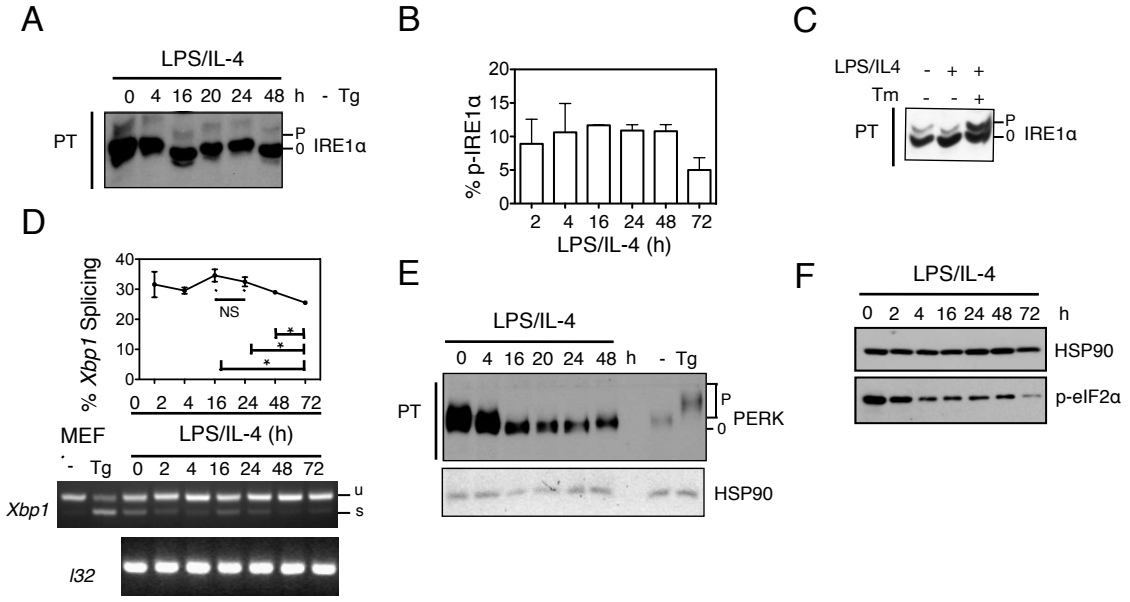

Figure A4 No overt UPR activation during B cell to plasma cell differentiation. (A) Immunoblots of IRE1α using Phos-tag gel (indicated by a bar at the left-hand side). 0-non-phosphorylated, p- phosphorylated. (B) Quantitation of the percent of phosphorylated IRE1α out of total IRE1α in panel A. (C) Immunoblots of IRE1α from LPS/IL4 or Tm treated purified B cells, using Phos-tag gel. (D) RT-PCR analysis of *Xbp1* mRNA splicing (bottom) and quantitation of the ratio of *Xbp1s* to total *Xbp1* from three independent experiments (top). L32, a loading control. Values are mean ± s.e.m.. NS, not significant; *, $P<0.05$ using unpaired two-tailed Student's t-test. Representatives of at least two independent experiments shown. (E) Immunoblots of PERK using Phos-tag gels (indicated by a bar at the left-hand side). Two additional controls, MEF either mock (-) or 75 nM Tg treated for 4 h, included for the PERK blot. (F) Immunoblots of PERK downstream target p-eIF2α on regular SDS PAGE gel. Hsp90, a loading control.

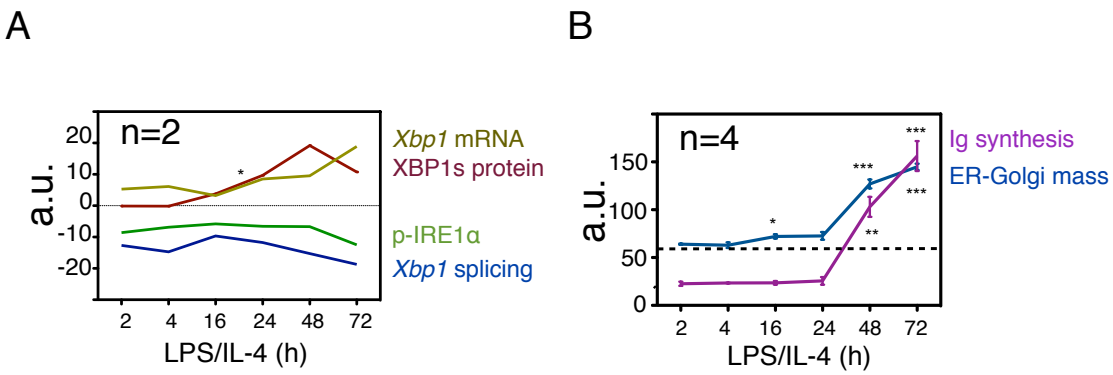

Figure A5 Event dynamics during plasma cell differentiation (Summary of Figure A2-4). (A) Event dynamics of the IRE1α-XBP1 pathway. (B) Event dynamics related to ER volume and protein synthesis. *, P<0.05; **, P<0.01, ***,P<0.001; using unpaired two-tailed Student's t-test.

A.4 DISCUSSION

Our results lead us to conclude that, in contrast to the current dogma, massive Ig synthesis does not cause overt ER stress during differentiation; rather, an increase in *Xbp1 mRNA* (the substrate) induced by differentiation signals at early stages of differentiation (Iwakoshi et al., 2003; Todd et al., 2008) results in accumulation of XBP1s protein via basal IRE1α RNase enzymatic activity. Elevated XBP1s protein is responsible for the augmented ER mass/chaperones and thereby ER homeostasis for the subsequent Ig biosynthesis (Fig A5). The lack of ER stress and subsequent UPR during plasma cell differentiation circumvents the consequences of PERK activation on blockade of protein synthesis. Our model provides another explanation of the functional disparities between the IRE1α-XBP1 and PERK pathways in plasma cell differentiation(Gass et al., 2008; Iwakoshi et al., 2003; Ma et al., 2009; Reimold et al., 2001; Zhang et al., 2005). This scenario seems to be reminiscent of the situation in hormone-stimulated thyrocytes (Christis et al., 2010), where ER chaperones were dramatically increased ahead of large protein load.

XBP1s activation depends on the differentiation signals provided by LPS and IL-4, rather than Ig biosynthesis. Indeed, several recent studies show that XBP1 activation occurs normally in IgM-deficient cells (Hu et al., 2009; McGehee et al., 2009) and precedes an increase in Ig synthesis (Gass et al., 2002). Thus, XBP1s activation is a differentiation- and transcriptional-dependent and UPR-independent event during plasma cell differentiation. As many cell or tissue types have basal levels of IRE1α activity (Yang et

al., 2010), hence *Xbp1* mRNA can be spliced to generate XBP1s protein even in the absence of an overt UPR.

Our data show that, in a choreographed sequence of events, B cells differentiate into plasma cells without the activation of an overt UPR. This represents an alternative model of UPR activation in physiological settings. Previously, we have shown the UPR activation in fasting-refeeding pancreas (Yang et al., 2010), which we speculate may allow the secretion of pancreatic zymogens directly correlated with the amount of food intake and content of nutrients in a more acute setting. As chronically UPR is associated with cell death, we propose that in some physiological events ER stress may be circumvented by the XBP1-mediated upregulation of ER chaperones and capacity and thereby reset of ER homeostasis. This mechanism seems to be evolutionally conserved as a similar mode of transcriptional upregulation of XBP1 homolog Hac1 without overt IRE1 activation has been reported in yeast (Leber et al., 2004).

In summary, our results challenge the notion that plasma cell differentiation is associated with overt ER stress and UPR activation. As cells have high stress adaptability and flexibility in ER homeostasis (Federovitch et al., 2005; Sha et al., 2011), the on/off switch provided by ER stress may not be the only regulatory step of IRE1α-XBP1 pathway in mammals; rather, a transcriptional program-triggered XBP1s induction may provide an alternative molecular mechanism underlying homeostatic regulation of the ER and allow the cell to differentiate and survive. From evolution perspective, this intriguing mechanism may be preferentially selected for specialized secretory cell types such as B cells to fulfill their functional requirement.

APPENDIX B. FARP1, A NOVEL IRE1A INTERACTING PROTEIN

B.1 INTRODUCTION

Under ER stress conditions, IRE1α is activated by direct binding of unfolded protein, and/or disassociated of BIP from IRE1α luminal linker region, which leads to autophosphorylation and oligomerization. Recent studies point out that the activation of IRE1α can be fine-tuned by additional binding proteins, which are together termed as IRE1α interactome or "UPRosome" (Hetz et al., 2011). Reported IRE1α accessory proteins include BAX, BAK, PUMA and BIM, loss of which significantly influence IRE1α activation (Hetz et al., 2006). In addition to the regulatory effects on IRE1α activity, some adaptor proteins initiate a variety of physiological outcomes in responsible to ER stress. For instance, activation of IRE1α leads to phosphorylation of the binding partner TRAF2 and thus activates caspase-12, JNK, ERK, p38 and NFκB, which regulate apoptosis, autophagy and inflammation (Hetz and Glimcher, 2009).

One of the research directions in our lab is to define the detailed mechanism of IRE1α activation. To this end, our lab performed a proteomic screening. The screening successfully identified multiple previously unknown IRE1α interacting proteins. One of the novel adaptor proteins, the non-muscle myosin heavy chain IIB (NMHCIIB), has been proved to be critical for full IRE1α activation including IRE1α foci formation, *Xbp1* splicing and downstream upregulation of XBP1 targets (He et al., 2012). However, how NMHCIIB mediates the activation of IRE1α remains to be unclear.

The fact that NMHCIIB is associated with actin filaments and migrates along the filament network for cargo transportation suggests a potential role of the cytoskeleton system in precise control of IRE1α foci formation and activation. Interestingly, the proteomic screening identified another putative IRE1α- interacting factor, FARP1 (FERM, RhoGEF and pleckstrin domain-containing protein 1), which also involve in cytoskeletal dynamics and organization. FARP1 belongs to the Rho GEF (guanine nucleotide exchange factor) family with a cytoskeleton-associating ezrin-like domain (Koyano et al., 1997). It has been shown to be important for trans-synaptic organization, axonal repulsion and dendritic growth of neurons (Cheadle and Biederer, 2012; Toyofuku et al., 2005; Zhuang et al., 2009). Here, we tested whether FARP1 is physically associated with UPR sensors IRE1α and PERK, and regulates the UPR signaling pathways.

B.2 MATERIALS AND METHODS

Cells

Mouse embryonic fibroblast (MEF) cells were maintained in DMEM supplemented with 10% FBS and 1% penicillin/streptomycin.

Immunoprecipitation

Cells were lyzed in lysis buffer (150 mM NaCl, 1% Triton X-100, 1mM EDTA, 50 mM Tris HCl, pH 7.5) supplemented with protease inhibitor cocktail (Sigma) and 1 mM DTT. Immunoprecipitation was recovered by anti-HA agarose beads for overnight at 4°C. Beads were washed with washing buffer (137 mM NaCl, 1% Triton X-100, 20mM

EDTA, 20 mM Tris HCl, 10% glycerol, pH 7.5) for 5 min at room temperature for a total of four times, and eluted with 2X SDS sample buffer for future Western blot.

Western blots

Bradford assay (BioRad) was used to measure protein concentrations of whole cell lysate or nuclear extraction. 20 μg of whole cell lysates or 5-10 μg of nuclear extracts were used for regular western blot on mini SDS-PAGE gels. GRP78 (goat, 1:1,000), XBP1 (XBP1u/s-specific, rabbit, 1:1,000), CHOP (mouse, 1:500), HA-HRP (1:1000) and HSP90 (rabbit, 1:5,000) were purchased from Santa Cruz; (p)-eIF2α, IRE1α and PERK (rabbit) antibodies were purchased from Cell Signaling and used at 1:1,000–2,000. SEL1L (rabbit, 1:2000) was from Abcam. GAPDH (mouse, 1:20,000) was from Novus Biologicals. CREB antibody (rabbit, 1:6,000) was from Dr. Marc Montminy (Salk Institute). Primary antibodies were diluted in 5% milk/TBST or 2% BSA/TBST and incubated with PVDF membrane overnight at 4°C. Secondary antibodies were goat anti-rabbit IgG HRP, goat anti-mouse IgG HRP (Biorad) and donkey anti-goat IgG HRP (Jackson ImmunoResearch), all of which were used at 1:10,000.

RNA extraction and Q-PCR

RNA extraction and Q-PCR were performed as described previously (Sha et al., 2009). All Q-PCR data were normalized to ribosomal L32 gene in the corresponding sample. Primer sequences as listed below: L32 F: 5'-GAGCAACAAGAAAACCAAGCA-3', R: 5'-TGCACACAAGCCATCTACTCA-3'; Xbp1s F: 5'-TGCTGAGTCCGCAGCAGGTG-3', R: 5'-ACTAGCAGACTCTGGGGAAG-3'

Sel1L F: 5'-TGGGTTTTCTCTCTCTCCTCTG-3', R: 5'-CCTTTGTTCCGGTTACTTCTTG-3'; Chop F: 5'-TATCTCATCCCCAGGAAACG-3', R: 5'-GGGCACTGACCACTCTGTTT-3'; Erdj4 F: 5'-CTTAGGTGTGCCAAAGTCTGC-3', R: 5'-GGCATCCGAGAGTGTTTCATA-3'; Pdia6 F: 5'- TGGTTCCTTTCCTACCATCACT-3', R: 5'-ACTTTCACTGCTGGAAAACTGC-3'; FARP1 F: 5'-ATCACAGAGATGGTGGCACA-3'; R 5'-AGAACATGCGCTGCTGAAG-3'.

Plasmids and transfection

Plasmid expressing HA-tagged mouse FARP1 was a gift from Dr. Shan Sockanathan (John Hopkins University). Plasmids were transfected into MEFs via lipofectamine^{2000} according to the supplier's protocol. Tg treatment was performed 24 h post-transfection followed by Western blot or immunoprecipitation.

RNAi

Retroviral transduction and stable knockdown were performred as described previously (Sha et al., 2009). Stable cell lines with shRNA expressing were selected in media with 5ug/ml puromycin.

FARP1 shRNA were designed online using Thermo-Scientific siDESIGN center. Sequences of the three shRNA constructs are as followed: FARP1.14/FARP1.18 are two different clones resulted from the same shRNA constract: 5'-

GGATAAGGAGTAAGATGTA-3'; FARP2 target to sequence: 5'-GGTTCTAAGTACTAACAAA-3'.

B.3 RESULTS

FARP1 interacts with IRE1α and PERK in an ER stress-independent manner.

First of all, semi-endogenous immunoprecipitation (IP) was carried out to confirm the proteomic screen result. HA-tagged mouse FARP1 or GFP proteins were overexpressed in MEF cells. To our surprise, IP against HA-FARP1 pulled down not only endogenous IRE1α but also PERK when HA-FARP1 is expressed, indicating a physical interaction between FARP1 and both UPR sensors IRE1α and PERK (Fig. B1). As elevated interaction between NMHCIIB and IRE1α was observed upon ER stress-inducer Tg treatment, immunoprecipitation against FARP1 was also performed under 300nM Tg treatment for 2 hours. However, Tg treatment didn't increased interaction between FARP1 and either IRE1α or PERK (Fig. B1). Thus, FARP1 interacts with UPR sensors independently of ER stress.

Overexpression of FARP1 is not sufficient to promote UPR activation by ER stress.

To determine whether the interaction of FARP1 and UPR sensors is important for UPR activation, we checked the Tg-induced upregulation of UPR downstream targets in MEF cells expressing EGFP control plasmid or plasmid expressing FARP1. We observed similar levels of phosphorylation on PERK target eIF2α as well as XBP1s and CHOP proteins in the nuclei (Fig. B2-A). At the mRNA level, *Xbp1s* and other UPR genes including *GRP78, Erdj4* and *Chop* are comparable between the two cell lines (Fig. B2-B).

The dramatic increase of Farp1 mRNA and western blot against HA demonstrated the high transfection efficiency (Fig. B2-A,B).

FARP1 is not required for UPR activation

We next tested whether FARP1 deficiency impaired UPR activation under ER stress. The knockdown is highly efficient as indicated by the over 80% reduction of FARP1 mRNA (Fig. B3-A). However, we observed no changes of UPR mRNA induction by Tg in control knockdown (CONi) and three different FARP1i cell lines (Fig. B3-A). Both CONi and FARP1i exhibited similar dynamic patterns of phosphorylation increase on IRE1α and PERK, protein induction of GRP78, and nuclear transcription factors CHOP and XBP1s by Tg treatment. Neither p-eIF2α nor SEL1L increase much in either cell lines (Fig. B3-B). Thus, we concluded that FARP1 is not necessary for the upregulation of UPR under ER stress conditions.

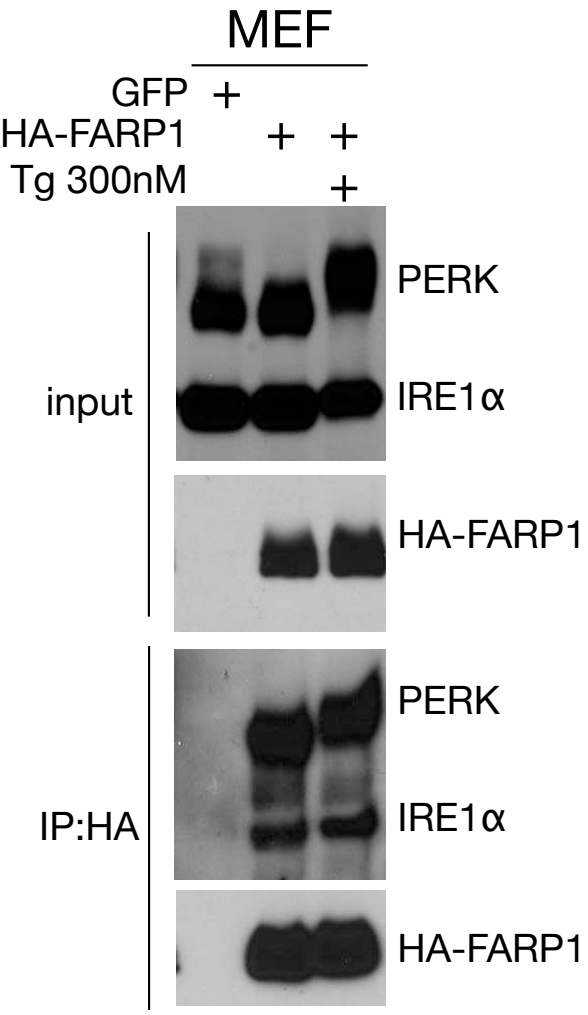

Figure B1 FARP1 interacts with both IRE1α and PERK independently of ER stress. Western blots against HA-FARP and UPR sensors – IRE1α and PERK from input and immunoprecipitates (IP) with anti-HA agarose. MEF cells transfected with GFP control or HA-FARP1 were treated with or without 300nM Tg for 2h.

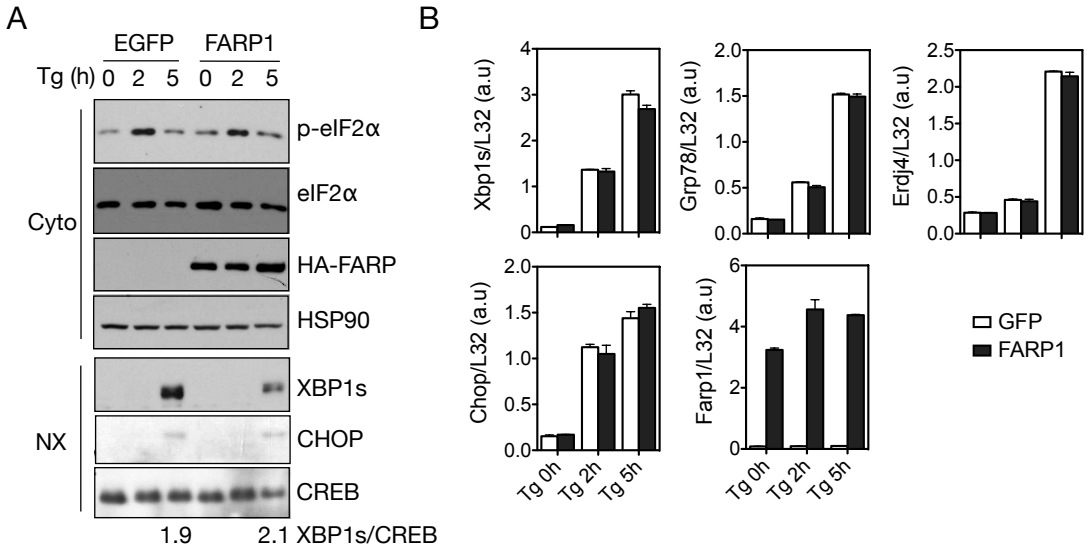

Figure B2 Over-expression of FARP1 doesn't promote UPR activation. (A) Western blots against UPR genes in MEF cells overexpressing EGFP control or mouse FARP1 under 300nM Tg for indicated time. Cell fractionation was performed to separate the cytosolic (Cyto) and nuclear fractions (NX). HSP90: the loading control for the cytosolic fraction. CREB: the loading control for the nuclear extraction. Quantification of XBP1s protein level normalized to CREB was shown below the gel. (B) Q-PCR showing the mRNA levels of UPR genes and *Farp1* in the cells as in (A). Ribosomal L32 gene as control.

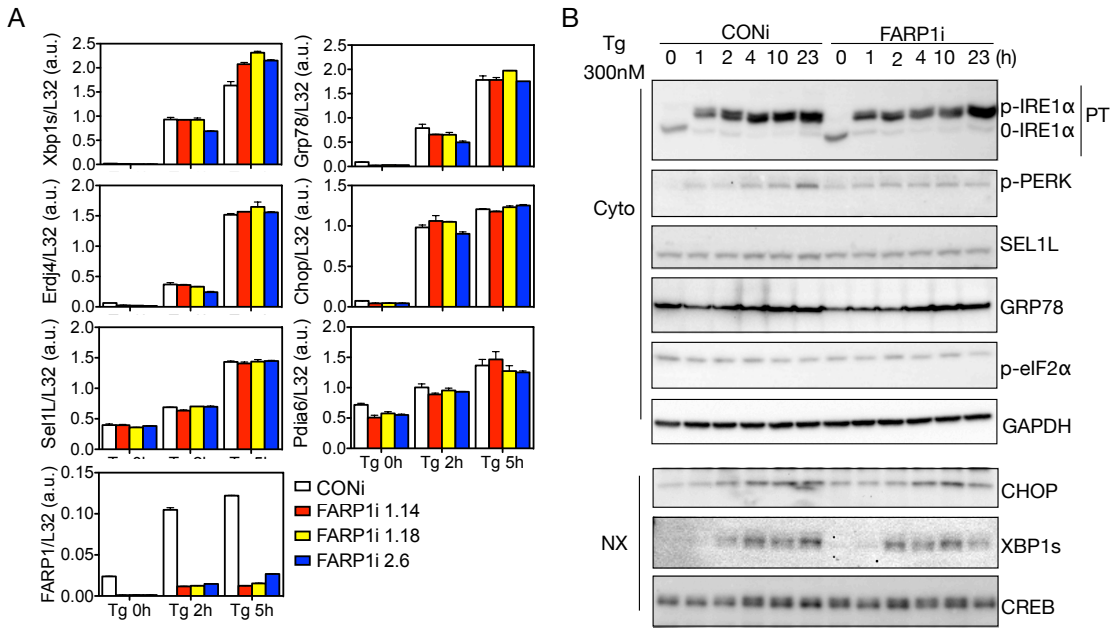

Figure B3 Knockdown of FARP1 doesn't impair UPR activation. (A) mRNA levels of UPR genes including *Xbp1s (spliced), Grp78, Erdj4, Chop, Sel1L, Pdia6* in MEF cells stabling expressing control shRNA (CONi) or three different FARP1 shRNA (FARP1i 1.14(red)/1.18(yellow)/2.6(blue)). (B) Western blots against UPR genes in cytosolic fraction (Cyto) or nuclear extraction (NX). IRE1α was separated on phos-tag gels indicated by the bar on the right with PT. p-: phosphorylated, 0-: non-phosphorylated. GAPDH: the loading control for cytosolic fraction. CREB: the loading control for nuclear extraction.

B.4 DISCUSSION

Here our data show that the FARP1 interacts with both IRE1α and PERK in basal and stressed conditions. The strength of interaction is not affected by ER stress. In addition, neither overexpression nor knockdown of FARP1 affects UPR activation. It is possible that the nature of FARP1 binding to IRE1α and PERK is non-specific, when FARP1 is highly overexpressed. Co-immunoprecipitation of endogenous FARP1 and IRE1α /PERK may help to clarify the possibility of non-specific binding. Nevertheless, the regulatory role of cytoskeleton networks in UPR activation remains to be an interesting future direction, which is worth of more investigation.

APPENDIX C. CIRCADIAN EXPRESSION OF UPR GENES IN MULTIPLE ORGANS

C.1 INTRODUCTION

Mammalian circadian rhythm orchestrates the temporal cycling of many physiological activities including metabolism, thus allowing organisms to adjust to the environmental cycles of light and nutrients caused by the 24 h rotation of the earth (Green et al., 2008). Dysregulation of circadian clock has been linked to a number of human diseases, such as sleep disorder, obesity, diabetes, and cardiovascular diseases (Maury et al., 2010). Mammalian circadian clock is composed of a master clock located in the suprachiasmatic nucleus (SCN) of the hypothalamus as well as peripheral clocks in various tissues (Kohsaka et al., 2007; Ralph et al., 1990). Despite tissue specificity, circadian rhythm is generated and maintained by the same master regulatory transcription factors, CLOCK and BMAL1. Heterodimeric CLOCK/BMAL1 binds to the E-box motif (CACGTGA) at the promoter regions of four other core clock transcription factors, PERIOD (PER), CRYPTOCHROME (CRY), nuclear receptors RORα and REV-ERBα, and activates their transcription. Heterodimeric PER/CRY suppresses their own expression by inhibiting CLOCK/BMAL1 activity, while RORα and REV-ERBα activate and suppress BMAL1 transcription respectively. The two interlocking regulatory loops trigger the oscillation of these core clock genes and orchestrate the periodic expression of a wide range of downstream genes involved in various biological pathways and are especially relevant in lipid and glucose metabolism (Green et al., 2008).

A large portion of metabolic genes (*Pdk4, Pepck, Pgc-1a, Hmgcr, Fasn, Ldlr*) have been shown to cycle with a period of 24h in key metabolic tissues such as liver and fat, many of which encode rate-limiting enzymes (Kohsaka et al., 2007; Panda et al., 2002; Storch et al., 2002). Disruption of circadian clock dampens the oscillation of those genes and thus interrupts metabolic homeostasis. For example, inactivation of BMAL1 and CLOCK impairs gluconeogenesis and suppresses the diurnal variations of serum metabolites such as glucose, triglycerides, and corticosterone (Rudic et al., 2004). Interestingly, circadian rhythm can also be influenced by metabolic status. Food restriction and high fat diet are known to affect the period and persistence of circadian rhythm (Kohsaka et al., 2007). However, despite the recent identification of several metabolic genes such as Retinoid X receptor alpha (RXRα), peroxisome-proliferation-activator-receptor alpha (PPARα) and PPARγ coactivator-1 alpha (PGC-1α), as potential modulators of BMAL and CLOCK expression, the mechanisms by which different physiological challenges and metabolic stress contribute to the regulation of circadian clock remains largely unknown (Canaple et al., 2006; Liu et al., 2007; McNamara et al., 2001).

Several reports have suggested a potential reciprocal regulation between UPR and circadian rhythm. ER dilation, a common outcome of UPR activation has been reported to exhibit a diurnal pattern, implying a link between UPR and circadian rhythm (Uchiyama and Watanabe, 1987). Moreover, the potential link between these two pathways may also be reflected by the functional similarities shared between them. Both UPR and circadian rhythm have pivotal roles in lipid metabolism, gluconeogenesis, and are implicated in the pathogenesis of obesity, diabetes, and cardiovascular diseases

(Hotamisligil, 2010; Maury et al., 2010). Interestingly, the E-box motif also contains the core CRE site "-ACGT-", the binding site for XBP1, suggesting a possible regulation of clock genes and clock-controlled genes by XBP1. In addition, the recent report hinted at the existence of a cycling canonical UPR without *Xbp1* mRNA change in mouse liver (Cretenet et al., 2010) directly links UPR to circadian rhythm. Thus we are interested in the regulation of UPR by circadian rhythm, and the physiological importance of the oscillating UPR in various tissues. This study is a pilot investigation describing the phenotypic UPR circadian rhythm in metabolic tissues as the first step.

C.2 MATERIALS AND METHODS

Animals

Wildtype C57BL/6 mice were either purchased from the Jackson Laboratory or bred in the Cornell Weill Mouse Facility. 4 mice were used for each time point. Tissues were frozen immediately in liquid nitrogen and stored at -80°C for later protein or RNA extraction.

Cell lines

HEK293T, 3T3L1 and Macrophage cell line RAW267.4 cells were maintained in DMEM supplemented with 10% FBS and 1% penicillin/streptomycin.

Western blots

Western blotting against IRE1α was performed according to previously published paper (Yang et al., 2010). IRE1α antibody (rabbit 1:1000) was purchased from Cell Signaling

while XBP1 antibody (rabbit 1:1000) from Santa Cruz. Secondary antibodies were goat anti-rabbit IgG HRP was used at 1:10,000

RNAi

Stable knockdown was performred as described in (Sha et al., 2009). To knockdown XBP1, shRNA were designed targeting to the mouse XBP1 sequence (GGATTCATGAATGGCCTTA) at 3' UTR. Stable cell lines with shRNA expressing were selected in media with 5ug/ml puromycin. XBP1i 3T3L1 as described in (Yang et al., 2013) while XBP1i RAW267.4 cells as in (He, 2013).

RNA extraction and Q-PCR

RNA extraction and Q-PCR were performed as described previously (Sha et al., 2009; Yang et al., 2010). All Q-PCR data were normalized to ribosomal l32 gene in the corresponding sample. Primer sequences as listed below: L32 F: 5'-GAGCAACAAGAAAACCAAGCA-3', R: 5'-TGCACACAAGCCATCTACTCA-3'; Xbp1 F: 5'-ACATCTTCCCATGGACTCTG-3', R: 5'-TAGGTCCTTCTGGGTAGACC-3'; Xbp1s F: 5'-TGCTGAGTCCGCAGCAGGTG-3', R: 5'-ACTAGCAGACTCTGGGGAAG-3'; Chop F: 5'-TATCTCATCCCCAGGAAACG-3', R: 5'-GGGCACTGACCACTCTGTTT-3'; Erdj4 F: 5'-CTTAGGTGTGCCAAAGTCTGC-3', R: 5'-GGCATCCGAGAGTGTTTCATA-3'; Grp78 F: 5'-TGTGGTACCCACCAAGAAGTC-3', R: 5'-TTCAGCTGTCACTCGGAGAAT-3'; p58ipk F: 5'-GTGGCATCCAGATAATTTCCAG-3', R: 5'-GAGTTCCAACTTCTGTGGAAGG-3';

Dgat2 F: 5'-TTCCTGGCATAAGGCCCTATT-3', R: 5'-AGTCTATGGTGTCTCGGTTGAC-3'; Acc2 F: 5'-CACCATCCGTGAAAACATCA-3', R: 5'-AGCAGCTGAGCCACCTGTAT-3'; Per1 F: 5'-AACGGGATGTGTTTCGGGGTGC-3', R: 5'-AGGACCTCCTCTGATTCGGCAG-3'; Per2 F: 5'-TGTGCGATGATGATTCGTGA-3', R: 5'-GGTGAAGGTACGTTTGGTTTGC-3'; Clock F: 5'-ACCACAGCAACAGCAACAAC-3', R: 5'- GGCTGCTGAACTGAAGGAAG-3'; Bmal1 F: 5'-CCACCTCAGAGCCATTGATACA-3', R: 5'-GAGCAGGTTTAGTTCCACTTTGTCT-3'; RXRα F: 5'-CACCCTGCTTGGAGATTCAT-3", R: 5'-CCCTGTGGTCATCTTCGTTT-3'; Rev-erbα F: 5'-ATGCCCATGACAAGTTAGGC-3', R: 5'-GGGCTACCTGATGCATGATT-3'; Rev-erbβ F: 5'-CGCACATTGCCGATATAGGAGG-3', R: 5'-GAGACTGCCACCACCACGTACT-3'; Cry1 F: 5'-AGCGCAGGTGTCGGTTATGAGC-3', R: 5'-ATAGACGCAGCGGATGGTGTCG-3'; Pgc1α F: 5'-TGTACTTTTGTGGACGGAAGC-3', R: 5'-TCCCATGAGGTATTGACCATC-3'; Pgc1β F: 5'-GCCAGAAGCACGGTTTTATC-3', R: 5'-GAAGGGACTCCTCAGATGTG-3'; aP2 F: 5'-AGCATCATAACCCTAGATGG-3', R: 5'-TCACGCCTTTCATAACACAT-3'; AdipoQ F: 5'-GGAACTTGTGCAGGTTGGAT-3', R: 5'-GCTTCTCCAGGCTCTCCTTT-3'.

Luciferase assay

Luciferase assay was performed in HEK293T cells with PEI-based transfection of PGC1α or control construct as in (Sha et al., 2009).

Statistics

Results are expressed as mean ± s.e.m. Comparisons between groups from each time point were made by unpaired two-tailed Student t-test. $P<0.05$ was considered as statistically significant. All experiments were repeated at least twice and representative data or data on average are shown.

C.3 RESULTS

***Xbp1* and its downstream targets' mRNA levels exhibit circadian rhythm in the heart, liver and WAT.**

Quantitative PCR (qPCR) was used to analyze UPR gene expression patterns in wild type C57BL/6J mouse hearts during a 24h period. Mice were accommodated under 12 hour light: 12 hour dark conditions. The mice were active during the dark period, which lasted from ZT*12* to ZT*0*.

Total *Xbp1* mRNA and *Xbp1s* oscillated with a peak around ZT8, started to decrease at ZT 12 (start of active phase), and reached nadir at ZT16- ZT20, suggesting a circadian-clock-dependent transcriptional regulation of *Xbp1* mRNA. In addition, PERK downstream target *Chop* and XBP1 downstream targets *Erdj4*, *Grp78* and *P58ipk* exhibited 24-hour cycles with peaking time around ZT8-ZT12. Per2, and Clock are used as control here and exhibits dramatic mRNA level changes as expected (Fig. C1).

As ER stress and IRE1 activation are the upstream events of XBP1 activation in most known cases, I applied a Phos-tag based method previously developed to sensitively

assess the phosphorylation status of IRE1α as an indicator of ER stress level (Yang et al., 2010). Unexpectedly, the Phos-tag based western blot showed no obvious oscillation of phospho-IRE1α (p-IRE1α) level. The lack of diurnal variation in IRE1α phosphorylation indicates unchanged IRE1 activity. It also suggests that the splicing rate of *Xbp1* mRNA by IRE1α is constant and that the force driving UPR oscillation *in heart* may be ER stress-independent (Fig. C2).

Interestingly, the oscillation of *Xbp1* and *Xbp1s* is very unique in heart, while in liver and white adipose tissue (WAT), the chaperone genes such as *Grp78, Erdj4,* and *P58ipk,* as well as *Chop* exhibit significant circadian patterns, even without cycling of *Xbp1/Xbp1s* mRNA levels (Fig. C3, C4). Metabolic genes (*Dgat2, Acc2, AdipoQ, aP2* and *Pgc-1β)* and circadian clock genes (*Per2* and *Clock)* showed circadian clock with 24-hour cycling period as expected in liver and WAT (Fig. C3, C4).

XBP1 may transcriptionally regulate circadian clock components.

The relationship between XBP1s and clock components was further tested in a cell line stably expressing shRNA against XBP1 (XBP1i). In Xbp1-deficient 3T3L1 cells, an ER stress agent, thapsigargin (Tg), failed to induce XBP1s protein, confirming very high knockdown efficiency (data in Chapter 3 and (Yang et al., 2013)). Intriguingly, core clock gene *Bmal1* as well as *Rxrα* was significantly reduced in XBP1i (Fig. C5-A). Furthermore, we observed that a similar circadian phase was shared between hepatic *Xbp1s* and *Pgc1α,* the *Bmal1* activator (Fig. C5-B). To confirm the link between XBP1 and PGC1α, we performed a luciferase reporter assay in which XBP1s elevated the

expression of a luciferase construct driven by mouse PGC1α promoter for four fold (Fig. C5-C). Influences of XBP1 on circadian clock were also observed in macrophages with XBP1 knockdown, arguing against cell specificity (Fig. C6). Taken together, these data suggest that XBP1 may not only be controlled by circadian clock but may also feedback into circadian clock maintenance.

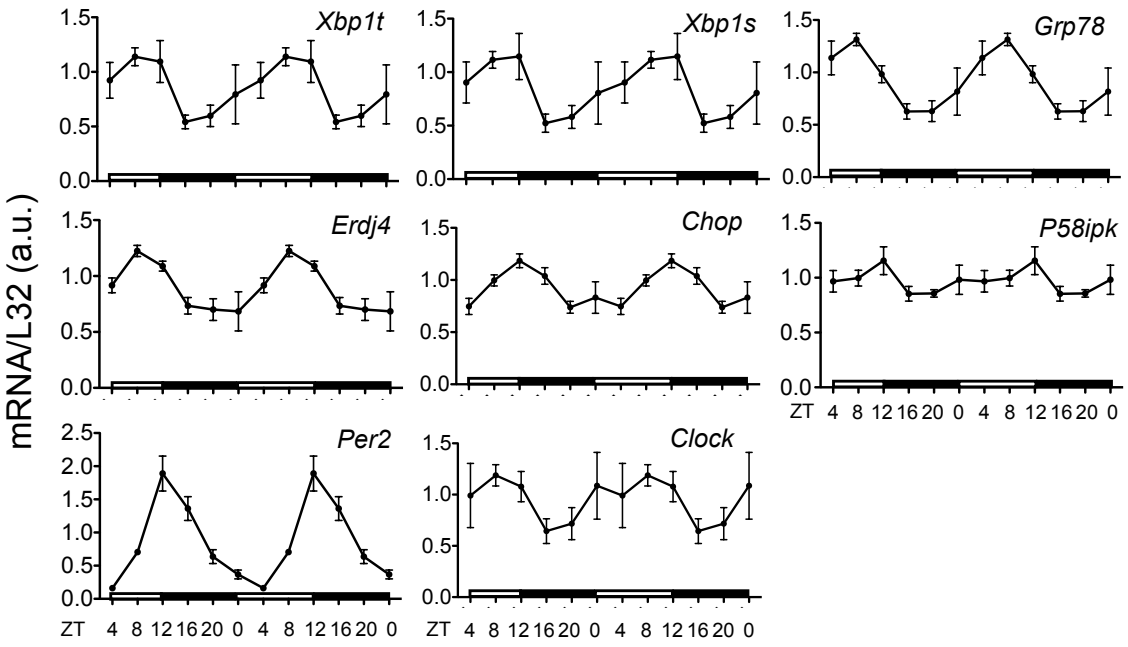

Figure C1 Circadian rhythm of UPR genes in heart. Hearts were harvested every 4 hours from 9 week-old male B6 mice. 4 mice per time point. Q-PCR showing the mRNA levels of *Xbp1t (total), Xbp1s (spliced), Grp78, Erdj4, P58ipk, Chop, Per2, Clock*. mRNA levels were normalized to ribosomal L32. a.u.: arbitrary unit. Values are mean ± s.e.m. White bar: light period. Black bar: dark period. ZT: Zeitgeber time. ZT0: start of light period. ZT 12: start of dark period.

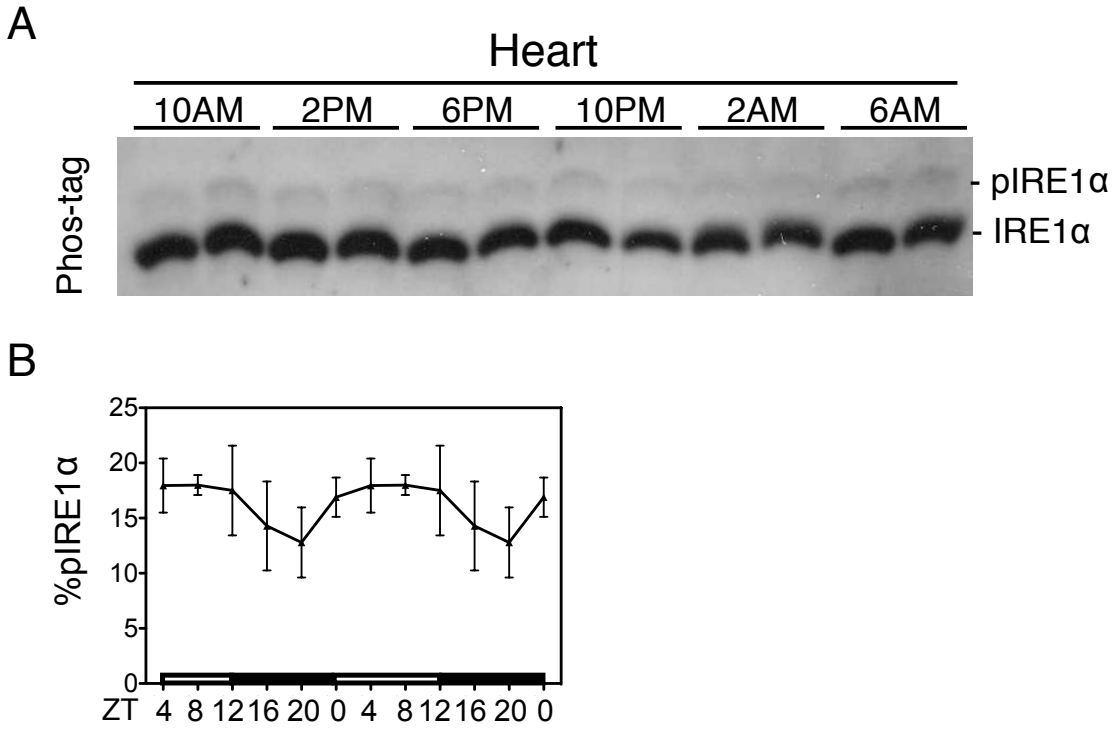

Figure C2 Activity of ER stress sensor IRE1α remains constant in heart. (A) Levels of phosphorylated- (P) and non-phosphorylated IRE1α revealed via Phos-tag based western blot. Same samples are used as in Fig.C1. Duplicates are shown for each time point. (B) Quantitation of percent of phosphorylated IRE1α (pIRE1α). Values are mean ± s.e.m (n=4 per time point).

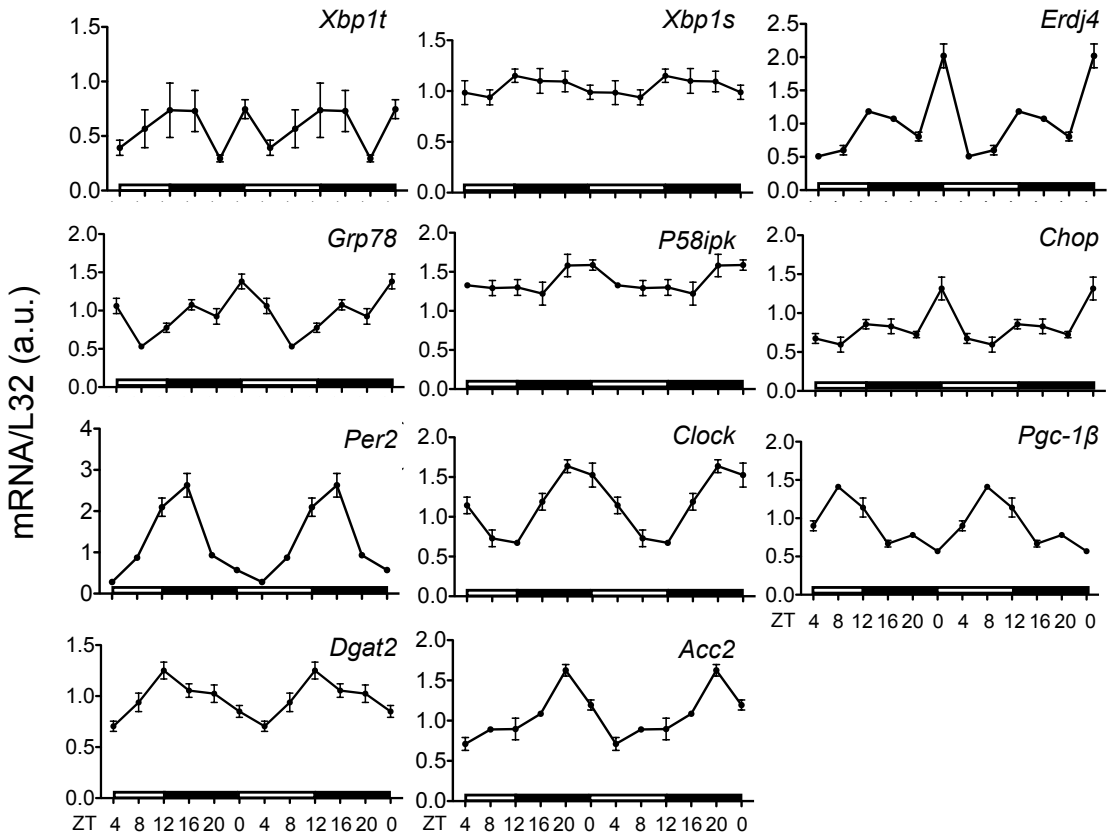

Figure C3 Circadian rhythm of UPR genes in liver. Livers were harvested every 4 hours from 9 week-old male B6 mice. 4 mice per time point. Q-PCR showing the mRNA levels of *Xbp1t (total), Xbp1s (spliced), Erdj4, Grp78, P58ipk, Chop, Per2, Clock, Pgc-1β, Dgat2, Acc2*. mRNA levels were normalized to ribosomal L32. a.u.: arbitrary unit. Values are mean ± s.e.m. White bar: light period. Black bar: dark period. ZT: Zeitgeber time. ZT0: start of light period. ZT 12: start of dark period.

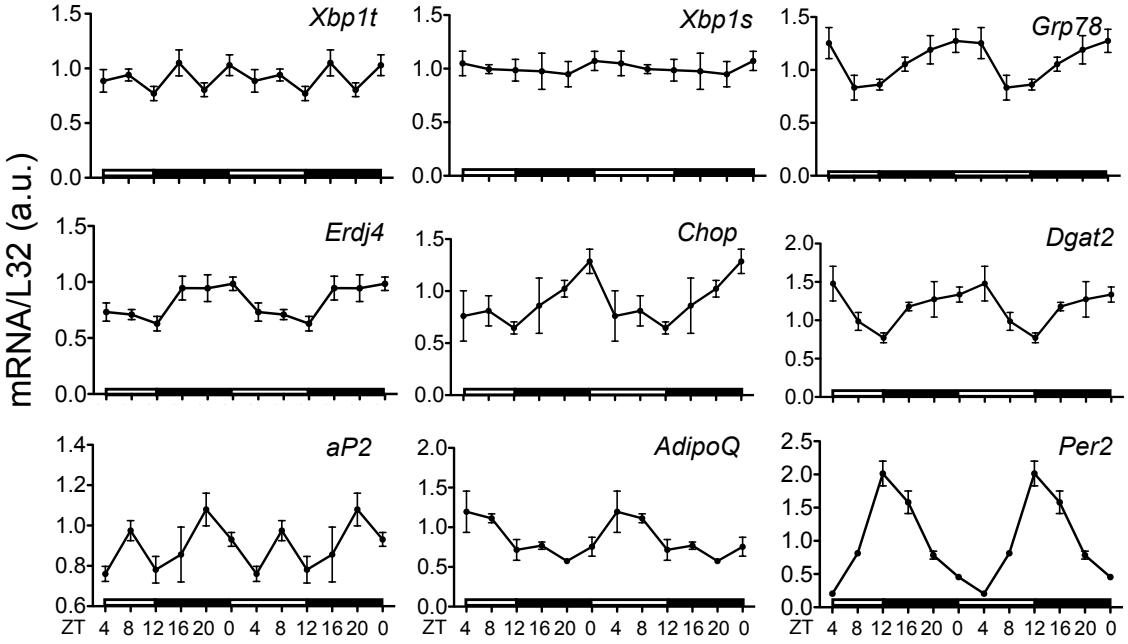

Figure C4 Circadian rhythm of UPR genes in white adipose tissue (WAT). WAT were harvested every 4 hours from 9 week-old male B6 mice. 4 mice per time point. Q-PCR showing the mRNA levels of *Xbp1t (total), Xbp1s (spliced), Grp78, Erdj4, Chop, Dgat2, aP2, AdipoQ, Per2*. mRNA levels were normalized to ribosomal L32. a.u.: arbitrary unit. Values are mean ± s.e.m. White bar: light period. Black bar: dark period. ZT: Zeitgeber time. ZT0: start of light period. ZT 12: start of dark period.

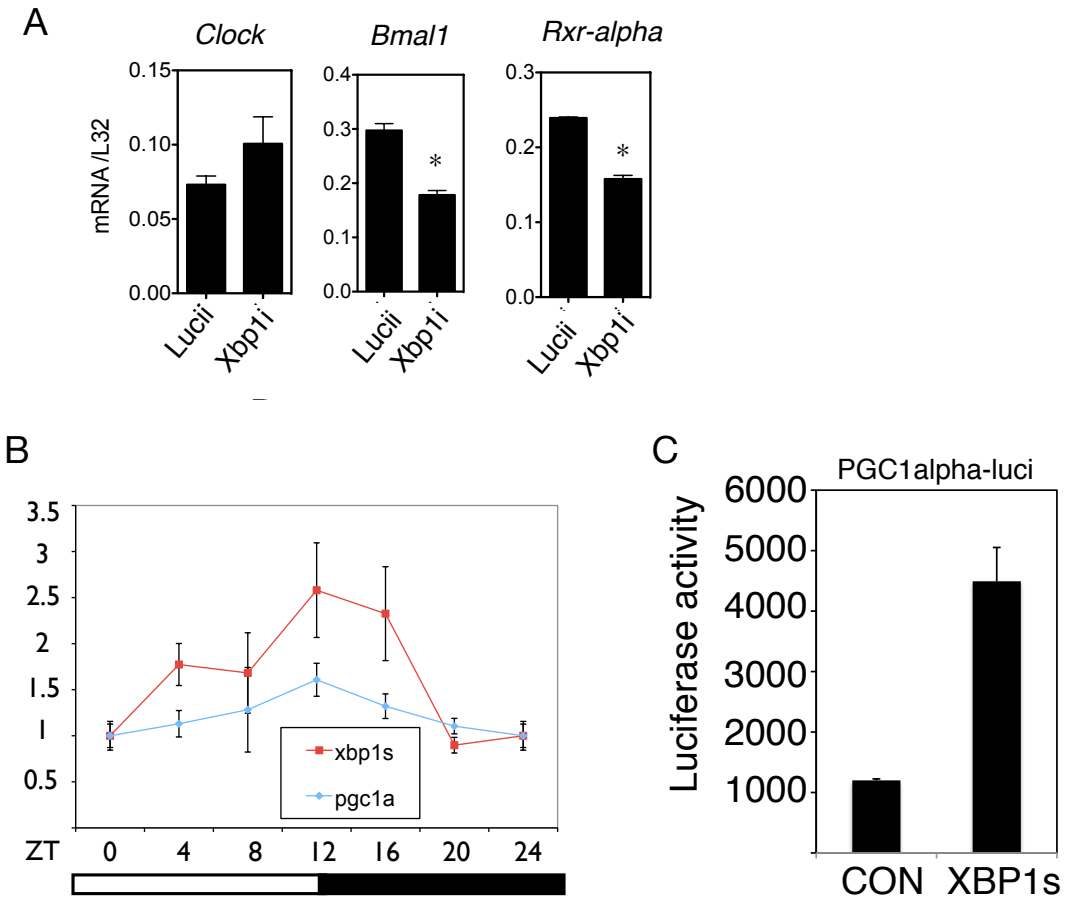

Figure C5 XBP1 regulates core circadian components at transcriptional level. (A) Q-PCR analysis *of Clock, Bmal1, Rxrα* in Lucii or Xbp1i 3T3-L1 cells. Values are mean ± s.e.m. *, p<0.05 (B) Q-PCR analysis of hepatic *Xbp1s* and *Pgc1α* mRNA in a 24h period from C57BL/6J mice. Values are mean ± s.e.m. (C) Luciferase activity of HEK293T cells transiently co-transfected with PGC1α promoter-luciferase construct (-170 to +68) and Xbp1s or EGFP control.

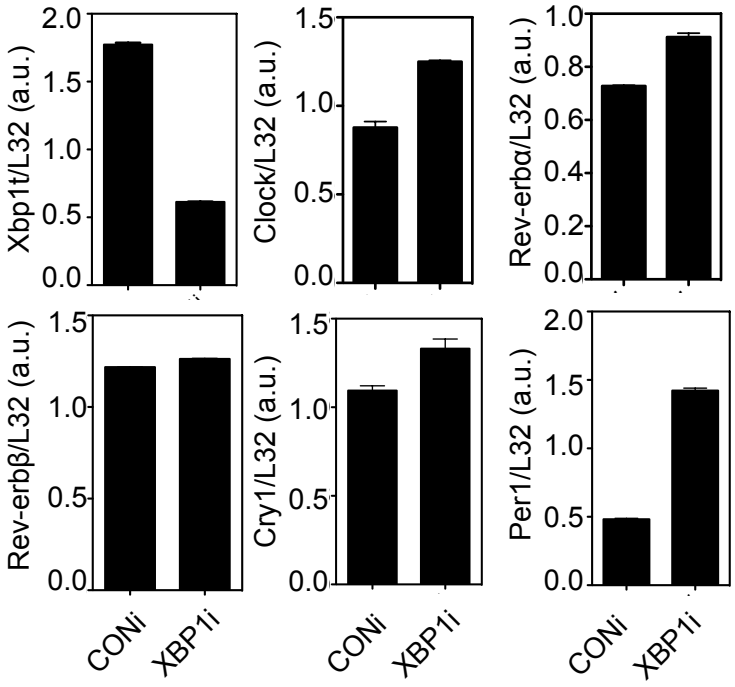

Figure C6 Knockdown of XBP1 influences multiple circadian genes. Q-PCR showing the mRNA levels of *Xbp1t (total)*, and circadian genes including Clock, *Rev-erbα, Rev-erbβ, Cry1,* and *Per1* in RAW267.4 cells with control knockdown (CONi) or XBP1 knockdown (XBP1i). mRNA normalized to ribosomal L32 level. a.u.: arbitrary unit. Values are mean ± s.e.m.

C.4 DISCUSSION

My preliminary data reveal the circadian oscillation of total *Xbp1* mRNA, *Xbp1s* in hearts, and other UPR downstream targets in multiple tissues with a 24hour-circadian period. The *Xbp1* circadian rhythm is independent of IRE1α activation in mouse hearts. This is indicative of a unique circadian UPR under basal physiological conditions. Strikingly, our results also showed that knockdown of XBP1 significantly affects the mRNA level of several clock genes in multiple cell models. Furthermore, a luciferase reporter assay demonstrated that XBP1 transcriptionally activated PGC1α (peroxisome proliferator activated receptor coactivator-1 alpha), a transcription cofactor critical for maintaining rhythmic oscillations of both clock and metabolic genes. Considering the link between disrupted circadian rhythm and multiple diseases, it is of great interest to investigate whether UPR maintains tissue homeostasis in a circadian manner to allow appropriate and rapid adaptation of the organ to environmental changes, and how the circadian rhythm of UPR is regulated.

REFERENCE

Aiba, Y., Kameyama, M., Yamazaki, T., Tedder, T.F., and Kurosaki, T. (2008). Regulation of B-cell development by BCAP and CD19 through their binding to phosphoinositide 3-kinase. Blood *111*, 1497–1503.

Akopian, D., Shen, K., Zhang, X., and Shan, S.-O. (2013). Signal Recognition Particle: An Essential Protein-Targeting Machine. Annu Rev Biochem.

Ali, M.M.U., Bagratuni, T., Davenport, E.L., Nowak, P.R., Silva-Santisteban, M.C., Hardcastle, A., McAndrews, C., Rowlands, M.G., Morgan, G.J., Aherne, W., et al. (2011). Structure of the Ire1 autophosphorylation complex and implications for the unfolded protein response. Embo J *30*, 894–905.

Allagnat, F., Christulia, F., Ortis, F., Pirot, P., Lortz, S., Lenzen, S., Eizirik, D.L., and Cardozo, A.K. (2010). Sustained production of spliced X-box binding protein 1 (XBP1) induces pancreatic beta cell dysfunction and apoptosis. Diabetologia *53*, 1120–1130.

Appenzeller-Herzog, C., and Hall, M.N. (2012). Bidirectional crosstalk between endoplasmic reticulum stress and mTOR signaling. Trends Cell Biol *22*, 274–282.

Appleyard, M.V.C.L., Murray, K.E., Coates, P.J., Wullschleger, S., Bray, S.E., Kernohan, N.M., Fleming, S., Alessi, D.R., and Thompson, A.M. (2012). Phenformin as prophylaxis and therapy in breast cancer xenografts. Br J Cancer *106*, 1117–1122.

Aragon, I.V., Barrington, R.A., Jackowski, S., Mori, K., and Brewer, J.W. (2012). The specialized unfolded protein response of B lymphocytes: ATF6α-independent development of antibody-secreting B cells. Mol Immunol *51*, 347–355.

Ariyama, H., Kono, N., Matsuda, S., Inoue, T., and Arai, H. (2010). Decrease in membrane phospholipid unsaturation induces unfolded protein response. J Biol Chem.

Armstrong, J.L., Flockhart, R., Veal, G.J., Lovat, P.E., and Redfern, C.P.F. (2010). Regulation of endoplasmic reticulum stress-induced cell death by ATF4 in neuroectodermal tumor cells. J Biol Chem *285*, 6091–6100.

Assan, R., Heuclin, C., Girard, J.R., LeMaire, F., and Attali, J.R. (1975). Phenformin-induced lactic acidosis in diabetic patients. Diabetes *24*, 791–800.

Back, S.H., Scheuner, D., Han, J., Song, B., Ribick, M., Wang, J., Gildersleeve, R.D., Pennathur, S., and Kaufman, R.J. (2009). Translation attenuation through eIF2alpha phosphorylation prevents oxidative stress and maintains the differentiated state in beta cells. Cell Metab *10*, 13–26.

Bagola, K., Delbrück, von, M., Dittmar, G., Scheffner, M., Ziv, I., Glickman, M.H., Ciechanover, A., and Sommer, T. (2013). Ubiquitin Binding by a CUE Domain Regulates Ubiquitin Chain Formation by ERAD E3 Ligases. Mol Cell.

Bagola, K., Mehnert, M., Jarosch, E., and Sommer, T. (2011). Protein dislocation from the ER. Biochim Biophys Acta *1808*, 925–936.

Balch, W.E., Morimoto, R.I., Dillin, A., and Kelly, J.W. (2008). Adapting proteostasis for disease intervention. Science *319*, 916–919.

Baltzis, D., Pluquet, O., Papadakis, A.I., Kazemi, S., Qu, L.-K., and Koromilas, A.E. (2007). The eIF2alpha kinases PERK and PKR activate glycogen synthase kinase 3 to promote the proteasomal degradation of p53. J Biol Chem *282*, 31675–31687.

Basseri, S., Lhoták, S., Sharma, A.M., and Austin, R.C. (2009). The chemical chaperone 4-phenylbutyrate inhibits adipogenesis by modulating the unfolded protein response. J Lipid Res *50*, 2486–2501.

Bazirgan, O.A., Garza, R.M., and Hampton, R.Y. (2006). Determinants of RING-E2 fidelity for Hrd1p, a membrane-anchored ubiquitin ligase. J Biol Chem *281*, 38989–39001.

Bernasconi, R., Galli, C., Calanca, V., Nakajima, T., and Molinari, M. (2010). Stringent requirement for HRD1, SEL1L, and OS-9/XTP3-B for disposal of ERAD-LS substrates. J Cell Biol *188*, 223–235.

Bertolotti, A., Wang, X., Novoa, I., Jungreis, R., Schlessinger, K., Cho, J.H., West, A.B., and Ron, D. (2001). Increased sensitivity to dextran sodium sulfate colitis in IRE1beta-deficient mice. J Clin Invest *107*, 585–593.

Bertolotti, A., Zhang, Y., Hendershot, L.M., Harding, H.P., and Ron, D. (2000). Dynamic interaction of BiP and ER stress transducers in the unfolded-protein response. Nat Cell Biol *2*, 326–332.

Biunno, I., Cattaneo, M., Orlandi, R., Canton, C., Biagiotti, L., Ferrero, S., Barberis, M., Pupa, S.M., Scarpa, A., and Ménard, S. (2006). SEL1L a multifaceted protein playing a role in tumor progression. J Cell Physiol *208*, 23–38.

Black, V.H., Sanjay, A., van Leyen, K., Lauring, B., and Kreibich, G. (2005). Cholesterol and steroid synthesizing smooth endoplasmic reticulum of adrenocortical cells contains high levels of proteins associated with the translocation channel. Endocrinology *146*, 4234–4249.

Braun, S., Matuschewski, K., Rape, M., Thoms, S., and Jentsch, S. (2002). Role of the ubiquitin-selective CDC48(UFD1/NPL4)chaperone (segregase) in ERAD of OLE1 and other substrates. Embo J *21*, 615–621.

Brewer, J.W., Cleveland, J.L., and Hendershot, L.M. (1997). A pathway distinct from the mammalian unfolded protein response regulates expression of endoplasmic reticulum chaperones in non-stressed cells. Embo J *16*, 7207–7216.

Brouns, G.S., de Vries, E., Neefjes, J.J., and Borst, J. (1996). Assembled pre-B cell

receptor complexes are retained in the endoplasmic reticulum by a mechanism that is not selective for the pseudo-light chain. J Biol Chem *271*, 19272–19278.

Brown, E.J., Albers, M.W., Shin, T.B., Ichikawa, K., Keith, C.T., Lane, W.S., and Schreiber, S.L. (1994). A mammalian protein targeted by G1-arresting rapamycin-receptor complex. Nature *369*, 756–758.

Canaple, L., Rambaud, J., Dkhissi-Benyahya, O., Rayet, B., Tan, N.S., Michalik, L., Delaunay, F., Wahli, W., and Laudet, V. (2006). Reciprocal regulation of brain and muscle Arnt-like protein 1 and peroxisome proliferator-activated receptor alpha defines a novel positive feedback loop in the rodent liver circadian clock. Mol Endocrinol *20*, 1715–1727.

Caraci, F., Chisari, M., Frasca, G., Chiechio, S., Salomone, S., Pinto, A., Sortino, M.A., and Bianchi, A. (2003). Effects of phenformin on the proliferation of human tumor cell lines. Life Sci. *74*, 643–650.

Caro, L.G., and Palade, G.E. (1964). Protein Synthesis, Storage, And Discharge In The Pancreatic Exocrine Cell. An Autoradiographic Study. J Cell Biol *20*, 473–495.

Casas-Tinto, S., Zhang, Y., Sanchez-Garcia, J., Gomez-Velazquez, M., Rincon-Limas, D.E., and Fernandez-Funez, P. (2011). The ER stress factor XBP1s prevents amyloid-beta neurotoxicity. Hum Mol Genet *20*, 2144–2160.

Castillo, K., Rojas-Rivera, D., Lisbona, F., Caballero, B.I.N., Nassif, M., Court, F.A., Schuck, S., Ibar, C., Walter, P., Sierralta, J., et al. (2011). BAX inhibitor-1 regulates autophagy by controlling the IRE1α branch of the unfolded protein response. Embo J *30*, 4465–4478.

Cattaneo, M., Lotti, L.V., MARTINO, S., Alessio, M., Conti, A., Bachi, A., Mariani-Costantini, R., and Biunno, I. (2011). Secretion of Novel SEL1L Endogenous Variants Is Promoted by ER Stress/UPR via Endosomes and Shed Vesicles in Human Cancer Cells. PLoS ONE *6*, e17206.

Cattaneo, M., Orlandini, S., Beghelli, S., Moore, P.S., Sorio, C., Bonora, A., Bassi, C., Talamini, G., Zamboni, G., Orlandi, R., et al. (2003). SEL1L expression in pancreatic adenocarcinoma parallels SMAD4 expression and delays tumor growth in vitro and in vivo. Oncogene *22*, 6359–6368.

Chan, V.W., Meng, F., Soriano, P., DeFranco, A.L., and Lowell, C.A. (1997). Characterization of the B lymphocyte populations in Lyn-deficient mice and the role of Lyn in signal initiation and down-regulation. Immunity *7*, 69–81.

Chance, B., Williams, G.R., and Hollunger, G. (1963). Inhibition of electron and energy transfer in mitochondria. I. Effects of Amytal, thiopental, rotenone, progesterone, and methylene glycol. J Biol Chem *238*, 418–431.

Cheadle, L., and Biederer, T. (2012). The novel synaptogenic protein Farp1 links

postsynaptic cytoskeletal dynamics and transsynaptic organization. J Cell Biol *199*, 985–1001.

Chen, H., and Qi, L. (2010). SUMO modification regulates the transcriptional activity of XBP1. Biochem J *429*, 95–102.

Chen, X., Shen, J., and Prywes, R. (2002a). The luminal domain of ATF6 senses endoplasmic reticulum (ER) stress and causes translocation of ATF6 from the ER to the Golgi. J Biol Chem *277*, 13045–13052.

Chen, X., Ding, Y., Liu, C.-G., Mikhail, S., and Yang, C.S. (2002b). Overexpression of glucose-regulated protein 94 (Grp94) in esophageal adenocarcinomas of a rat surgical model and humans. Carcinogenesis *23*, 123–130.

Christianson, J.C., Olzmann, J.A., Shaler, T.A., Sowa, M.E., Bennett, E.J., Richter, C.M., Tyler, R.E., Greenblatt, E.J., Harper, J.W., and Kopito, R.R. (2012). Defining human ERAD networks through an integrative mapping strategy. Nat Cell Biol *14*, 93–105.

Christianson, J.C., Shaler, T.A., Tyler, R.E., and Kopito, R.R. (2008). OS-9 and GRP94 deliver mutant alpha1-antitrypsin to the Hrd1-SEL1L ubiquitin ligase complex for ERAD. Nat Cell Biol *10*, 272–282.

Christis, C., Fullaondo, A., Schildknegt, D., Mkrtchian, S., Heck, A.J.R., and Braakman, I. (2010). Regulated increase in folding capacity prevents unfolded protein stress in the ER. J Cell Sci *123*, 787–794.

Cohen, S., Haimovich, J., and Hollander, N. (2013). Distinct processing of the pre-B cell receptor and the B cell receptor. Mol Immunol *54*, 115–121.

Cormier, J.H., Tamura, T., Sunryd, J.C., and Hebert, D.N. (2009). EDEM1 recognition and delivery of misfolded proteins to the SEL1L-containing ERAD complex. Mol Cell *34*, 627–633.

Cornejo, V.H., and Hetz, C. (2013). The unfolded protein response in Alzheimer's disease. Semin Immunopathol *35*, 277–292.

Cox, J.S., and Walter, P. (1996). A novel mechanism for regulating activity of a transcription factor that controls the unfolded protein response. Cell *87*, 391–404.

Cox, J.S., Shamu, C.E., and Walter, P. (1993). Transcriptional induction of genes encoding endoplasmic reticulum resident proteins requires a transmembrane protein kinase. Cell *73*, 1197–1206.

Credle, J.J., Finer-Moore, J.S., Papa, F.R., Stroud, R.M., and Walter, P. (2005). On the mechanism of sensing unfolded protein in the endoplasmic reticulum. Proc Natl Acad Sci USA *102*, 18773–18784.

Cretenet, G., Le Clech, M., and Gachon, F. (2010). Circadian clock-coordinated 12 Hr

period rhythmic activation of the IRE1alpha pathway controls lipid metabolism in mouse liver. Cell Metab *11*, 47–57.

Cullinan, S.B., Zhang, D., Hannink, M., Arvisais, E., Kaufman, R.J., and Diehl, J.A. (2003). Nrf2 is a direct PERK substrate and effector of PERK-dependent cell survival. Mol Cell Biol *23*, 7198–7209.

Custer, S.K., Neumann, M., Lu, H., Wright, A.C., and Taylor, J.P. (2010). Transgenic mice expressing mutant forms VCP/p97 recapitulate the full spectrum of IBMPFD including degeneration in muscle, brain and bone. Hum Mol Genet *19*, 1741–1755.

Davidoff, F. (1968). Effects of guanidine derivatives on mitochondrial function. I. Phenethylbiguanide inhibition of respiration in mitochondria from guinea pig and rat tissues. J Clin Invest *47*, 2331–2343.

Davies, F.E., Dring, A.M., Li, C., Rawstron, A.C., Shammas, M.A., O'Connor, S.M., Fenton, J.A.L., Hideshima, T., Chauhan, D., Tai, I.T., et al. (2003). Insights into the multistep transformation of MGUS to myeloma using microarray expression analysis. Blood *102*, 4504–4511.

Delépine, M., Nicolino, M., Barrett, T., Golamaully, M., Lathrop, G.M., and Julier, C. (2000). EIF2AK3, encoding translation initiation factor 2-alpha kinase 3, is mutated in patients with Wolcott-Rallison syndrome. Nat Genet *25*, 406–409.

Dennis, J.W., Granovsky, M., and Warren, C.E. (1999). Protein glycosylation in development and disease. Bioessays *21*, 412–421.

Dong, Y., Zhang, M., Wang, S., Liang, B., Zhao, Z., Liu, C., Wu, M., Choi, H.C., Lyons, T.J., and Zou, M.-H. (2010). Activation of AMP-activated protein kinase inhibits oxidized LDL-triggered endoplasmic reticulum stress in vivo. Diabetes *59*, 1386–1396.

Dougan, S.K., Hu, C.-C.A., Paquet, M.-E., Greenblatt, M.B., Kim, J., Lilley, B.N., Watson, N., and Ploegh, H.L. (2011). Derlin-2-deficient mice reveal an essential role for protein dislocation in chondrocytes. Mol Cell Biol *31*, 1145–1159.

Drogat, B., Auguste, P., Nguyên, D.T., Bouchecareilh, M., Pineau, R., Nalbantoglu, J., Kaufman, R.J., Chevet, E., Bikfalvi, A., and Moenner, M. (2007). IRE1 signaling is essential for ischemia-induced vascular endothelial growth factor-A expression and contributes to angiogenesis and tumor growth in vivo. Cancer Res *67*, 6700–6707.

Duennwald, M.L., and Lindquist, S. (2008). Impaired ERAD and ER stress are early and specific events in polyglutamine toxicity. Genes Dev *22*, 3308–3319.

Elkabetz, Y., Ofir, A., Argon, Y., and Bar-Nun, S. (2008). Alternative pathways of disulfide bond formation yield secretion-competent, stable and functional immunoglobulins. Mol Immunol *46*, 97–105.

Eura, Y., Yanamoto, H., Arai, Y., Okuda, T., Miyata, T., and Kokame, K. (2012). Derlin-

1 deficiency is embryonic lethal, derlin-3 deficiency appears normal, and herp deficiency is intolerant to glucose load and ischemia in mice. PLoS ONE *7*, e34298.

Fagioli, C., and Sitia, R. (2001). Glycoprotein quality control in the endoplasmic reticulum. Mannose trimming by endoplasmic reticulum mannosidase I times the proteasomal degradation of unassembled immunoglobulin subunits. J Biol Chem *276*, 12885–12892.

Fang, T., Smith, B.P., and Roman, C.A. (2001). Conventional and surrogate light chains differentially regulate Ig mu and Dmu heavy chain maturation and surface expression. J Immunol *167*, 3846–3857.

Federovitch, C.M., Ron, D., and Hampton, R.Y. (2005). The dynamic ER: experimental approaches and current questions. Curr Opin Cell Biol *17*, 409–414.

Feng, B., Yao, P.M., Li, Y., Devlin, C.M., Zhang, D., Harding, H.P., Sweeney, M., Rong, J.X., Kuriakose, G., Fisher, E.A., et al. (2003). The endoplasmic reticulum is the site of cholesterol-induced cytotoxicity in macrophages. Nat Cell Biol *5*, 781–792.

Fernandez, P.M., Tabbara, S.O., Jacobs, L.K., Manning, F.C., Tsangaris, T.N., Schwartz, A.M., Kennedy, K.A., and Patierno, S.R. (2000). Overexpression of the glucose-regulated stress gene GRP78 in malignant but not benign human breast lesions. Breast Cancer Res. Treat. *59*, 15–26.

Flaherty, D.P., Golden, J.E., Liu, C., Hedrick, M., Gosalia, P., Li, Y., Milewski, M., Sugarman, E., Suyama, E., Nguyen, K., et al. (2012). Selective small molecule activator of the apoptotic arm of the UPR (Bethesda (MD): National Center for Biotechnology Information (US)).

Flaswinkel, H., and Reth, M. (1994). Dual role of the tyrosine activation motif of the Ig-alpha protein during signal transduction via the B cell antigen receptor. Embo J *13*, 83–89.

Francisco, A.B., Singh, R., Li, S., Vani, A.K., Yang, L., Munroe, R.J., Diaferia, G., Cardano, M., Biunno, I., Qi, L., et al. (2010). Deficiency of suppressor enhancer Lin12 1 like (SEL1L) in mice leads to systemic endoplasmic reticulum stress and embryonic lethality. J Biol Chem *285*, 13694–13703.

Francisco, A.B., Singh, R., Sha, H., Yan, X., Qi, L., Lei, X., and Long, Q. (2011). Haploid insufficiency of suppressor enhancer Lin12 1 like (SEL1L) predisposes mice to high fat diet-induced hyperglycemia. J Biol Chem.

Fu, S., Yang, L., Li, P., Hofmann, O., Dicker, L., Hide, W., Lin, X., Watkins, S.M., Ivanov, A.R., and Hotamisligil, G.S. (2011). Aberrant lipid metabolism disrupts calcium homeostasis causing liver endoplasmic reticulum stress in obesity. Nature.

Gardner, B.M., and Walter, P. (2011). Unfolded proteins are Ire1-activating ligands that directly induce the unfolded protein response. Science *333*, 1891–1894.

Gardner, R.G., Swarbrick, G.M., Bays, N.W., Cronin, S.R., Wilhovsky, S., Seelig, L., Kim, C., and Hampton, R.Y. (2000). Endoplasmic reticulum degradation requires lumen to cytosol signaling. Transmembrane control of Hrd1p by Hrd3p. J Cell Biol *151*, 69–82.

Gass, J.N., Gifford, N.M., and Brewer, J.W. (2002). Activation of an unfolded protein response during differentiation of antibody-secreting B cells. J Biol Chem *277*, 49047–49054.

Gass, J.N., Jiang, H.-Y., Wek, R.C., and Brewer, J.W. (2008). The unfolded protein response of B-lymphocytes: PERK-independent development of antibody-secreting cells. Mol Immunol *45*, 1035–1043.

Gauld, S.B., and Cambier, J.C. (2004). Src-family kinases in B-cell development and signaling. Oncogene *23*, 8001–8006.

Gauss, R., Jarosch, E., Sommer, T., and Hirsch, C. (2006a). A complex of Yos9p and the HRD ligase integrates endoplasmic reticulum quality control into the degradation machinery. Nat Cell Biol *8*, 849–854.

Gauss, R., Sommer, T., and Jarosch, E. (2006b). The Hrd1p ligase complex forms a linchpin between ER-lumenal substrate selection and Cdc48p recruitment. Embo J *25*, 1827–1835.

Gomez, B.P., Riggins, R.B., Shajahan, A.N., Klimach, U., Wang, A., Crawford, A.C., Zhu, Y., Zwart, A., Wang, M., and Clarke, R. (2007). Human X-box binding protein-1 confers both estrogen independence and antiestrogen resistance in breast cancer cell lines. Faseb J. *21*, 4013–4027.

Gomez, E., Powell, M.L., Bevington, A., and Herbert, T.P. (2008). A decrease in cellular energy status stimulates PERK-dependent eIF2alpha phosphorylation and regulates protein synthesis in pancreatic beta-cells. Biochem J *410*, 485–493.

Green, C.B., Takahashi, J.S., and Bass, J. (2008). The meter of metabolism. Cell *134*, 728–742.

Greenblatt, E.J., Olzmann, J.A., and Kopito, R.R. (2011). Derlin-1 is a rhomboid pseudoprotease required for the dislocation of mutant α-1 antitrypsin from the endoplasmic reticulum. Nat. Struct. Mol. Biol. *18*, 1147–1152.

Gupta, S., McGrath, B., and Cavener, D.R. (2010). PERK (EIF2AK3) regulates proinsulin trafficking and quality control in the secretory pathway. Diabetes *59*, 1937–1947.

Gwinn, D.M., Shackelford, D.B., Egan, D.F., Mihaylova, M.M., Mery, A., Vasquez, D.S., Turk, B.E., and Shaw, R.J. (2008). AMPK phosphorylation of raptor mediates a metabolic checkpoint. Mol Cell *30*, 214–226.

Han, D., Lerner, A.G., Vande Walle, L., Upton, J.-P., Xu, W., Hagen, A., Backes, B.J.,

Oakes, S.A., and Papa, F.R. (2009). IRE1alpha kinase activation modes control alternate endoribonuclease outputs to determine divergent cell fates. Cell *138*, 562–575.

Harding, H.P., Zeng, H., Zhang, Y., Jungries, R., Chung, P., Plesken, H., Sabatini, D.D., and Ron, D. (2001). Diabetes mellitus and exocrine pancreatic dysfunction in perk-/- mice reveals a role for translational control in secretory cell survival. Mol Cell *7*, 1153–1163.

Harding, H.P., Zhang, Y., and Ron, D. (1999). Protein translation and folding are coupled by an endoplasmic-reticulum-resident kinase. Nature *397*, 271–274.

Harding, H.P., Zhang, Y., Bertolotti, A., Zeng, H., and Ron, D. (2000). Perk is essential for translational regulation and cell survival during the unfolded protein response. Mol Cell *5*, 897–904.

Hardy, R.R., and Hayakawa, K. (2001). B cell development pathways. Annu Rev Immunol *19*, 595–621.

Hardy, R.R., Carmack, C.E., Shinton, S.A., Kemp, J.D., and Hayakawa, K. (1991). Resolution and characterization of pro-B and pre-pro-B cell stages in normal mouse bone marrow. J Exp Med *173*, 1213–1225.

Hawley, S.A., Boudeau, J., Reid, J.L., Mustard, K.J., Udd, L., Mäkelä, T.P., Alessi, D.R., and Hardie, D.G. (2003). Complexes between the LKB1 tumor suppressor, STRAD alpha/beta and MO25 alpha/beta are upstream kinases in the AMP-activated protein kinase cascade. J. Biol. *2*, 28.

Haze, K., Yoshida, H., Yanagi, H., Yura, T., and Mori, K. (1999). Mammalian transcription factor ATF6 is synthesized as a transmembrane protein and activated by proteolysis in response to endoplasmic reticulum stress. Mol Biol Cell *10*, 3787–3799.

He, Y. (2013). Investigating Mammalian Unfolded Protein Response: The Physiology And Regulatory Mechanisms Of IREα-Xbp1 Signaling (Thesis dissertation).

He, Y., Beatty, A., Han, X., Ji, Y., Ma, X., Adelstein, R.S., Yates, J.R., Kemphues, K., and Qi, L. (2012). Nonmuscle myosin IIB links cytoskeleton to IRE1α signaling during ER stress. Dev Cell *23*, 1141–1152.

He, Y., Sun, S., Sha, H., Liu, Z., Yang, L., Xue, Z., Chen, H., and Qi, L. (2010). Emerging roles for XBP1, a sUPeR transcription factor. Gene Expr *15*, 13–25.

Hebert, D.N., Foellmer, B., and Helenius, A. (1995). Glucose trimming and reglucosylation determine glycoprotein association with calnexin in the endoplasmic reticulum. Cell *81*, 425–433.

Heishi, M., Hayashi, K., Ichihara, J., Ishikawa, H., Kawamura, T., Kanaoka, M., Taiji, M., and Kimura, T. (2008). Comparison of gene expression changes induced by biguanides in db/db mice liver. The Journal of Toxicological Sciences *33*, 339–347.

Helenius, A., and Aebi, M. (2004). ROLES OF N-LINKED GLYCANS IN THE ENDOPLASMIC RETICULUM. Annu Rev Biochem *73*, 1019–1049.

Hendershot, L.M. (1990). Immunoglobulin heavy chain and binding protein complexes are dissociated in vivo by light chain addition. J Cell Biol *111*, 829–837.

Herzog, S., Reth, M., and Jumaa, H. (2009). Regulation of B-cell proliferation and differentiation by pre-B-cell receptor signalling. Nat Rev Immunol *9*, 195–205.

Hetz, C. (2012). The unfolded protein response: controlling cell fate decisions under ER stress and beyond. Nat Rev Mol Cell Biol *13*, 89–102.

Hetz, C., and Glimcher, L.H. (2009). Fine-tuning of the unfolded protein response: Assembling the IRE1alpha interactome. Mol Cell *35*, 551–561.

Hetz, C., Bernasconi, P., Fisher, J., Lee, A.-H., Bassik, M.C., Antonsson, B., Brandt, G.S., Iwakoshi, N.N., Schinzel, A., Glimcher, L.H., et al. (2006). Proapoptotic BAX and BAK modulate the unfolded protein response by a direct interaction with IRE1alpha. Science *312*, 572–576.

Hetz, C., Lee, A.-H., Gonzalez-Romero, D., Thielen, P., Castilla, J., Soto, C., and Glimcher, L.H. (2008). Unfolded protein response transcription factor XBP-1 does not influence prion replication or pathogenesis. Proc Natl Acad Sci USA *105*, 757–762.

Hetz, C., Martinon, F., Rodriguez, D., and Glimcher, L.H. (2011). The unfolded protein response: integrating stress signals through the stress sensor IRE1α. Physiol Rev *91*, 1219–1243.

Hetz, C., Russelakis-Carneiro, M., Maundrell, K., Castilla, J., and Soto, C. (2003). Caspase-12 and endoplasmic reticulum stress mediate neurotoxicity of pathological prion protein. Embo J *22*, 5435–5445.

Hetz, C., Russelakis-Carneiro, M., Wälchli, S., Carboni, S., Vial-Knecht, E., Maundrell, K., Castilla, J., and Soto, C. (2005). The disulfide isomerase Grp58 is a protective factor against prion neurotoxicity. J Neurosci *25*, 2793–2802.

Hetz, C., Thielen, P., Matus, S., Nassif, M., Court, F., Kiffin, R., Martinez, G., Cuervo, A.M., Brown, R.H., and Glimcher, L.H. (2009). XBP-1 deficiency in the nervous system protects against amyotrophic lateral sclerosis by increasing autophagy. Genes Dev *23*, 2294–2306.

Hollien, J., and Weissman, J.S. (2006). Decay of endoplasmic reticulum-localized mRNAs during the unfolded protein response. Science *313*, 104–107.

Hollien, J., Lin, J.H., Li, H., Stevens, N., Walter, P., and Weissman, J.S. (2009). Regulated Ire1-dependent decay of messenger RNAs in mammalian cells. J Cell Biol *186*, 323–331.

Holtz, W.A., and O'Malley, K.L. (2003). Parkinsonian mimetics induce aspects of unfolded protein response in death of dopaminergic neurons. J Biol Chem *278*, 19367–19377.

Hotamisligil, G.S. (2010). Endoplasmic reticulum stress and the inflammatory basis of metabolic disease. Cell *140*, 900–917.

Hsu, T.A., and Betenbaugh, M.J. (1997). Coexpression of molecular chaperone BiP improves immunoglobulin solubility and IgG secretion from Trichoplusia ni insect cells. Biotechnol. Prog. *13*, 96–104.

Hu, C.-C.A., Dougan, S.K., McGehee, A.M., Love, J.C., and Ploegh, H.L. (2009). XBP-1 regulates signal transduction, transcription factors and bone marrow colonization in B cells. Embo J *28*, 1624.

Hu, J., Prinz, W.A., and Rapoport, T.A. (2011). Weaving the web of ER tubules. Cell *147*, 1226–1231.

Hu, P., Han, Z., Couvillon, A.D., Kaufman, R.J., and Exton, J.H. (2006). Autocrine tumor necrosis factor alpha links endoplasmic reticulum stress to the membrane death receptor pathway through IRE1alpha-mediated NF-kappaB activation and down-regulation of TRAF2 expression. Mol Cell Biol *26*, 3071–3084.

Iida, Y., Fujimori, T., Okawa, K., Nagata, K., Wada, I., and Hosokawa, N. (2011). SEL1L protein critically determines the stability of the HRD1-SEL1L endoplasmic reticulum-associated degradation (ERAD) complex to optimize the degradation kinetics of ERAD substrates. J Biol Chem *286*, 16929–16939.

Iwakoshi, N.N., Lee, A.-H., Vallabhajosyula, P., Otipoby, K.L., Rajewsky, K., and Glimcher, L.H. (2003). Plasma cell differentiation and the unfolded protein response intersect at the transcription factor XBP-1. Nat Immunol *4*, 321–329.

Iwakoshi, N.N., Pypaert, M., and Glimcher, L.H. (2007). The transcription factor XBP-1 is essential for the development and survival of dendritic cells. J Exp Med *204*, 2267–2275.

Iwawaki, T., and Tokuda, M. (2011). Function of yeast and amphioxus tRNA ligase in IRE1alpha-dependent XBP1 mRNA splicing. Biochem Biophys Res Commun *413*, 527–531.

Iwawaki, T., Akai, R., Kohno, K., and Miura, M. (2004). A transgenic mouse model for monitoring endoplasmic reticulum stress. Nat Med *10*, 98–102.

Jakob, C.A., Bodmer, D., Spirig, U., Battig, P., Marcil, A., Dignard, D., Bergeron, J.J., Thomas, D.Y., and Aebi, M. (2001). Htm1p, a mannosidase-like protein, is involved in glycoprotein degradation in yeast. EMBO Rep *2*, 423–430.

Jakob, C.A., Burda, P., Roth, J., and Aebi, M. (1998). Degradation of misfolded

endoplasmic reticulum glycoproteins in Saccharomyces cerevisiae is determined by a specific oligosaccharide structure. J Cell Biol *142*, 1223–1233.

Jamora, C., Dennert, G., and Lee, A.S. (1996). Inhibition of tumor progression by suppression of stress protein GRP78/BiP induction in fibrosarcoma B/C10ME. Proc Natl Acad Sci USA *93*, 7690–7694.

Jessop, C.E., Chakravarthi, S., Garbi, N., Hämmerling, G.J., Lovell, S., and Bulleid, N.J. (2007). ERp57 is essential for efficient folding of glycoproteins sharing common structural domains. Embo J *26*, 28–40.

Jiang, H.-Y., Wek, S.A., McGrath, B.C., Lu, D., Hai, T., Harding, H.P., Wang, X., Ron, D., Cavener, D.R., and Wek, R.C. (2004). Activating transcription factor 3 is integral to the eukaryotic initiation factor 2 kinase stress response. Mol Cell Biol *24*, 1365–1377.

Kabani, M., Kelley, S.S., Morrow, M.W., Montgomery, D.L., Sivendran, R., Rose, M.D., Gierasch, L.M., and Brodsky, J.L. (2003). Dependence of endoplasmic reticulum-associated degradation on the peptide binding domain and concentration of BiP. Mol Biol Cell *14*, 3437–3448.

Kaneko, M., Koike, H., Saito, R., Kitamura, Y., Okuma, Y., and Nomura, Y. (2010). Loss of HRD1-mediated protein degradation causes amyloid precursor protein accumulation and amyloid-beta generation. J Neurosci *30*, 3924–3932.

Kaser, A., Lee, A.-H., Franke, A., Glickman, J.N., Zeissig, S., Tilg, H., Nieuwenhuis, E.E.S., Higgins, D.E., Schreiber, S., Glimcher, L.H., et al. (2008). XBP1 links ER stress to intestinal inflammation and confers genetic risk for human inflammatory bowel disease. Cell *134*, 743–756.

Kaufman, R.J. (1999). Stress signaling from the lumen of the endoplasmic reticulum: coordination of gene transcriptional and translational controls. Genes Dev *13*, 1211–1233.

Kikkert, M., Doolman, R., Dai, M., Avner, R., Hassink, G., van Voorden, S., Thanedar, S., Roitelman, J., Chau, V., and Wiertz, E. (2004). Human HRD1 is an E3 ubiquitin ligase involved in degradation of proteins from the endoplasmic reticulum. J Biol Chem *279*, 3525–3534.

Kim, I., Xu, W., and Reed, J.C. (2008). Cell death and endoplasmic reticulum stress: disease relevance and therapeutic opportunities. Nature Reviews Drug Discovery *7*, 1013–1030.

Kim, Y.H., Joo, H.S., and Kim, D.-S. (2010). Nitric oxide induction of IRE1-alpha-dependent CREB phosphorylation in human glioma cells. Nitric Oxide *23*, 112–120.

Kimata, Y., Ishiwata-Kimata, Y., Ito, T., Hirata, A., Suzuki, T., Oikawa, D., Takeuchi, M., and Kohno, K. (2007). Two regulatory steps of ER-stress sensor Ire1 involving its cluster formation and interaction with unfolded proteins. J Cell Biol *179*, 75–86.

Kinoshita, E., Kinoshita-Kikuta, E., Takiyama, K., and Koike, T. (2006). Phosphate-binding tag, a new tool to visualize phosphorylated proteins. Mol Cell Proteomics *5*, 749–757.

Kohsaka, A., Laposky, A.D., Ramsey, K.M., Estrada, C., Joshu, C., Kobayashi, Y., Turek, F.W., and Bass, J. (2007). High-fat diet disrupts behavioral and molecular circadian rhythms in mice. Cell Metab *6*, 414–421.

Kondo, S., Murakami, T., Tatsumi, K., Ogata, M., Kanemoto, S., Otori, K., Iseki, K., Wanaka, A., and Imaizumi, K. (2005). OASIS, a CREB/ATF-family member, modulates UPR signalling in astrocytes. Nat Cell Biol *7*, 186–194.

Korennykh, A.V., Egea, P.F., Korostelev, A.A., Finer-Moore, J., Zhang, C., Shokat, K.M., Stroud, R.M., and Walter, P. (2009). The unfolded protein response signals through high-order assembly of Ire1. Nature *457*, 687–693.

Koyano, Y., Kawamoto, T., Shen, M., Yan, W., Noshiro, M., Fujii, K., and Kato, Y. (1997). Molecular cloning and characterization of CDEP, a novel human protein containing the ezrin-like domain of the band 4.1 superfamily and the Dbl homology domain of Rho guanine nucleotide exchange factors. Biochem Biophys Res Commun *241*, 369–375.

Kozutsumi, Y., Segal, M., Normington, K., Gething, M.J., and Sambrook, J. (1988). The presence of malfolded proteins in the endoplasmic reticulum signals the induction of glucose-regulated proteins. Nature *332*, 462–464.

Kraut-Cohen, J., and Gerst, J.E. (2010). Addressing mRNAs to the ER: cis sequences act up! Trends Biochem Sci *35*, 459–469.

Kusio-Kobialka, M., Podszywalow-Bartnicka, P., Peidis, P., Glodkowska-Mrowka, E., Wolanin, K., Leszak, G., Seferynska, I., Stoklosa, T., Koromilas, A.E., and Piwocka, K. (2012). The PERK-eIF2α phosphorylation arm is a pro-survival pathway of BCR-ABL signaling and confers resistance to imatinib treatment in chronic myeloid leukemia cells. Cell Cycle *11*, 4069–4078.

Kyöstilä, K., Cizinauskas, S., Seppälä, E.H., Suhonen, E., Jeserevics, J., Sukura, A., Syrjä, P., and Lohi, H. (2012). A SEL1L Mutation Links a Canine Progressive Early-Onset Cerebellar Ataxia to the Endoplasmic Reticulum-Associated Protein Degradation (ERAD) Machinery. PLoS Genet *8*, e1002759.

Lacroix, M., and Leclercq, G. (2004). About GATA3, HNF3A, and XBP1, three genes co-expressed with the oestrogen receptor-alpha gene (ESR1) in breast cancer. Mol Cell Endocrinol *219*, 1–7.

Leber, J.H., Bernales, S., and Walter, P. (2004). IRE1-independent gain control of the unfolded protein response. PLoS Biol *2*, E235.

Lee, A.-H., Chu, G.C., Iwakoshi, N.N., and Glimcher, L.H. (2005). XBP-1 is required for

biogenesis of cellular secretory machinery of exocrine glands. Embo J *24*, 4368–4380.

Lee, A.-H., Heidtman, K., Hotamisligil, G.S., and Glimcher, L.H. (2011). Dual and opposing roles of the unfolded protein response regulated by IRE1alpha and XBP1 in proinsulin processing and insulin secretion. Proc Natl Acad Sci USA *108*, 8885–8890.

Lee, A.-H., Iwakoshi, N.N., Anderson, K.C., and Glimcher, L.H. (2003). Proteasome inhibitors disrupt the unfolded protein response in myeloma cells. Proc Natl Acad Sci USA *100*, 9946–9951.

Lee, A.-H., Scapa, E.F., Cohen, D.E., and Glimcher, L.H. (2008). Regulation of hepatic lipogenesis by the transcription factor XBP1. Science *320*, 1492–1496.

Lee, E.K., Jeong, J.U., Chang, J.W., Yang, W.S., Kim, S.B., Park, S.K., Park, J.S., and Lee, S.K. (2012). Activation of AMP-activated protein kinase inhibits albumin-induced endoplasmic reticulum stress and apoptosis through inhibition of reactive oxygen species. Nephron Exp. Nephrol. *121*, e38–e48.

Li, H., Korennykh, A.V., Behrman, S.L., and Walter, P. (2010a). Mammalian endoplasmic reticulum stress sensor IRE1 signals by dynamic clustering. Proc Natl Acad Sci USA *107*, 16113–16118.

Li, S., Francisco, A.B., Munroe, R.J., Schimenti, J.C., and Long, Q. (2010b). SEL1L deficiency impairs growth and differentiation of pancreatic epithelial cells. BMC Developmental Biology *10*, 19.

Liang, G., Audas, T.E., Li, Y., Cockram, G.P., Dean, J.D., Martyn, A.C., Kokame, K., and Lu, R. (2006). Luman/CREB3 induces transcription of the endoplasmic reticulum (ER) stress response protein Herp through an ER stress response element. Mol Cell Biol *26*, 7999–8010.

Lilley, B.N., and Ploegh, H.L. (2004). A membrane protein required for dislocation of misfolded proteins from the ER. Nature *429*, 834–840.

Lin, J.H., Li, H., Yasumura, D., Cohen, H.R., Zhang, C., Panning, B., Shokat, K.M., Lavail, M.M., and Walter, P. (2007). IRE1 signaling affects cell fate during the unfolded protein response. Science *318*, 944–949.

Lin, J.H., Li, H., Zhang, Y., Ron, D., and Walter, P. (2009). Divergent effects of PERK and IRE1 signaling on cell viability. PLoS ONE *4*, e4170.

Liou, H.C., Boothby, M.R., Finn, P.W., Davidon, R., Nabavi, N., Zeleznik-Le, N.J., Ting, J.P., and Glimcher, L.H. (1990). A new member of the leucine zipper class of proteins that binds to the HLA DR alpha promoter. Science *247*, 1581–1584.

Lipson, K.L., Ghosh, R., and Urano, F. (2008). The role of IRE1alpha in the degradation of insulin mRNA in pancreatic beta-cells. PLoS ONE *3*, e1648.

Lisbona, F., Rojas-Rivera, D., Thielen, P., Zamorano, S., Todd, D., Martinon, F., Glavic, A., Kress, C., Lin, J.H., Walter, P., et al. (2009). BAX inhibitor-1 is a negative regulator of the ER stress sensor IRE1alpha. Mol Cell *33*, 679–691.

Liu, C.Y., Schröder, M., and Kaufman, R.J. (2000). Ligand-independent dimerization activates the stress response kinases IRE1 and PERK in the lumen of the endoplasmic reticulum. J Biol Chem *275*, 24881–24885.

Liu, C., Li, S., Liu, T., Borjigin, J., and Lin, J.D. (2007). Transcriptional coactivator PGC-1alpha integrates the mammalian clock and energy metabolism. Nature *447*, 477–481.

Liu, C.Y., Wong, H.N., Schauerte, J.A., and Kaufman, R.J. (2002). The protein kinase/endoribonuclease IRE1alpha that signals the unfolded protein response has a luminal N-terminal ligand-independent dimerization domain. J Biol Chem *277*, 18346–18356.

Lizcano, J.M., Göransson, O., Toth, R., Deak, M., Morrice, N.A., Boudeau, J., Hawley, S.A., Udd, L., Mäkelä, T.P., Hardie, D.G., et al. (2004). LKB1 is a master kinase that activates 13 kinases of the AMPK subfamily, including MARK/PAR-1. Embo J *23*, 833–843.

Loewen, C.A., and Feany, M.B. (2010). The unfolded protein response protects from tau neurotoxicity in vivo. PLoS ONE *5*.

Lu, J., Wang, Q., Huang, L., Dong, H., Lin, L., Lin, N., Zheng, F., and Tan, J. (2012). Palmitate causes endoplasmic reticulum stress and apoptosis in human mesenchymal stem cells: prevention by AMPK activator. Endocrinology *153*, 5275–5284.

Lu, P.D., Harding, H.P., and Ron, D. (2004a). Translation reinitiation at alternative open reading frames regulates gene expression in an integrated stress response. J Cell Biol *167*, 27–33.

Lu, P.D., Jousse, C., Marciniak, S.J., Zhang, Y., Novoa, I., Scheuner, D., Kaufman, R.J., Ron, D., and Harding, H.P. (2004b). Cytoprotection by pre-emptive conditional phosphorylation of translation initiation factor 2. Embo J *23*, 169–179.

Ma, K., Vattem, K.M., and Wek, R.C. (2002). Dimerization and release of molecular chaperone inhibition facilitate activation of eukaryotic initiation factor-2 kinase in response to endoplasmic reticulum stress. J Biol Chem *277*, 18728–18735.

Ma, Y., Shimizu, Y., Mann, M.J., Jin, Y., and Hendershot, L.M. (2009). Plasma cell differentiation initiates a limited ER stress response by specifically suppressing the PERK-dependent branch of the unfolded protein response. Cell Stress Chaperones.

Maeda, T., Wakasawa, T., Shima, Y., Tsuboi, I., Aizawa, S., and Tamai, I. (2006). Role of polyamines derived from arginine in differentiation and proliferation of human blood cells. Biol Pharm Bull *29*, 234–239.

Maestre, L., Tooze, R., Cañamero, M., Montes-Moreno, S., Ramos, R., Doody, G., Boll, M., Barrans, S., Baena, S., Piris, M.A., et al. (2009). Expression pattern of XBP1(S) in human B-cell lymphomas. Haematologica *94*, 419–422.

Malhotra, J.D., Miao, H., Zhang, K., Wolfson, A., Pennathur, S., Pipe, S.W., and Kaufman, R.J. (2008). Antioxidants reduce endoplasmic reticulum stress and improve protein secretion. Proc Natl Acad Sci USA *105*, 18525–18530.

Mao, T., Shao, M., Qiu, Y., Huang, J., Zhang, Y., Song, B., Wang, Q., Jiang, L., Liu, Y., Han, J.-D.J., et al. (2011). PKA phosphorylation couples hepatic inositol-requiring enzyme 1alpha to glucagon signaling in glucose metabolism. Proc Natl Acad Sci USA *108*, 15852–15857.

Marciniak, S.J., Garcia-Bonilla, L., Hu, J., Harding, H.P., and Ron, D. (2006). Activation-dependent substrate recruitment by the eukaryotic translation initiation factor 2 kinase PERK. J Cell Biol *172*, 201–209.

Martinon, F., Chen, X., Lee, A.-H., and Glimcher, L.H. (2010). TLR activation of the transcription factor XBP1 regulates innate immune responses in macrophages. Nat Immunol.

Masaki, T., Yoshida, M., and Noguchi, S. (1999). Targeted disruption of CRE-binding factor TREB5 gene leads to cellular necrosis in cardiac myocytes at the embryonic stage. Biochem Biophys Res Commun *261*, 350–356.

Matsumoto, M., Minami, M., Takeda, K., Sakao, Y., and Akira, S. (1996). Ectopic expression of CHOP (GADD153) induces apoptosis in M1 myeloblastic leukemia cells. FEBS Lett *395*, 143–147.

Maury, E., Ramsey, K., and Bass, J. (2010). Circadian Rhythms and Metabolic Syndrome: From Experimental Genetics to Human Disease. Circ Res *106*, 447.

Mayer, C.M., and Belsham, D.D. (2010). Palmitate attenuates insulin signaling and induces endoplasmic reticulum stress and apoptosis in hypothalamic neurons: rescue of resistance and apoptosis through adenosine 5' monophosphate-activated protein kinase activation. Endocrinology *151*, 576–585.

McCullough, K.D., Martindale, J.L., Klotz, L.O., Aw, T.Y., and Holbrook, N.J. (2001). Gadd153 sensitizes cells to endoplasmic reticulum stress by down-regulating Bcl2 and perturbing the cellular redox state. Mol Cell Biol *21*, 1249–1259.

McGehee, A.M., Dougan, S.K., Klemm, E.J., Shui, G., Park, B., Kim, Y.-M., Watson, N., Wenk, M.R., Ploegh, H.L., and Hu, C.-C.A. (2009). XBP-1-deficient plasmablasts show normal protein folding but altered glycosylation and lipid synthesis. J Immunol *183*, 3690–3699.

McNamara, P., Seo, S.B., Rudic, R.D., Sehgal, A., Chakravarti, D., and FitzGerald, G.A. (2001). Regulation of CLOCK and MOP4 by nuclear hormone receptors in the

vasculature: a humoral mechanism to reset a peripheral clock. Cell *105*, 877–889.

Meares, G.P., Hughes, K.J., Naatz, A., Papa, F.R., Urano, F., Hansen, P.A., Benveniste, E.N., and Corbett, J.A. (2011). IRE1-Dependent Activation of AMPK in Response to Nitric Oxide. Mol Cell Biol *31*, 4286–4297.

Meldolesi, J., and Pozzan, T. (1998). The endoplasmic reticulum Ca2+ store: a view from the lumen. Trends Biochem Sci *23*, 10–14.

Metzger, M.B., Liang, Y.-H., Das, R., Mariano, J., Li, S., Li, J., Kostova, Z., Byrd, R.A., Ji, X., and Weissman, A.M. (2013). A Structurally Unique E2-Binding Domain Activates Ubiquitination by the ERAD E2, Ubc7p, through Multiple Mechanisms. Mol Cell.

Milne, C.D., and Paige, C.J. (2006). IL-7: a key regulator of B lymphopoiesis. Semin. Immunol. *18*, 20–30.

Minegishi, Y., Hendershot, L.M., and Conley, M.E. (1999). Novel mechanisms control the folding and assembly of lambda5/14.1 and VpreB to produce an intact surrogate light chain. Proc Natl Acad Sci USA *96*, 3041–3046.

Mittl, P.R.E., and Schneider-Brachert, W. (2007). Sel1-like repeat proteins in signal transduction. Cell Signal *19*, 20–31.

Miyata, Y., Fukuhara, A., Matsuda, M., Komuro, R., and Shimomura, I. (2008). Insulin induces chaperone and CHOP gene expressions in adipocytes. Biochem Biophys Res Commun *365*, 826–832.

Mori, K., Ma, W., Gething, M.J., and Sambrook, J. (1993). A transmembrane protein with a cdc2+/CDC28-related kinase activity is required for signaling from the ER to the nucleus. Cell *74*, 743–756.

Morisset, J.A., and Webster, P.D. (1972). Effects of fasting and feeding on protein synthesis by the rat pancreas. J Clin Invest *51*, 1–8.

Mueller, B., Klemm, E.J., Spooner, E., Claessen, J.H., and Ploegh, H.L. (2008). SEL1L nucleates a protein complex required for dislocation of misfolded glycoproteins. Proc Natl Acad Sci USA *105*, 12325.

Mueller, B., Lilley, B.N., and Ploegh, H.L. (2006). SEL1L, the homologue of yeast Hrd3p, is involved in protein dislocation from the mammalian ER. J Cell Biol *175*, 261–270.

Mundt, C., Licence, S., Shimizu, T., Melchers, F., and Mårtensson, I.L. (2001). Loss of precursor B cell expansion but not allelic exclusion in VpreB1/VpreB2 double-deficient mice. J Exp Med *193*, 435–445.

Müller, J.M.M., Deinhardt, K., Rosewell, I., Warren, G., and Shima, D.T. (2007). Targeted deletion of p97 (VCP/CDC48) in mouse results in early embryonic lethality.

Biochem Biophys Res Commun *354*, 459–465.

Nagai, A., Kadowaki, H., Maruyama, T., Takeda, K., Nishitoh, H., and Ichijo, H. (2009). USP14 inhibits ER-associated degradation via interaction with IRE1alpha. Biochem Biophys Res Commun *379*, 995–1000.

Nagasawa, T. (2006). Microenvironmental niches in the bone marrow required for B-cell development. Nat Rev Immunol *6*, 107–116.

Nakatsukasa, K., Nishikawa, S., Hosokawa, N., Nagata, K., and Endo, T. (2001). Mnl1p, an alpha -mannosidase-like protein in yeast Saccharomyces cerevisiae, is required for endoplasmic reticulum-associated degradation of glycoproteins. J Biol Chem *276*, 8635–8638.

Nguyen, T.H., Law, D.T., and Williams, D.B. (1991). Binding protein BiP is required for translocation of secretory proteins into the endoplasmic reticulum in Saccharomyces cerevisiae. Proc Natl Acad Sci USA *88*, 1565–1569.

Nguyên, D.T., Kebache, S., Fazel, A., Wong, H.N., Jenna, S., Emadali, A., Lee, E.-H., Bergeron, J.J.M., Kaufman, R.J., Larose, L., et al. (2004). Nck-dependent activation of extracellular signal-regulated kinase-1 and regulation of cell survival during endoplasmic reticulum stress. Mol Biol Cell *15*, 4248–4260.

Nicchitta, C.V. (2002). A platform for compartmentalized protein synthesis: protein translation and translocation in the ER. Curr Opin Cell Biol *14*, 412–416.

Nikawa, J., and Yamashita, S. (1992). IRE1 encodes a putative protein kinase containing a membrane-spanning domain and is required for inositol phototrophy in Saccharomyces cerevisiae. Mol. Microbiol. *6*, 1441–1446.

Nishikawa, S.I., Fewell, S.W., Kato, Y., Brodsky, J.L., and Endo, T. (2001). Molecular chaperones in the yeast endoplasmic reticulum maintain the solubility of proteins for retrotranslocation and degradation. J Cell Biol *153*, 1061–1070.

Nishimoto, N., Kubagawa, H., Ohno, T., Gartland, G.L., Stankovic, A.K., and Cooper, M.D. (1991). Normal pre-B cells express a receptor complex of mu heavy chains and surrogate light-chain proteins. Proc Natl Acad Sci USA *88*, 6284–6288.

Nishitoh, H., Kadowaki, H., Nagai, A., Maruyama, T., Yokota, T., Fukutomi, H., Noguchi, T., Matsuzawa, A., Takeda, K., and Ichijo, H. (2008). ALS-linked mutant SOD1 induces ER stress- and ASK1-dependent motor neuron death by targeting Derlin-1. Genes Dev *22*, 1451–1464.

Nishitoh, H., Matsuzawa, A., Tobiume, K., Saegusa, K., Takeda, K., Inoue, K., Hori, S., Kakizuka, A., and Ichijo, H. (2002). ASK1 is essential for endoplasmic reticulum stress-induced neuronal cell death triggered by expanded polyglutamine repeats. Genes Dev *16*, 1345–1355.

Oda, Y., Hosokawa, N., Wada, I., and Nagata, K. (2003). EDEM as an acceptor of terminally misfolded glycoproteins released from calnexin. Science *299*, 1394–1397.

Ohoka, N., Yoshii, S., Hattori, T., Onozaki, K., and Hayashi, H. (2005). TRB3, a novel ER stress-inducible gene, is induced via ATF4-CHOP pathway and is involved in cell death. Embo J *24*, 1243–1255.

Oikawa, D., Tokuda, M., and Iwawaki, T. (2007). Site-specific cleavage of CD59 mRNA by endoplasmic reticulum-localized ribonuclease, IRE1. Biochem Biophys Res Commun *360*, 122–127.

Oikawa, D., Tokuda, M., Hosoda, A., and Iwawaki, T. (2010). Identification of a consensus element recognized and cleaved by IRE1 alpha. Nucleic Acids Res *38*, 6265–6273.

Orlandi, R., Cattaneo, M., Troglio, F., Casalini, P., Ronchini, C., Ménard, S., and Biunno, I. (2002). SEL1L expression decreases breast tumor cell aggressiveness in vivo and in vitro. Cancer Res *62*, 567–574.

Oyadomari, S., Harding, H.P., Zhang, Y., Oyadomari, M., and Ron, D. (2008). Dephosphorylation of translation initiation factor 2alpha enhances glucose tolerance and attenuates hepatosteatosis in mice. Cell Metab *7*, 520–532.

Ozcan, L., Ergin, A.S., Lu, A., Chung, J., Sarkar, S., Nie, D., Myers, M.G., and Ozcan, U. (2009). Endoplasmic reticulum stress plays a central role in development of leptin resistance. Cell Metab *9*, 35–51.

Ozcan, U., Cao, Q., Yilmaz, E., Lee, A.-H., Iwakoshi, N.N., Ozdelen, E., Tuncman, G., Görgün, C., Glimcher, L.H., and Hotamisligil, G.S. (2004). Endoplasmic reticulum stress links obesity, insulin action, and type 2 diabetes. Science *306*, 457–461.

Ozcan, U., Yilmaz, E., Ozcan, L., Furuhashi, M., Vaillancourt, E., Smith, R.O., Görgün, C.Z., and Hotamisligil, G.S. (2006). Chemical chaperones reduce ER stress and restore glucose homeostasis in a mouse model of type 2 diabetes. Science *313*, 1137–1140.

Panda, S., Antoch, M.P., Miller, B.H., Su, A.I., Schook, A.B., Straume, M., Schultz, P.G., Kay, S.A., Takahashi, J.S., and Hogenesch, J.B. (2002). Coordinated transcription of key pathways in the mouse by the circadian clock. Cell *109*, 307–320.

Papavasiliou, F., Jankovic, M., and Nussenzweig, M.C. (1996). Surrogate or conventional light chains are required for membrane immunoglobulin mu to activate the precursor B cell transition. J Exp Med *184*, 2025–2030.

Park, S.W., Zhou, Y., Lee, J., Lu, A., Sun, C., Chung, J., Ueki, K., and Ozcan, U. (2010). The regulatory subunits of PI3K, p85alpha and p85beta, interact with XBP-1 and increase its nuclear translocation. Nat Med.

Parodi, A.J. (2000). Protein glucosylation and its role in protein folding. Annu Rev

Biochem *69*, 69–93.

Peschon, J.J., Morrissey, P.J., Grabstein, K.H., Ramsdell, F.J., Maraskovsky, E., Gliniak, B.C., Park, L.S., Ziegler, S.F., Williams, D.E., Ware, C.B., et al. (1994). Early lymphocyte expansion is severely impaired in interleukin 7 receptor-deficient mice. J Exp Med *180*, 1955–1960.

Pincus, D., Chevalier, M.W., Aragón, T., van Anken, E., Vidal, S.E., El-Samad, H., and Walter, P. (2010). BiP binding to the ER-stress sensor Ire1 tunes the homeostatic behavior of the unfolded protein response. PLoS Biol *8*, e1000415.

Pineau, L., Colas, J., Dupont, S., Beney, L., Fleurat-Lessard, P., Berjeaud, J.-M., Bergès, T., and Ferreira, T. (2009). Lipid-induced ER stress: synergistic effects of sterols and saturated fatty acids. Traffic *10*, 673–690.

Plemper, R.K., Böhmler, S., Bordallo, J., Sommer, T., and Wolf, D.H. (1997). Mutant analysis links the translocon and BiP to retrograde protein transport for ER degradation. Nature *388*, 891–895.

Powers, E.T., Morimoto, R.I., Dillin, A., Kelly, J.W., and Balch, W.E. (2009). Biological and chemical approaches to diseases of proteostasis deficiency. Annu Rev Biochem *78*, 959–991.

Prabhu, A., Sarcar, B., Kahali, S., Shan, Y., and Chinnaiyan, P. (2012). Targeting the unfolded protein response in glioblastoma cells with the fusion protein EGF-SubA. PLoS ONE *7*, e52265.

Puthalakath, H., O'Reilly, L.A., Gunn, P., Lee, L., Kelly, P.N., Huntington, N.D., Hughes, P.D., Michalak, E.M., McKimm-Breschkin, J., Motoyama, N., et al. (2007). ER stress triggers apoptosis by activating BH3-only protein Bim. Cell *129*, 1337–1349.

Qi, L., Heredia, J.E., Altarejos, J.Y., Screaton, R., Goebel, N., Niessen, S., Macleod, I.X., Liew, C.W., Kulkarni, R.N., Bain, J., et al. (2006). TRB3 links the E3 ubiquitin ligase COP1 to lipid metabolism. Science *312*, 1763–1766.

Qi, L., Saberi, M., Zmuda, E., Wang, Y., Altarejos, J., Zhang, X., Dentin, R., Hedrick, S., Bandyopadhyay, G., Hai, T., et al. (2009). Adipocyte CREB promotes insulin resistance in obesity. Cell Metab *9*, 277–286.

Qi, L., Yang, L., and Chen, H. (2011). Detecting and quantitating physiological endoplasmic reticulum stress. Meth Enzymol *490*, 137–146.

Qin, L., Wang, Z., Tao, L., and Wang, Y. (2010). ER stress negatively regulates AKT/TSC/mTOR pathway to enhance autophagy. Autophagy *6*.

Qiu, Y., Mao, T., Zhang, Y., Shao, M., You, J., Ding, Q., Chen, Y., Wu, D., Xie, D., Lin, X., et al. (2010). A crucial role for RACK1 in the regulation of glucose-stimulated IRE1alpha activation in pancreatic beta cells. Sci Signal *3*, ra7.

Quan, E.M., Kamiya, Y., Kamiya, D., Denic, V., Weibezahn, J., Kato, K., and Weissman, J.S. (2008). Defining the glycan destruction signal for endoplasmic reticulum-associated degradation. Mol Cell *32*, 870–877.

Quentin, T., Steinmetz, M., Poppe, A., and Thoms, S. (2011). Metformin differentially activates ER stress signaling pathways without inducing apoptosis. Disease Models & Mechanisms 1–11.

Raggo, C., Rapin, N., Stirling, J., Gobeil, P., Smith-Windsor, E., O'Hare, P., and Misra, V. (2002). Luman, the cellular counterpart of herpes simplex virus VP16, is processed by regulated intramembrane proteolysis. Mol Cell Biol *22*, 5639–5649.

Ralph, M.R., Foster, R.G., Davis, F.C., and Menaker, M. (1990). Transplanted suprachiasmatic nucleus determines circadian period. Science *247*, 975–978.

Rapoport, T.A., Matlack, K.E., Plath, K., Misselwitz, B., and Staeck, O. (1999). Posttranslational protein translocation across the membrane of the endoplasmic reticulum. Biol. Chem. *380*, 1143–1150.

Rehm, A., Engelsberg, A., Tortorella, D., Körner, I.J., Lehmann, I., Ploegh, H.L., and Höpken, U.E. (2002). Human cytomegalovirus gene products US2 and US11 differ in their ability to attack major histocompatibility class I heavy chains in dendritic cells. J. Virol. *76*, 5043–5050.

Reimold, A.M., Etkin, A., Clauss, I., Perkins, A., Friend, D.S., Zhang, J., Horton, H.F., Scott, A., Orkin, S.H., Byrne, M.C., et al. (2000). An essential role in liver development for transcription factor XBP-1. Genes Dev *14*, 152–157.

Reimold, A.M., Iwakoshi, N.N., Manis, J., Vallabhajosyula, P., Szomolanyi-Tsuda, E., Gravallese, E.M., Friend, D., Grusby, M.J., Alt, F., and Glimcher, L.H. (2001). Plasma cell differentiation requires the transcription factor XBP-1. Nature *412*, 300–307.

Reimold, A.M., Ponath, P.D., Li, Y.S., Hardy, R.R., David, C.S., Strominger, J.L., and Glimcher, L.H. (1996). Transcription factor B cell lineage-specific activator protein regulates the gene for human X-box binding protein 1. J Exp Med *183*, 393–401.

Reynaud, D., Demarco, I.A., Reddy, K.L., Schjerven, H., Bertolino, E., Chen, Z., Smale, S.T., Winandy, S., and Singh, H. (2008). Regulation of B cell fate commitment and immunoglobulin heavy-chain gene rearrangements by Ikaros. Nat Immunol *9*, 927–936.

Richardson, C.E., Kooistra, T., and Kim, D.H. (2010). An essential role for XBP-1 in host protection against immune activation in C. elegans. Nature *463*, 1092–1095.

Rickert, R.C., Roes, J., and Rajewsky, K. (1997). B lymphocyte-specific, Cre-mediated mutagenesis in mice. Nucleic Acids Res *25*, 1317–1318.

Ritter, C., and Helenius, A. (2000). Recognition of local glycoprotein misfolding by the ER folding sensor UDP-glucose:glycoprotein glucosyltransferase. Nat. Struct. Biol. *7*,

278–280.

Rodriguez, D.A., Zamorano, S., Lisbona, F., Rojas-Rivera, D., Urra, H., Cubillos-Ruiz, J.R., Armisen, R., Henriquez, D.R., H Cheng, E., Letek, M., et al. (2012). BH3-only proteins are part of a regulatory network that control the sustained signalling of the unfolded protein response sensor IRE1α. Embo J *31*, 2322–2335.

Ron, D., and Walter, P. (2007). Signal integration in the endoplasmic reticulum unfolded protein response. Nat Rev Mol Cell Biol *8*, 519–529.

Ruddock, L.W., and Molinari, M. (2006). N-glycan processing in ER quality control. J Cell Sci *119*, 4373–4380.

Rudic, R.D., McNamara, P., Curtis, A.-M., Boston, R.C., Panda, S., Hogenesch, J.B., and Fitzgerald, G.A. (2004). BMAL1 and CLOCK, two essential components of the circadian clock, are involved in glucose homeostasis. PLoS Biol *2*, e377.

Rutkowski, D.T., and Kaufman, R.J. (2007). That which does not kill me makes me stronger: adapting to chronic ER stress. Trends Biochem Sci *32*, 469–476.

Rüegsegger, U., Leber, J.H., and Walter, P. (2001). Block of HAC1 mRNA translation by long-range base pairing is released by cytoplasmic splicing upon induction of the unfolded protein response. Cell *107*, 103–114.

Sado, M., Yamasaki, Y., Iwanaga, T., Onaka, Y., Ibuki, T., Nishihara, S., Mizuguchi, H., Momota, H., Kishibuchi, R., Hashimoto, T., et al. (2009). Protective effect against Parkinson's disease-related insults through the activation of XBP1. Brain Res *1257*, 16–24.

Saito, T., Chiba, S., Ichikawa, M., Kunisato, A., Asai, T., Shimizu, K., Yamaguchi, T., Yamamoto, G., Seo, S., Kumano, K., et al. (2003). Notch2 is preferentially expressed in mature B cells and indispensable for marginal zone B lineage development. Immunity *18*, 675–685.

Schelhaas, M., Malmström, J., Pelkmans, L., Haugstetter, J., Ellgaard, L., Grünewald, K., and Helenius, A. (2007). Simian Virus 40 depends on ER protein folding and quality control factors for entry into host cells. Cell *131*, 516–529.

Scheuner, D., Song, B., McEwen, E., Liu, C., Laybutt, R., Gillespie, P., Saunders, T., Bonner-Weir, S., and Kaufman, R.J. (2001). Translational control is required for the unfolded protein response and in vivo glucose homeostasis. Mol Cell *7*, 1165–1176.

Sha, H., He, Y., Chen, H., Wang, C., Zenno, A., Shi, H., Yang, X., Zhang, X., and Qi, L. (2009). The IRE1alpha-XBP1 pathway of the unfolded protein response is required for adipogenesis. Cell Metab *9*, 556–564.

Sha, H., He, Y., Yang, L., and Qi, L. (2011). Stressed out about obesity: IRE1α-XBP1 in metabolic disorders. Trends Endocrinol Metab *22*, 374–381.

Shaffer, A.L., Shapiro-Shelef, M., Iwakoshi, N.N., Lee, A.-H., Qian, S.-B., Zhao, H., Yu, X., Yang, L., Tan, B.K., Rosenwald, A., et al. (2004). XBP1, downstream of Blimp-1, expands the secretory apparatus and other organelles, and increases protein synthesis in plasma cell differentiation. Immunity *21*, 81–93.

Shamu, C.E., and Walter, P. (1996). Oligomerization and phosphorylation of the Ire1p kinase during intracellular signaling from the endoplasmic reticulum to the nucleus. Embo J *15*, 3028–3039.

Shearer, A.G., and Hampton, R.Y. (2005). Lipid-mediated, reversible misfolding of a sterol-sensing domain protein. Embo J *24*, 149–159.

Shen, J., Chen, X., Hendershot, L., and Prywes, R. (2002). ER stress regulation of ATF6 localization by dissociation of BiP/GRP78 binding and unmasking of Golgi localization signals. Dev Cell *3*, 99–111.

Shenkman, M.M., Groisman, B.B., Ron, E.E., Avezov, E.E., Hendershot, L.M.L., and Lederkremer, G.Z.G. (2013). A Shared Endoplasmic Reticulum-associated Degradation Pathway Involving the EDEM1 Protein for Glycosylated and Nonglycosylated Proteins. J Biol Chem *288*, 2167–2178.

Shibata, Y., Voeltz, G.K., and Rapoport, T.A. (2006). Rough sheets and smooth tubules. Cell *126*, 435–439.

Shimizu, T., Mundt, C., Licence, S., Melchers, F., and Mårtensson, I.-L. (2002). VpreB1/VpreB2/lambda 5 triple-deficient mice show impaired B cell development but functional allelic exclusion of the IgH locus. J Immunol *168*, 6286–6293.

Shuda, M., Kondoh, N., Imazeki, N., Tanaka, K., Okada, T., Mori, K., Hada, A., Arai, M., Wakatsuki, T., Matsubara, O., et al. (2003). Activation of the ATF6, XBP1 and grp78 genes in human hepatocellular carcinoma: a possible involvement of the ER stress pathway in hepatocarcinogenesis. J. Hepatol. *38*, 605–614.

Sidrauski, C., and Walter, P. (1997). The transmembrane kinase Ire1p is a site-specific endonuclease that initiates mRNA splicing in the unfolded protein response. Cell *90*, 1031–1039.

Sidrauski, C., Cox, J.S., and Walter, P. (1996). tRNA ligase is required for regulated mRNA splicing in the unfolded protein response. Cell *87*, 405–413.

Sifers, R.N., Brashears-Macatee, S., Kidd, V.J., Muensch, H., and Woo, S.L. (1988). A frameshift mutation results in a truncated alpha 1-antitrypsin that is retained within the rough endoplasmic reticulum. J Biol Chem *263*, 7330–7335.

Slot, J.W., and Geuze, J.J. (1979). A morphometrical study of the exocrine pancreatic cell in fasted and fed frogs. J Cell Biol *80*, 692–707.

Slot, J.W., Strous, G.J., and Geuze, J.J. (1979). Effect of fasting and feeding on synthesis

and intracellular transport of proteins in the frog exocrine pancreas. J Cell Biol *80*, 708–714.

Smith, J.A., Turner, M.J., DeLay, M.L., Klenk, E.I., Sowders, D.P., and Colbert, R.A. (2008). Endoplasmic reticulum stress and the unfolded protein response are linked to synergistic IFN-beta induction via X-box binding protein 1. Eur J Immunol *38*, 1194–1203.

Smith, M.H., Ploegh, H.L., and Weissman, J.S. (2011). Road to ruin: targeting proteins for degradation in the endoplasmic reticulum. Science *334*, 1086–1090.

Sok, J., Wang, X.Z., Batchvarova, N., Kuroda, M., Harding, H., and Ron, D. (1999). CHOP-Dependent stress-inducible expression of a novel form of carbonic anhydrase VI. Mol Cell Biol *19*, 495–504.

SOLS, A., and CRANE, R.K. (1954). Substrate specificity of brain hexokinase. J Biol Chem *210*, 581–595.

Song, B.-L., Sever, N., and DeBose-Boyd, R.A. (2005). Gp78, a membrane-anchored ubiquitin ligase, associates with Insig-1 and couples sterol-regulated ubiquitination to degradation of HMG CoA reductase. Mol Cell *19*, 829–840.

Song, B., Scheuner, D., Ron, D., Pennathur, S., and Kaufman, R.J. (2008). Chop deletion reduces oxidative stress, improves beta cell function, and promotes cell survival in multiple mouse models of diabetes. J Clin Invest *118*, 3378–3389.

Song, M.S., Park, Y.K., Lee, J.H., and Park, K. (2001). Induction of glucose-regulated protein 78 by chronic hypoxia in human gastric tumor cells through a protein kinase C-epsilon/ERK/AP-1 signaling cascade. Cancer Res *61*, 8322–8330.

Souabni, A., Cobaleda, C., Schebesta, M., and Busslinger, M. (2002). Pax5 promotes B lymphopoiesis and blocks T cell development by repressing Notch1. Immunity *17*, 781–793.

Stephens, S.B., and Nicchitta, C.V. (2008). Divergent regulation of protein synthesis in the cytosol and endoplasmic reticulum compartments of mammalian cells. Mol Biol Cell *19*, 623–632.

Storch, K.-F., Lipan, O., Leykin, I., Viswanathan, N., Davis, F.C., Wong, W.H., and Weitz, C.J. (2002). Extensive and divergent circadian gene expression in liver and heart. Nature *417*, 78–83.

Sullivan, J.E., Brocklehurst, K.J., Marley, A.E., Carey, F., Carling, D., and Beri, R.K. (1994). Inhibition of lipolysis and lipogenesis in isolated rat adipocytes with AICAR, a cell-permeable activator of AMP-activated protein kinase. FEBS Lett *353*, 33–36.

Sundaram, M., and Greenwald, I. (1993). Suppressors of a lin-12 hypomorph define genes that interact with both lin-12 and glp-1 in Caenorhabditis elegans. Genetics *135*,

765–783.

Tabas, I., and Ron, D. (2011). Integrating the mechanisms of apoptosis induced by endoplasmic reticulum stress. Nat Cell Biol *13*, 184–190.

Tatu, U., Braakman, I., and Helenius, A. (1993). Membrane glycoprotein folding, oligomerization and intracellular transport: effects of dithiothreitol in living cells. Embo J *12*, 2151–2157.

Terai, K., Hiramoto, Y., Masaki, M., Sugiyama, S., Kuroda, T., Hori, M., Kawase, I., and Hirota, H. (2005). AMP-activated protein kinase protects cardiomyocytes against hypoxic injury through attenuation of endoplasmic reticulum stress. Mol Cell Biol *25*, 9554–9575.

Thastrup, O., Cullen, P.J., Drøbak, B.K., Hanley, M.R., and Dawson, A.P. (1990). Thapsigargin, a tumor promoter, discharges intracellular Ca2+ stores by specific inhibition of the endoplasmic reticulum Ca2(+)-ATPase. Proc Natl Acad Sci USA *87*, 2466–2470.

Tirasophon, W., Lee, K., Callaghan, B., Welihinda, A., and Kaufman, R.J. (2000). The endoribonuclease activity of mammalian IRE1 autoregulates its mRNA and is required for the unfolded protein response. Genes Dev *14*, 2725–2736.

Tirasophon, W., Welihinda, A.A., and Kaufman, R.J. (1998). A stress response pathway from the endoplasmic reticulum to the nucleus requires a novel bifunctional protein kinase/endoribonuclease (Ire1p) in mammalian cells. Genes Dev *12*, 1812–1824.

Todd, D.J., Lee, A.-H., and Glimcher, L.H. (2008). The endoplasmic reticulum stress response in immunity and autoimmunity. Nat Rev Immunol *8*, 663–674.

Todd, D.J., McHeyzer-Williams, L.J., Kowal, C., Lee, A.-H., Volpe, B.T., Diamond, B., McHeyzer-Williams, M.G., and Glimcher, L.H. (2009). XBP1 governs late events in plasma cell differentiation and is not required for antigen-specific memory B cell development. J Exp Med *206*, 2151–2159.

Toyofuku, T., Yoshida, J., Sugimoto, T., Zhang, H., Kumanogoh, A., Hori, M., and Kikutani, H. (2005). FARP2 triggers signals for Sema3A-mediated axonal repulsion. Nat Neurosci *8*, 1712–1719.

Travers, K.J., Patil, C.K., Wodicka, L., Lockhart, D.J., Weissman, J.S., and Walter, P. (2000). Functional and genomic analyses reveal an essential coordination between the unfolded protein response and ER-associated degradation. Cell *101*, 249–258.

Tsai, B., Rodighiero, C., Lencer, W.I., and Rapoport, T.A. (2001). Protein disulfide isomerase acts as a redox-dependent chaperone to unfold cholera toxin. Cell *104*, 937–948.

Tsai, H.-Y., Yang, Y.-F., Wu, A.T., Yang, C.-J., Liu, Y.-P., Jan, Y.-H., Lee, C.-H., Hsiao, Y.-W., Yeh, C.-T., Shen, C.-N., et al. (2013). Endoplasmic reticulum ribosome-

binding protein 1 (RRBP1) overexpression is frequently found in lung cancer patients and alleviates intracellular stress-induced apoptosis through the enhancement of GRP78. Oncogene.

Uchiyama, Y., and Watanabe, M. (1987). Correlation of rhythmic variations in subcellular structures of rat hepatocytes, pancreatic acinar cells, and islet B cells. Prog Clin Biol Res *227A*, 153–162.

Unterberger, U., Höftberger, R., Gelpi, E., Flicker, H., Budka, H., and Voigtländer, T. (2006). Endoplasmic reticulum stress features are prominent in Alzheimer disease but not in prion diseases in vivo. J Neuropathol Exp Neurol *65*, 348–357.

Urano, F., Wang, X., Bertolotti, A., Zhang, Y., Chung, P., Harding, H.P., and Ron, D. (2000). Coupling of stress in the ER to activation of JNK protein kinases by transmembrane protein kinase IRE1. Science *287*, 664–666.

Vaccaro, A., Patten, S.A., Aggad, D., Julien, C., Maios, C., Kabashi, E., Drapeau, P., and Parker, J.A. (2013). Pharmacological reduction of ER stress protects against TDP-43 neuronal toxicity in vivo. Neurobiol Dis *55*, 64–75.

van Anken, E., Romijn, E.P., Maggioni, C., Mezghrani, A., Sitia, R., Braakman, I., and Heck, A.J.R. (2003). Sequential waves of functionally related proteins are expressed when B cells prepare for antibody secretion. Immunity *18*, 243–253.

Vinci, F., Catharino, S., Frey, S., Buchner, J., Marino, G., Pucci, P., and Ruoppolo, M. (2004). Hierarchical formation of disulfide bonds in the immunoglobulin Fc fragment is assisted by protein-disulfide isomerase. J Biol Chem *279*, 15059–15066.

Vogel, J.P., Misra, L.M., and Rose, M.D. (1990). Loss of BiP/GRP78 function blocks translocation of secretory proteins in yeast. J Cell Biol *110*, 1885–1895.

Volmer, R., Ploeg, K.V.D., and Ron, D. (2013). Membrane lipid saturation activates endoplasmic reticulum unfolded protein response transducers through their transmembrane domains. Proc Natl Acad Sci USA *110*, 4628–4633.

Wahlman, J., DeMartino, G.N., Skach, W.R., Bulleid, N.J., Brodsky, J.L., and Johnson, A.E. (2007). Real-time fluorescence detection of ERAD substrate retrotranslocation in a mammalian in vitro system. Cell *129*, 943–955.

Walter, P., and Ron, D. (2011). The Unfolded Protein Response: From Stress Pathway to Homeostatic Regulation. Science *334*, 1081–1086.

Wang, S., and Kaufman, R.J. (2012). The impact of the unfolded protein response on human disease. J Cell Biol *197*, 857–867.

Wang, X.Z., Lawson, B., Brewer, J.W., Zinszner, H., Sanjay, A., Mi, L.J., Boorstein, R., Kreibich, G., Hendershot, L.M., and Ron, D. (1996). Signals from the stressed endoplasmic reticulum induce C/EBP-homologous protein (CHOP/GADD153). Mol Cell

Biol *16*, 4273–4280.

Wang, Y.H., Nomura, J., Faye-Petersen, O.M., and Cooper, M.D. (1998). Surrogate light chain production during B cell differentiation: differential intracellular versus cell surface expression. J Immunol *161*, 1132–1139.

Wek, R.C., Jiang, H.-Y., and Anthony, T.G. (2006). Coping with stress: eIF2 kinases and translational control. Biochem Soc Trans *34*, 7–11.

Whitney, M.L., Jefferson, L.S., and Kimball, S.R. (2009). ATF4 is necessary and sufficient for ER stress-induced upregulation of REDD1 expression. Biochem Biophys Res Commun *379*, 451–455.

Wiertz, E.J., Tortorella, D., Bogyo, M., Yu, J., Mothes, W., Jones, T.R., Rapoport, T.A., and Ploegh, H.L. (1996). Sec61-mediated transfer of a membrane protein from the endoplasmic reticulum to the proteasome for destruction. Nature *384*, 432–438.

Wilkinson, B., and Gilbert, H.F. (2004). Protein disulfide isomerase. Biochim Biophys Acta *1699*, 35–44.

Winnay, J.N., Boucher, J., Mori, M.A., Ueki, K., and Kahn, C.R. (2010). A regulatory subunit of phosphoinositide 3-kinase increases the nuclear accumulation of X-box-binding protein-1 to modulate the unfolded protein response. Nat Med.

Wiseman, R.L., Zhang, Y., Lee, K.P.K., Harding, H.P., Haynes, C.M., Price, J., Sicheri, F., and Ron, D. (2010). Flavonol activation defines an unanticipated ligand-binding site in the kinase-RNase domain of IRE1. Mol Cell *38*, 291–304.

Woo, C., Cui, D., Arellano, J., Dorweiler, B., Harding, H., Fitzgerald, K., Ron, D., and Tabas, I. (2009). Adaptive suppression of the ATF4-CHOP branch of the unfolded protein response by toll-like receptor signalling. Nat Cell Biol.

Wray, S., and Burdyga, T. (2010). Sarcoplasmic reticulum function in smooth muscle. Physiol Rev *90*, 113–178.

Wu, J., and Kaufman, R.J. (2006). From acute ER stress to physiological roles of the Unfolded Protein Response. Cell Death Differ *13*, 374–384.

Xia, S., Sha, H., Yang, L., Ji, Y., Ostrand-Rosenberg, S., and Qi, L. (2011). Gr-1+ CD11b+ Myeloid-derived Suppressor Cells Suppress Inflammation and Promote Insulin Sensitivity in Obesity. J Biol Chem *286*, 23591–23599.

Xue, Z., He, Y., Ye, K., Gu, Z., Mao, Y., and Qi, L. (2011). A conserved structural determinant located at the interdomain region of mammalian inositol-requiring enzyme 1alpha. J Biol Chem *286*, 30859–30866.

Yagishita, N., Ohneda, K., Amano, T., Yamasaki, S., Sugiura, A., Tsuchimochi, K., Shin, H., Kawahara, K.-I., Ohneda, O., Ohta, T., et al. (2005). Essential role of synoviolin in

embryogenesis. J Biol Chem *280*, 7909–7916.

Yamaguchi, H., and Wang, H.-G. (2004). CHOP is involved in endoplasmic reticulum stress-induced apoptosis by enhancing DR5 expression in human carcinoma cells. J Biol Chem *279*, 45495–45502.

Yamamoto, K., Yoshida, H., Kokame, K., Kaufman, R.J., and Mori, K. (2004). Differential contributions of ATF6 and XBP1 to the activation of endoplasmic reticulum stress-responsive cis-acting elements ERSE, UPRE and ERSE-II. J Biochem *136*, 343–350.

Yan, W., Frank, C.L., Korth, M.J., Sopher, B.L., Novoa, I., Ron, D., and Katze, M.G. (2002). Control of PERK eIF2alpha kinase activity by the endoplasmic reticulum stress-induced molecular chaperone P58IPK. Proc Natl Acad Sci USA *99*, 15920–15925.

Yang, L., Sha, H., Davisson, R.L., and Qi, L. (2013). Phenformin Activates the Unfolded Protein Response in an AMP-activated Protein Kinase (AMPK)-dependent Manner. J Biol Chem *288*, 13631–13638.

Yang, L., Xue, Z., He, Y., Sun, S., Chen, H., and Qi, L. (2010). A Phos-Tag-Based Approach Reveals the Extent of Physiological Endoplasmic Reticulum Stress. PLoS ONE *5(7): e11621*.

Ye, J., Rawson, R.B., Komuro, R., Chen, X., Davé, U.P., Prywes, R., Brown, M.S., and Goldstein, J.L. (2000). ER stress induces cleavage of membrane-bound ATF6 by the same proteases that process SREBPs. Mol Cell *6*, 1355–1364.

Ye, R., Jung, D.Y., Jun, J.Y., Li, J., Luo, S., Ko, H.J., Kim, J.K., and Lee, A.S. (2010). Grp78 heterozygosity promotes adaptive unfolded protein response and attenuates diet-induced obesity and insulin resistance. Diabetes *59*, 6–16.

Ye, Y., Meyer, H.H., and Rapoport, T.A. (2001). The AAA ATPase Cdc48/p97 and its partners transport proteins from the ER into the cytosol. Nature *414*, 652–656.

Ye, Y., Meyer, H.H., and Rapoport, T.A. (2003). Function of the p97-Ufd1-Npl4 complex in retrotranslocation from the ER to the cytosol: dual recognition of nonubiquitinated polypeptide segments and polyubiquitin chains. J Cell Biol *162*, 71–84.

Ye, Y., Shibata, Y., Yun, C., Ron, D., and Rapoport, T.A. (2004). A membrane protein complex mediates retro-translocation from the ER lumen into the cytosol. Nature *429*, 841–847.

Yoshida, H., Matsui, T., Yamamoto, A., Okada, T., and Mori, K. (2001). XBP1 mRNA is induced by ATF6 and spliced by IRE1 in response to ER stress to produce a highly active transcription factor. Cell *107*, 881–891.

Yoshida, H., Oku, M., Suzuki, M., and Mori, K. (2006). pXBP1(U) encoded in XBP1 pre-mRNA negatively regulates unfolded protein response activator pXBP1(S) in

mammalian ER stress response. J Cell Biol *172*, 565–575.

Young, C.N., Cao, X., Guruju, M.R., Pierce, J.P., Morgan, D.A., Wang, G., Iadecola, C., Mark, A.L., and Davisson, R.L. (2012). ER stress in the brain subfornical organ mediates angiotensin-dependent hypertension. J Clin Invest *122*, 3960–3964.

Zeng, L., Liu, Y.-P., Sha, H., Chen, H., Qi, L., and Smith, J.A. (2010). XBP-1 couples endoplasmic reticulum stress to augmented IFN-beta induction via a cis-acting enhancer in macrophages. J Immunol *185*, 2324–2330.

Zeng, L., Zampetaki, A., Margariti, A., Pepe, A.E., Alam, S., Martin, D., Xiao, Q., Wang, W., Jin, Z.-G., Cockerill, G., et al. (2009). Sustained activation of XBP1 splicing leads to endothelial apoptosis and atherosclerosis development in response to disturbed flow. Proc Natl Acad Sci USA *106*, 8326–8331.

Zhang, K., Shen, X., Wu, J., Sakaki, K., Saunders, T., Rutkowski, D.T., Back, S.H., and Kaufman, R.J. (2006a). Endoplasmic reticulum stress activates cleavage of CREBH to induce a systemic inflammatory response. Cell *124*, 587–599.

Zhang, K., Wang, S., Malhotra, J., Hassler, J.R., Back, S.H., Wang, G., Chang, L., Xu, W., Miao, H., Leonardi, R., et al. (2011). The unfolded protein response transducer IRE1α prevents ER stress-induced hepatic steatosis. Embo J *30*, 1357–1375.

Zhang, K., Wong, H.N., Song, B., Miller, C.N., Scheuner, D., and Kaufman, R.J. (2005). The unfolded protein response sensor IRE1alpha is required at 2 distinct steps in B cell lymphopoiesis. J Clin Invest *115*, 268–281.

Zhang, P., McGrath, B., Li, S., Frank, A., Zambito, F., Reinert, J., Gannon, M., Ma, K., McNaughton, K., and Cavener, D.R. (2002). The PERK eukaryotic initiation factor 2 alpha kinase is required for the development of the skeletal system, postnatal growth, and the function and viability of the pancreas. Mol Cell Biol *22*, 3864–3874.

Zhang, W., Feng, D., Li, Y., Iida, K., McGrath, B., and Cavener, D.R. (2006b). PERK EIF2AK3 control of pancreatic beta cell differentiation and proliferation is required for postnatal glucose homeostasis. Cell Metab *4*, 491–497.

Zhang, X., Zhang, G., Zhang, H., Karin, M., Bai, H., and Cai, D. (2008). Hypothalamic IKKbeta/NF-kappaB and ER stress link overnutrition to energy imbalance and obesity. Cell *135*, 61–73.

Zhou, G., Myers, R., Li, Y., Chen, Y., Shen, X., Fenyk-Melody, J., Wu, M., Ventre, J., Doebber, T., Fujii, N., et al. (2001). Role of AMP-activated protein kinase in mechanism of metformin action. J Clin Invest *108*, 1167–1174.

Zhou, J., Liu, C.Y., Back, S.H., Clark, R.L., Peisach, D., Xu, Z., and Kaufman, R.J. (2006). The crystal structure of human IRE1 luminal domain reveals a conserved dimerization interface required for activation of the unfolded protein response. Proc Natl Acad Sci USA *103*, 14343–14348.

Zhuang, B., Su, Y.S., and Sockanathan, S. (2009). FARP1 promotes the dendritic growth of spinal motor neuron subtypes through transmembrane Semaphorin6A and PlexinA4 signaling. Neuron *61*, 359–372.